

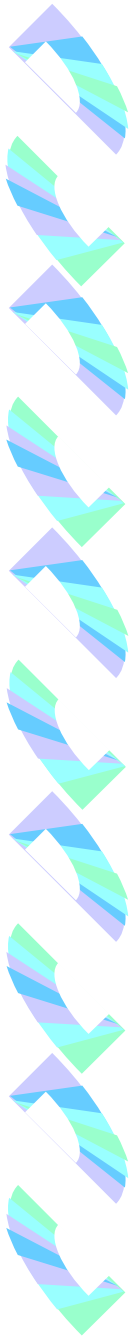
Preparation, Applications and Structural Determination of Nano-porous Materials

Soofin Cheng (鄭淑芬)

Department of Chemistry, National Taiwan University

台灣大學化學系

Email: chem1031@ntu.edu.tw



Nanostructured Materials

- Nanostructures represent the transition **from atom to bulky solid**.
- It is essential to obtain particles or pores with **uniform diameters and shapes** and, for the purpose of particular applications, **to arrange and embed them in a superstructure**.
- **Size quantization effects, high number of surface atoms, and special surface states.**
- **Special optical, electronic, magnetic, and chemical properties**
- Good applications in the areas of signal transmission, data and energy storage, catalysis, as well as biology.



Definition

What are **Nano-porous materials**



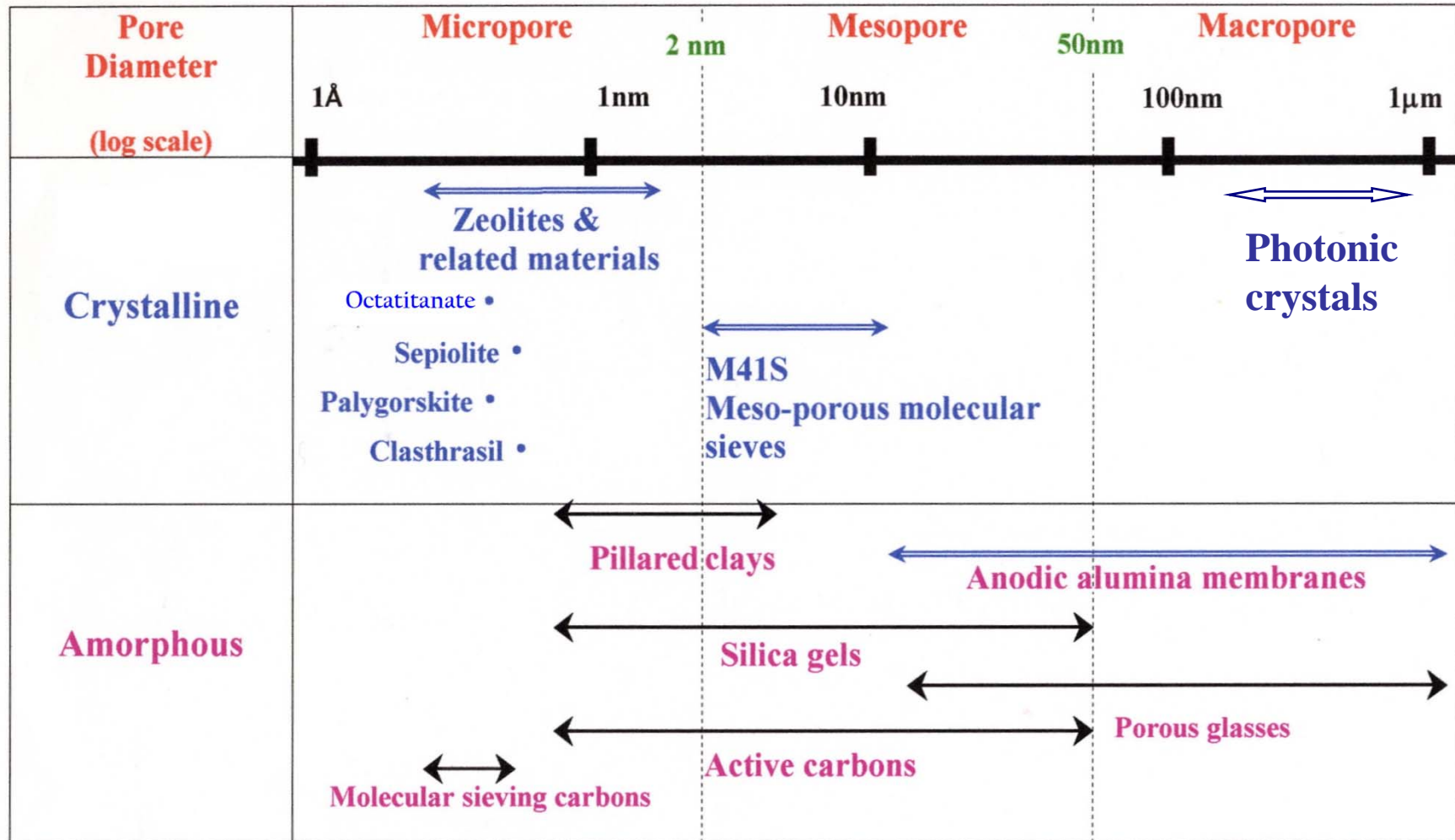


Nanoporous materials

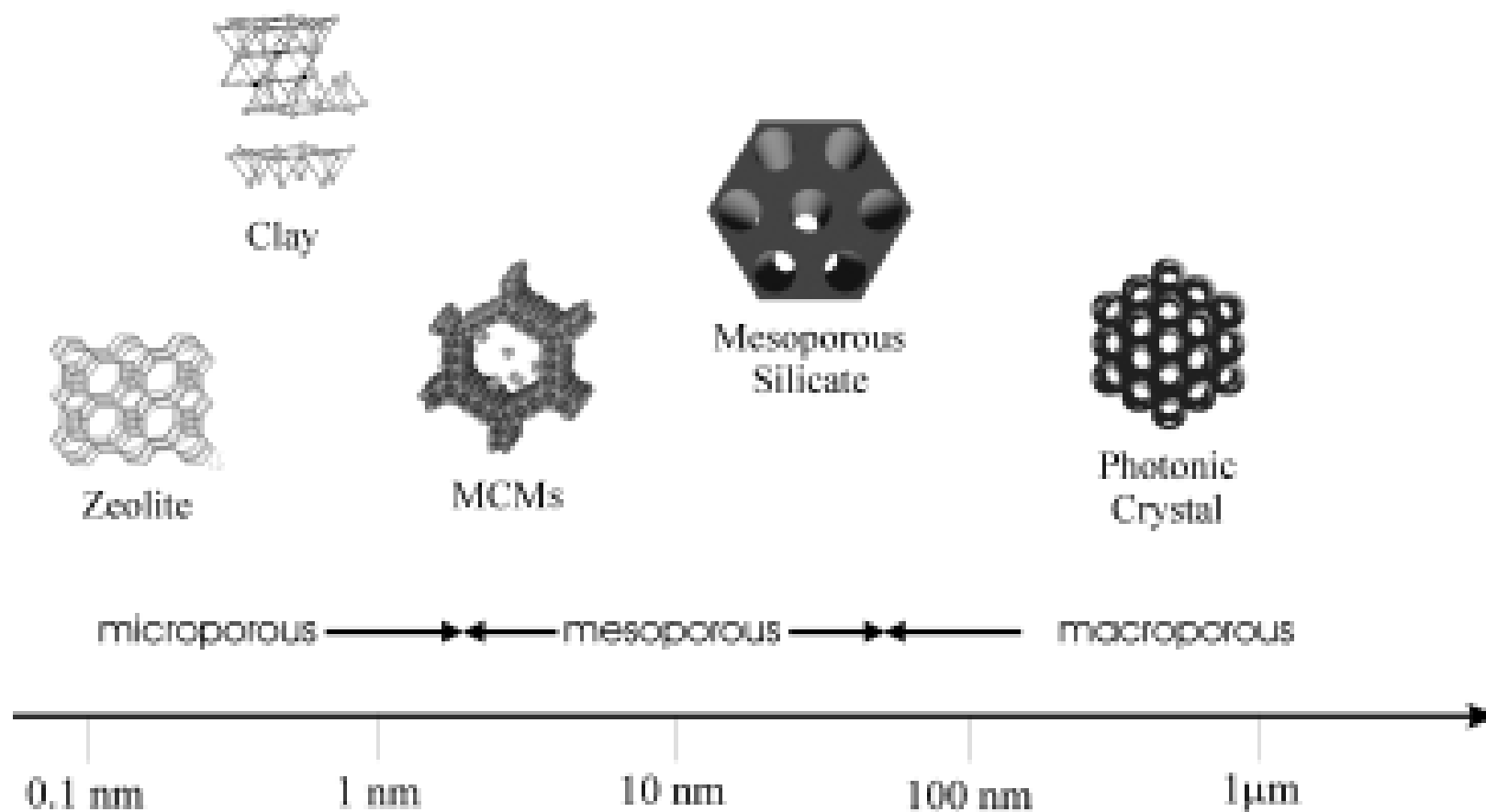
IUPAC (International Union of Pure and Applied Chemistry) classification:

- ♦ microporous , $d < 2 \text{ nm}$
- ♦ mesoporous , $2 \text{ nm} < d < 50 \text{ nm}$
- ♦ macroporous , $d > 50 \text{ nm}$

Scheme 1. Pore size distribution of various porous materials.



Nano-porous materials



Angew. Chem. Int. Ed. Vol. 41, pp. 688-714 (2002)

Anodic alumina

Appl. Phys. Lett., Vol. 71, No. 19, 10 November 1997

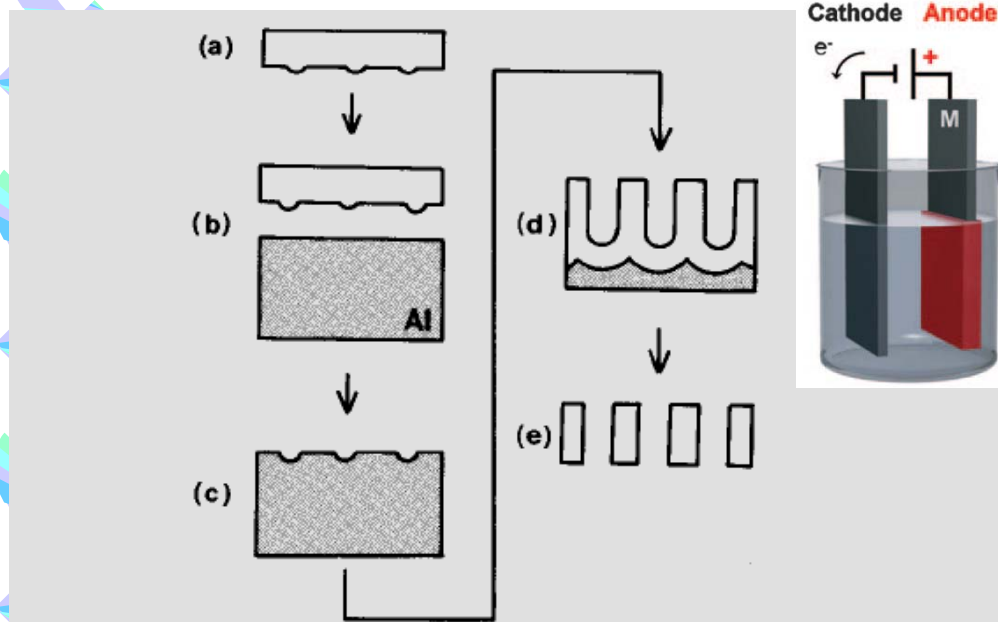


FIG. 1. Process for the ordered channel array; SiC mold with hexagonally ordered array of convexes (a), molding on the Al (b), textured Al (c), anodization and growth of channel architecture (d), removal of Al and barrier layer (e).

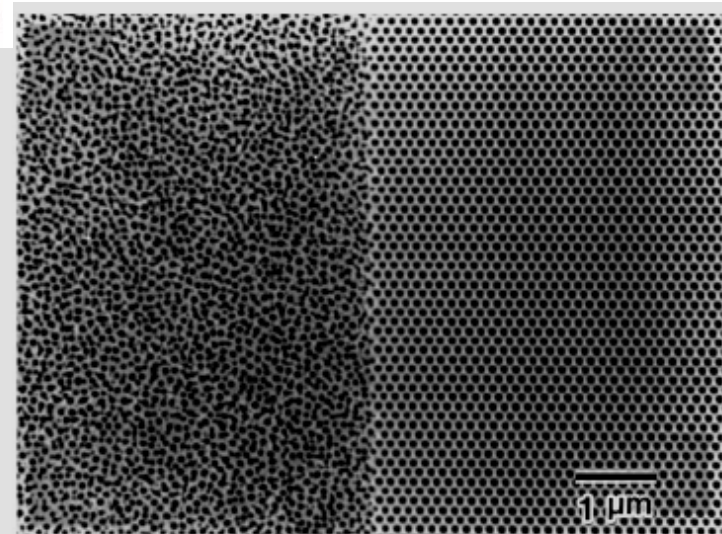


FIG. 2. SEM micrograph of surface view of anodized Al; pretexturing interval was 150 nm. Anodization was conducted in 0.3 M oxalic acid of 17 °C at 60 V for 36 min. Pore widening was carried out in 5 wt % phosphoric acid at 30 °C for 70 min.

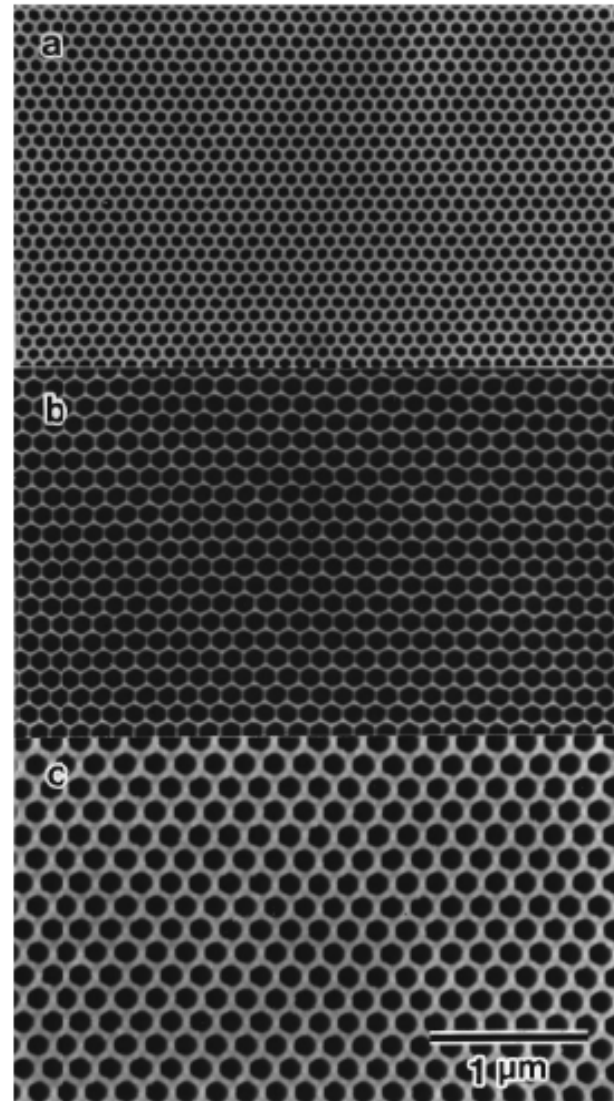
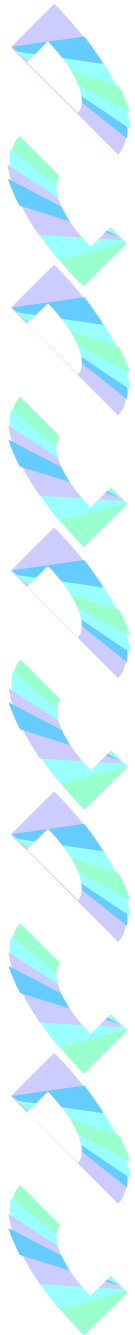


FIG. 5. SEM micrographs of cell configuration in barrier layer with different intervals of 100 nm (a), 150 nm (b), and 200 nm (c). Anodization voltage were 40 V (a), 60 V (b), and 80 V (c). Anodization was conducted in 0.3 M oxalic acid of 17 °C for (a) and (b), and 0.04 M oxalic acid of 3 °C for (c). Thickness of the oxide films was approximately 3 μm .

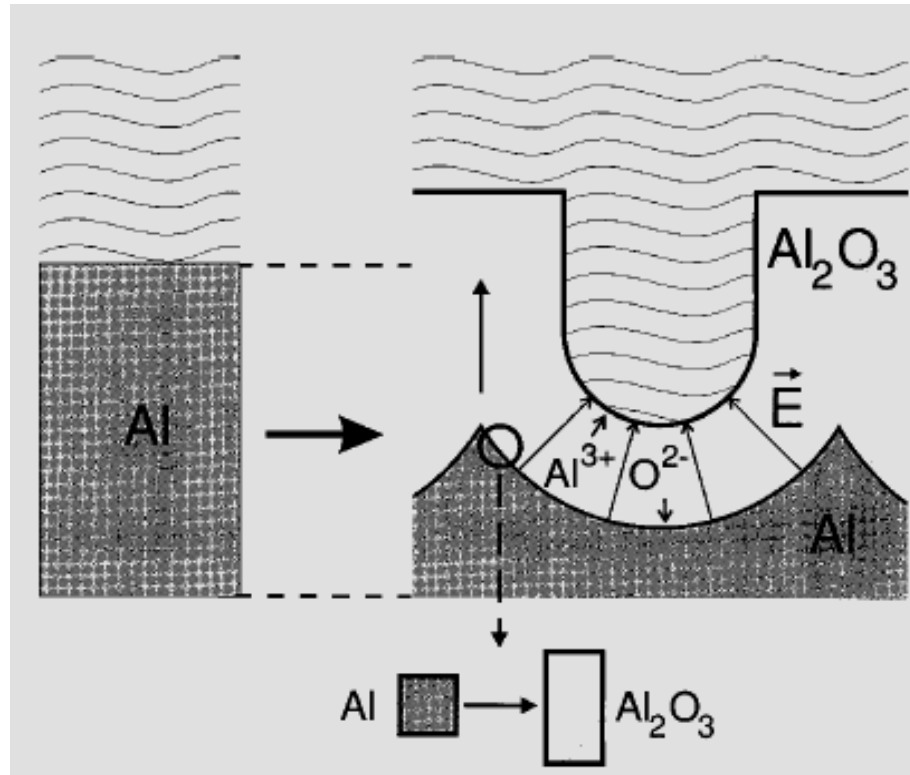
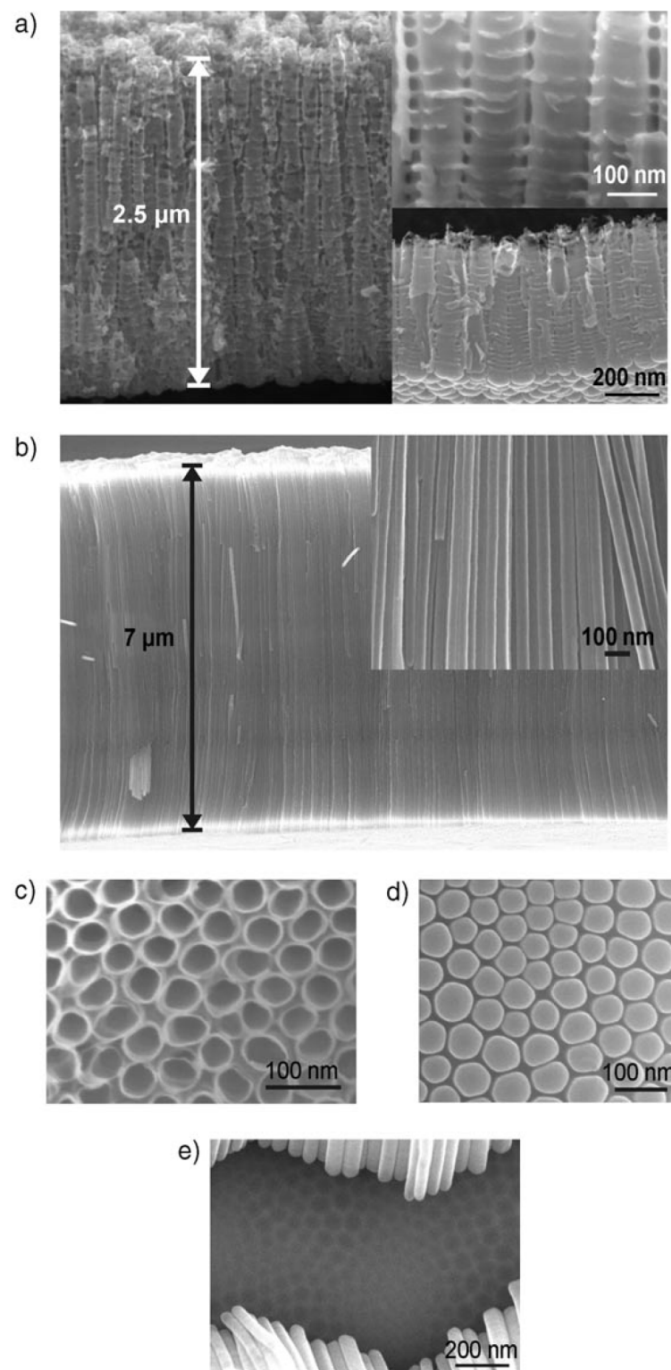
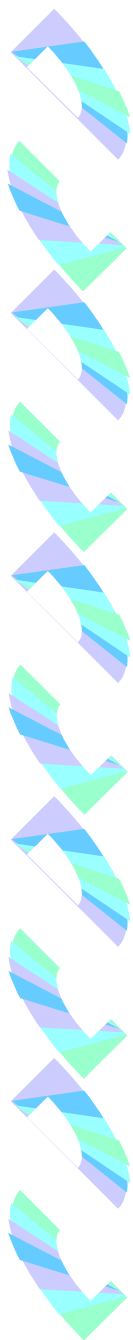


FIG. 1. Expansion of aluminum during anodic oxidation. On the left the level of the unoxidized metal surface is depicted.

The mechanical stress at the metal/oxide interface is proposed to cause repulsive forces between the neighboring pores which promote the formation of ordered hexagonal pore arrays.



Anodic TiO₂ nanotubes

Macak et al., Angew. Chem. Int. Ed. 2005, 44, 7463

Figure 1. a) SEM images of conventional anodic TiO₂ nanotubes with marked inhomogeneities (from Ref. [4]). The insets show a magnification of the structure (top) and an example of ripples on short tubes formed in 1m H₂SO₄ with 0.15 wt% HF (bottom). b) Smooth TiO₂ nanotubes 7-μm long produced in **glycerol electrolyte with 0.5 wt% NH₄F**. The inset shows the walls of the nanotubes in more detail. c)– e) SEM images of smooth TiO₂ nanotubes 7-μm long produced in glycerol electrolyte: c) top view; d) bottom view. The average nanotube diameter is approximately 40 nm and the average pore spacing is approximately 60 nm. e) Top view of an anodized sample after removal of some arrays of nanotubes. The lower part of the tubes and part of the Ti substrate surface are visible. Clearly the convex shape of the nanotube bottoms is reflected in the surface of the Ti substrate.

Anodic TiO₂ nanotubes

Macak et al., Angew. Chem. Int. Ed. 2005, 44, 7463

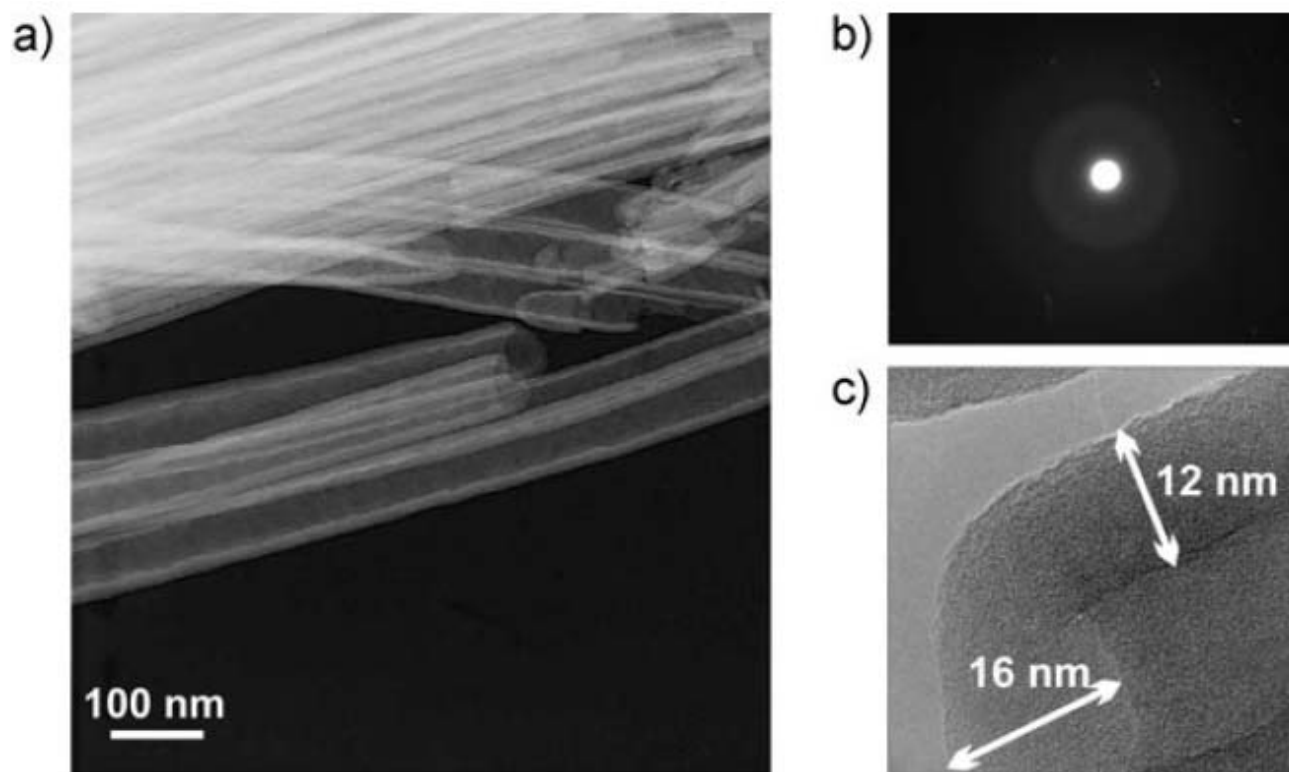


Figure 3. Smooth TiO₂ nanotubes produced in the glycerol electrolyte: a) TEM image of several TiO₂ nanotubes; b) TEM diffraction pattern of a nanotube wall; c) HRTEM image of a single nanotube.

TiO₂ Nanotubes: Synthesis and Applications

Roy et al. Angew. Chem. Int. Ed. **2011**, 50, 2904-2939

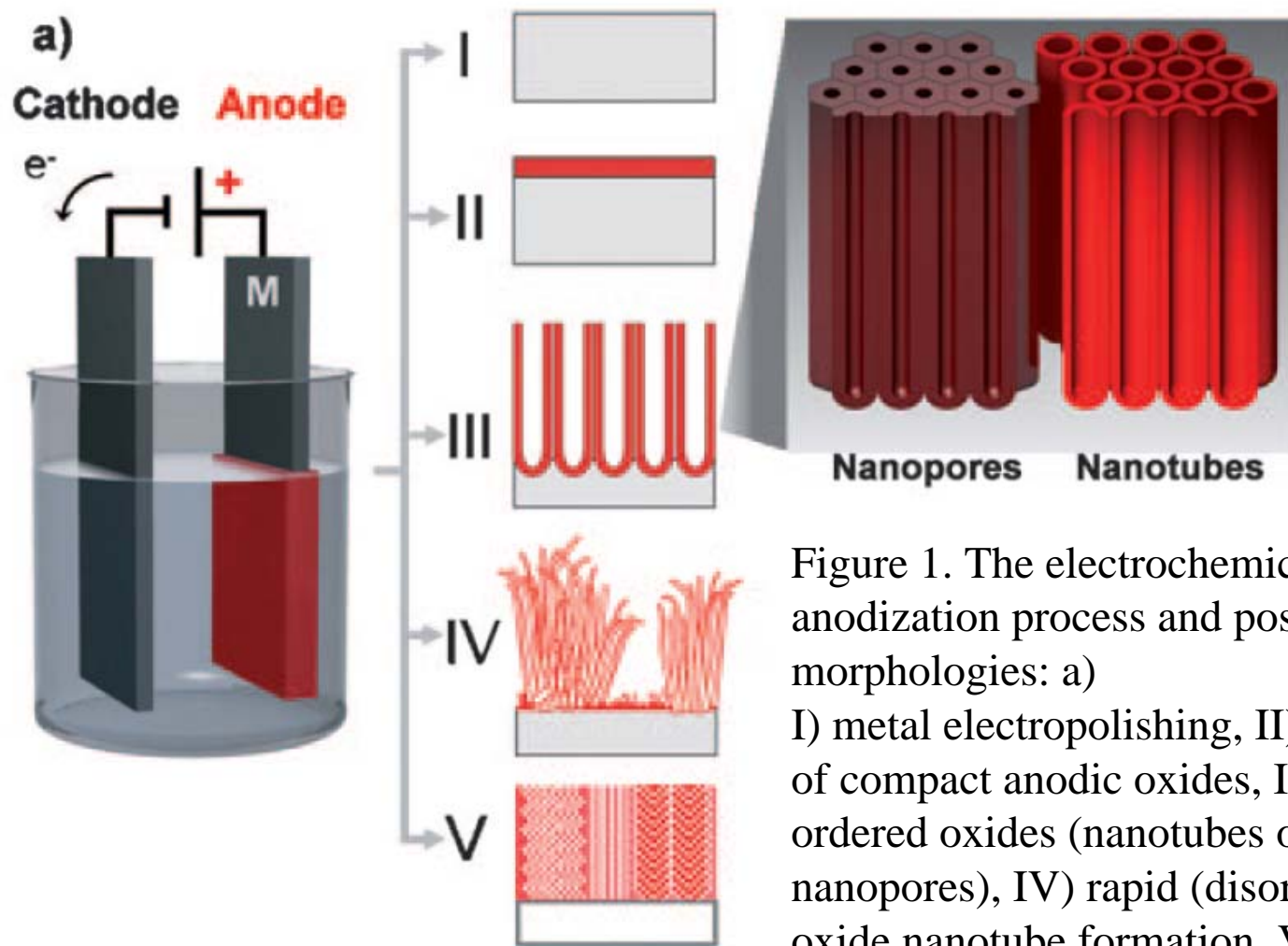


Figure 1. The electrochemical anodization process and possible anodic morphologies: a) I) metal electropolishing, II) formation of compact anodic oxides, III) self-ordered oxides (nanotubes or nanopores), IV) rapid (disorganized) oxide nanotube formation, V) ordered nanoporous layers.

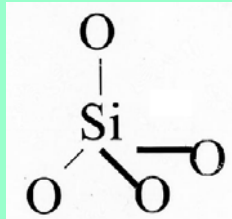


Zeolites (沸石) & Molecular Sieves (分子篩)

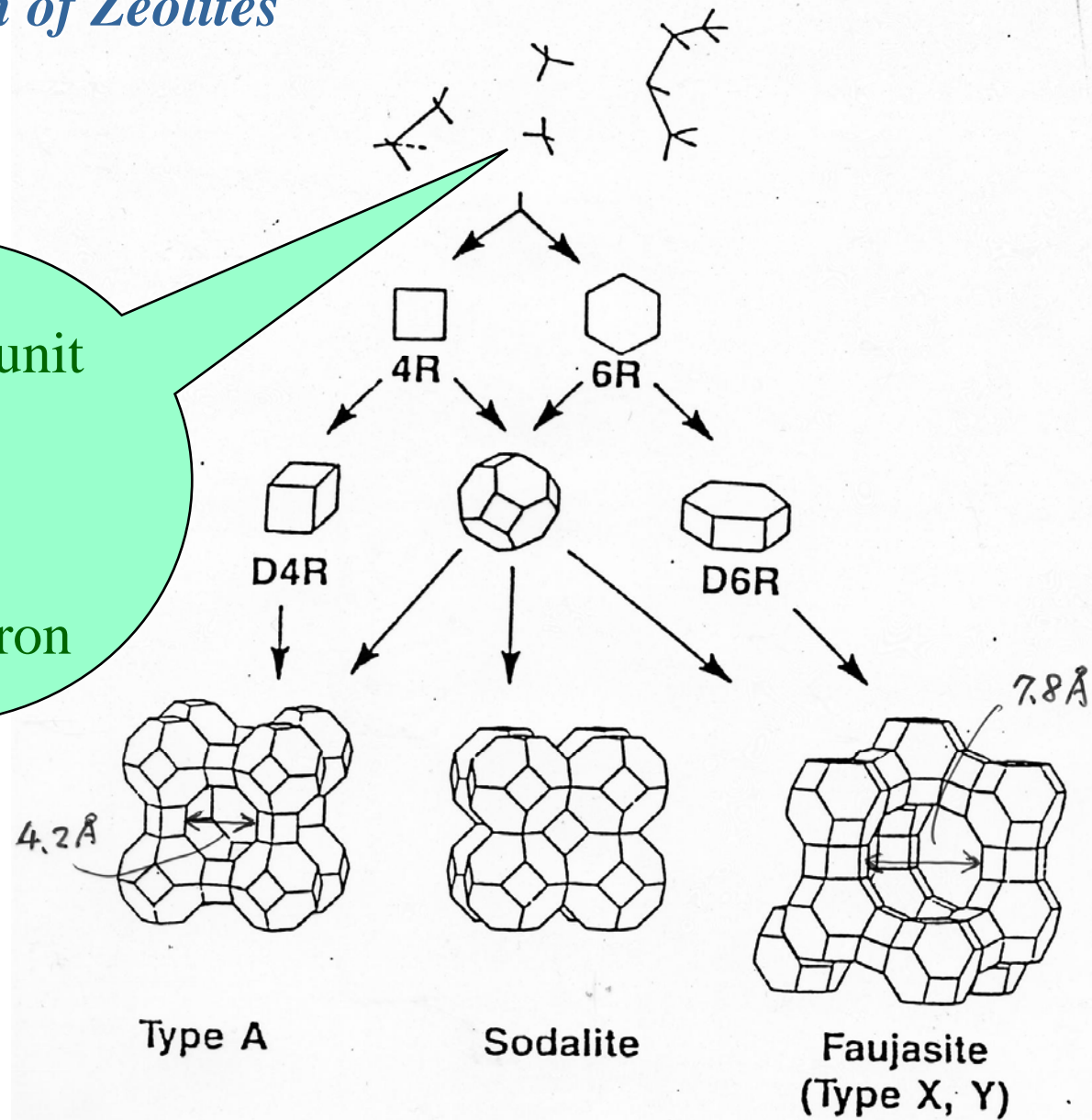
- ◆ Zeolites
 - ◆ - **crystalline** aluminosilicate with **open** structures
- ◆ Molecular Sieves
 - ◆ -materials which can **separate** gases based on **molecular size**

Construction of Zeolites

Building unit



Tetrahedron



Isomorphous substitution of Si in zeolite framework

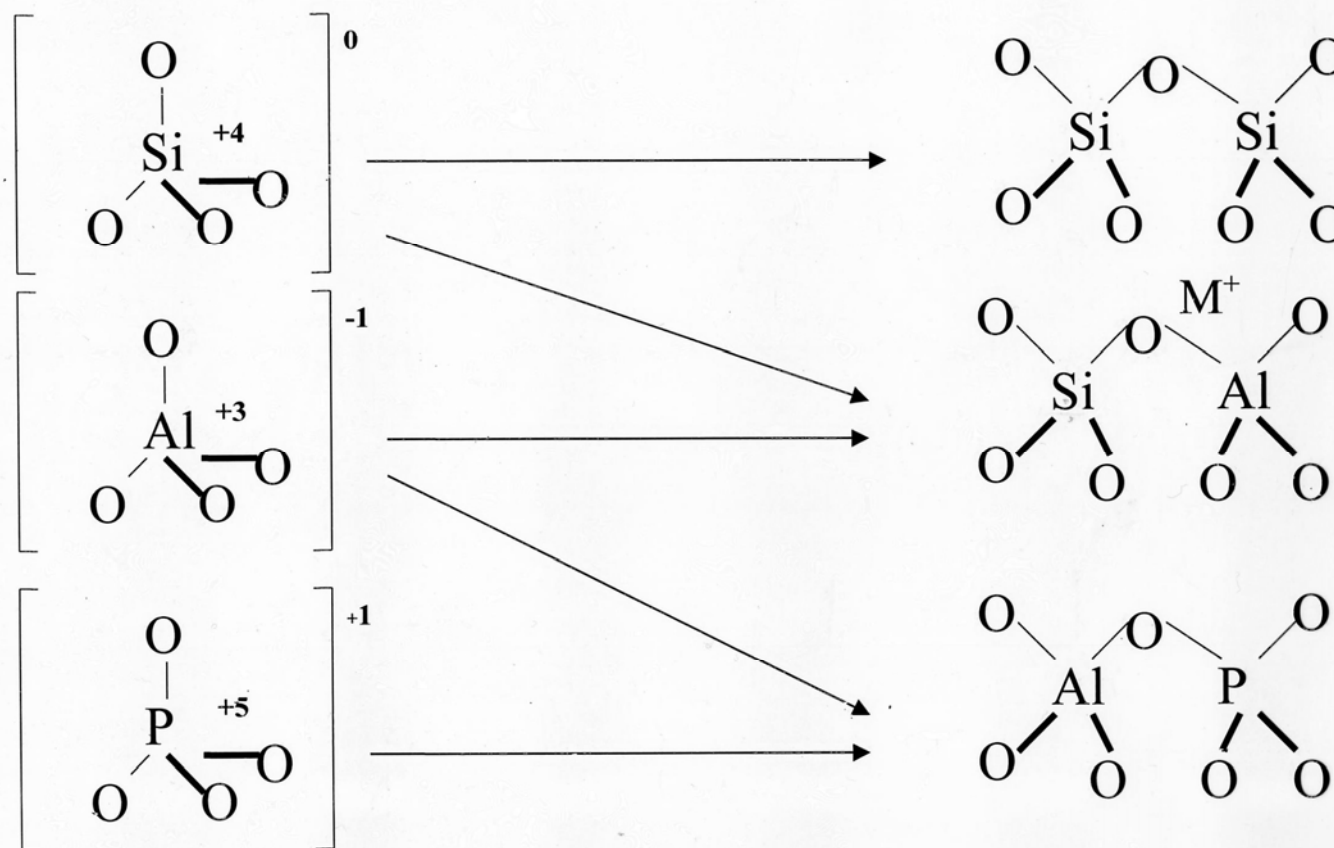
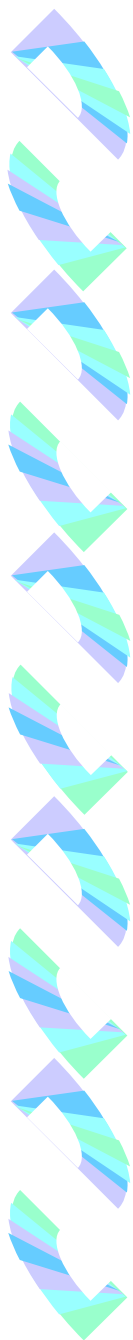


Figure 1. TO_4 units in zeolites and aluminophosphates.



Zeolites of various pore structures

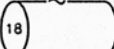

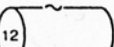
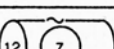
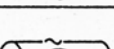
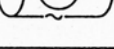

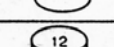
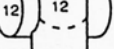

Framework Chemistry Channel/Cage System	Silicates		Phosphates, Arsenates & Germanates		
	SiO ₂	(Si,Al)O ₂	AlPO ₄	(Al,X)PO ₄	MXO ₄
			VFI VPI-5		
			AET AlPO ₄ -8		
	AFI SSZ-24	CAN Cancrinite	AFI AlPO ₄ -5	ATS MAPO-36	CAN AlGeO ₄ CAN BePO ₄ (tiptopite)
		MEI ZSM-18			
		BPH Linde Q GME gmelinite LTL Linde L MAZ mazzite MOR mordenite OFF offretite	ATO AlPO ₄ -31	AFS MAPSO-40 AFY CoAPO ₄ -50 AFY SAPO ₄ -40	BPH BePO ₄ -H (beryllo-phosphate-H)
		BOG boggsite			
		*BEA beta			
		EMT EMC-2 (hexagonal faujasite)			
		FAU faujasite		FAU SAPO ₄ -37	FAU BePO ₄ FAU ZnPO ₄ FAU BeAsO ₄ FAU ZnAsO ₄
					-CLO GaPO ₄ (cloverite)

Fig. 3. Framework chemistry and pore architecture of large pore zeolites.

J.B. Higgins, Catal. Today 19 (1994), 7-26

SOME PROPERTIES OF ZEOLITES

9

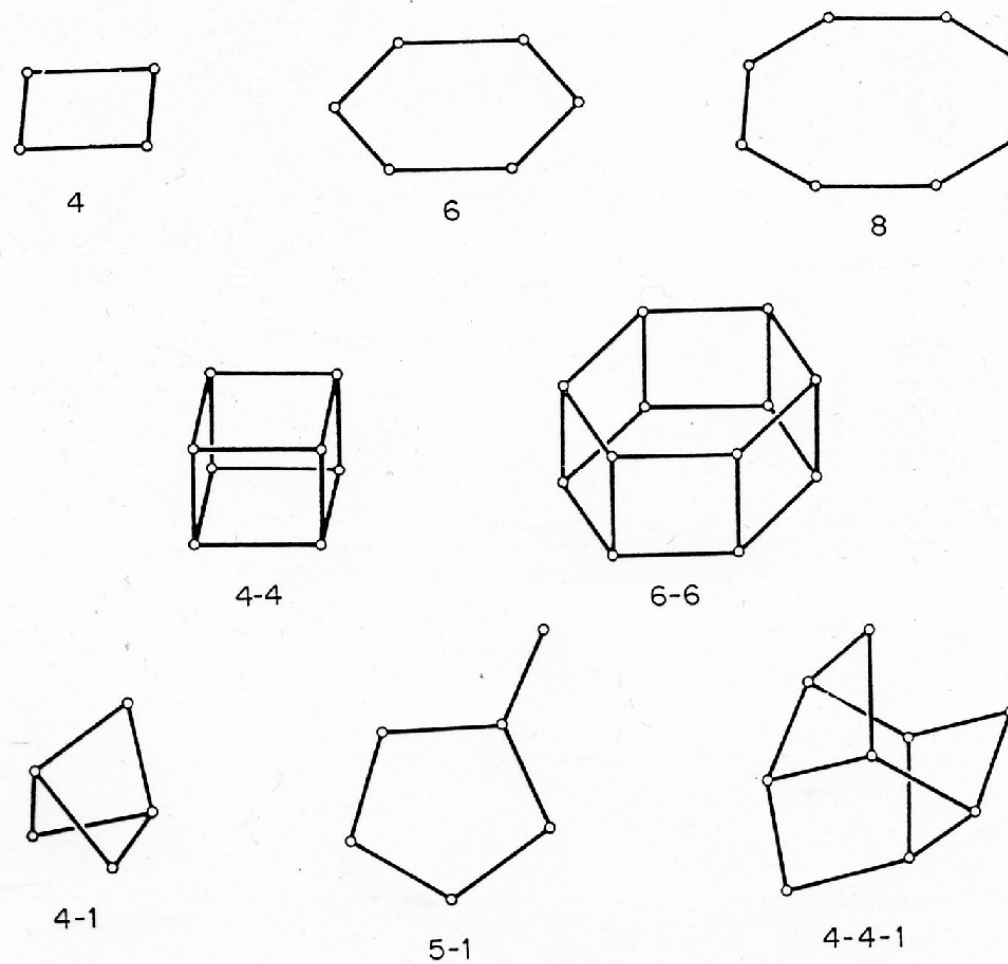


Fig. 4. Secondary building units identifiable in zeolite frameworks.⁽²⁹⁾

Structure of synthetic zeolite ZSM-5

pentasil zeolites

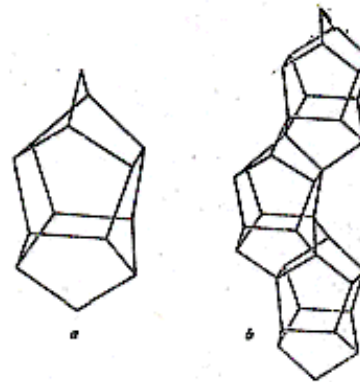


Fig. 1 Characteristic configuration (a) and its linkage within chains (b) in ZSM-5. These chains run parallel to $[001]$. Only T-atoms (Si, Al) are shown.

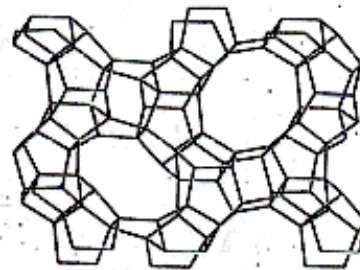


Fig. 2 Skeletal diagram of the (010)-face of the ZSM-5 unit cell. The x -axis is horizontal and the z -axis vertical. Oxygen atoms are not shown. The 10-membered ring apertures shown are the entrances to the straight channels which run parallel to $[010]$.

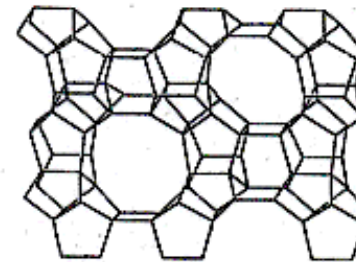


Fig. 3 Skeletal diagram of the (100)-face of the ZSM-5 unit cell. The y -axis is horizontal and the z -axis is vertical. Oxygen atoms are not shown. The nearly circular 10-membered ring apertures shown are the entrances to the sinusoidal channels which run parallel to $[100]$.

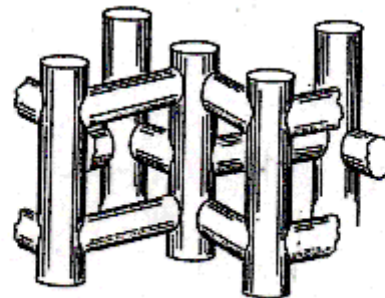


Fig. 4 The channel structure in ZSM-5.

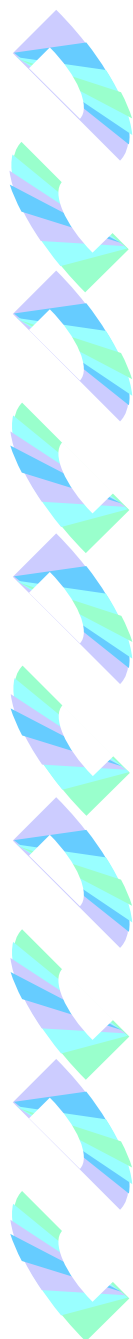
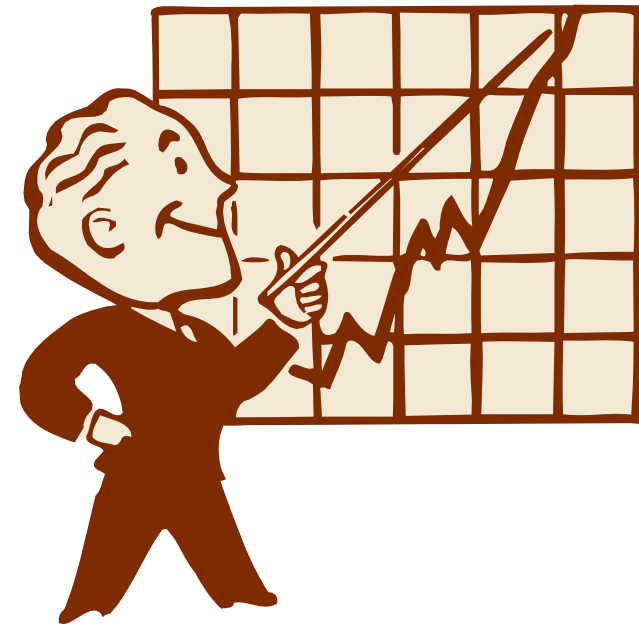


Table 3
Ideal and actual free dimensions of some *n*-rings

<u><i>n</i></u>	Free dimension (Å)	
	<u>Ideal planar^a</u>	Estimated from structures (max. and min.)
6	2·7 (2·8)	Sodalite: 2·1 hydrate
8	4·4 (4·5)	Zeolite A, LTA: 4·1 Chabazite: 4·1 and 3·9 Erionite: 5·2 and 3·6 Gmelinite: 4·1 and 3·4 Levynite: 5·1 and 3·2 Offretite: 5·2 and 3·6
10	6·0 (6·3)	Zeolite ZK-5, KFI: 3·9 Heulandite: 7·8 and 3·2 Stilbite: 6·2 and 4·1 Dachiardite: 6·7 and 3·7 Epistilbite: 5·3 and 3·2 Ferrierite: 5·5 and 4·3
12	7·7 (8·0)	Zeolite ZSM-5, MFI: 5·6 and 5·4 Gmelinite ^b : 6·9 Cancrinite ^b hydrate: 6·2 Mordenite ^b : 7·0 and 6·7 Offretite: 6·4 Mazzite: 7·1 Zeolite L, LTL: 7·1 Faujasite: 7·4

^a Figures in brackets are estimated assuming 2·8 Å as the diameters of the

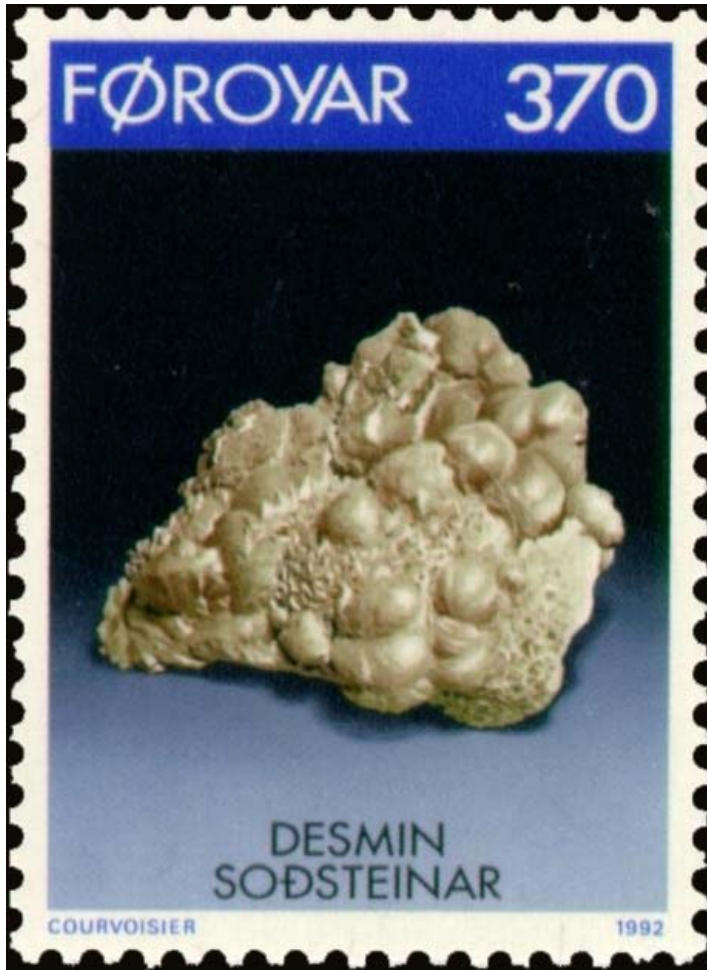
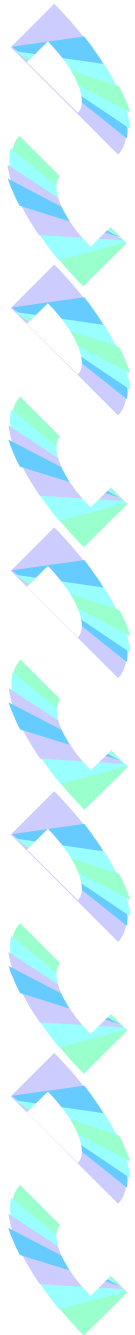
Historical development of Nano-porous Materials





Historical development

- **Natural zeolites**
 - discovery of “stilbite” by Swedish mineralogist A.F. Cronsted in 1756
 - since 1950s, >1000 zeolite minerals in >40 countries
- **“Zeolite” means “boiling stone”**
 - a frothy mass resulted from fusing zeolites in the blowpipe (zeolitic water forms bubbles within the melt)



a **stilbite** specimen from
Kiui Island, Alaska, USA

Desmine (**Stilbite**)

Stamp FR 229 of Postverk Forova, Faroe Islands

Date of issue: 9 June 1992

from wikipedia



Development of Zeolites

- 1950s

Linde company; Synthetic A-type zeolite for separation of normal and branched paraffins

- 1960s

X and Y-type zeolites for catalytic cracking

- 1968

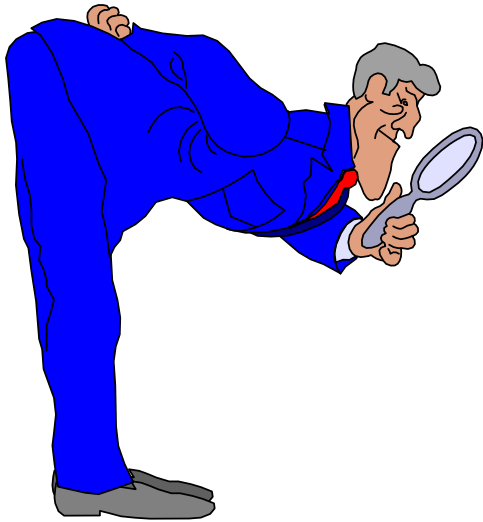
First use of “Shape Selectivity” properties of zeolites in selective hydrocracking on erionite

- In the past 40 years

Zeolites are used in refining and petrochemicals worldwide.

⇒ **Many synthetic zeolites are prepared.**

Structure



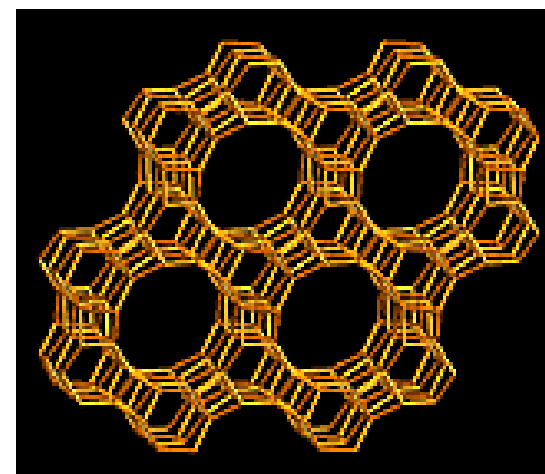
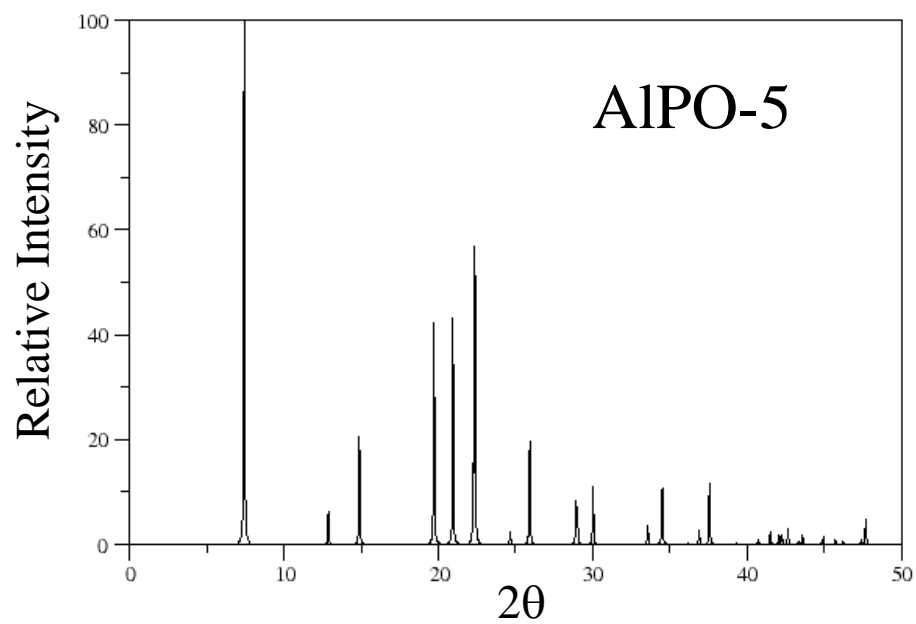
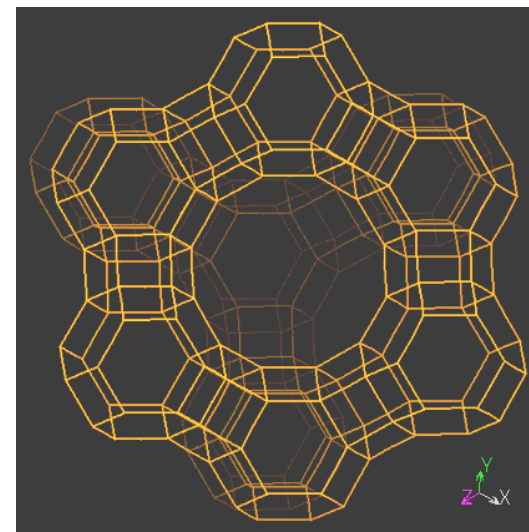
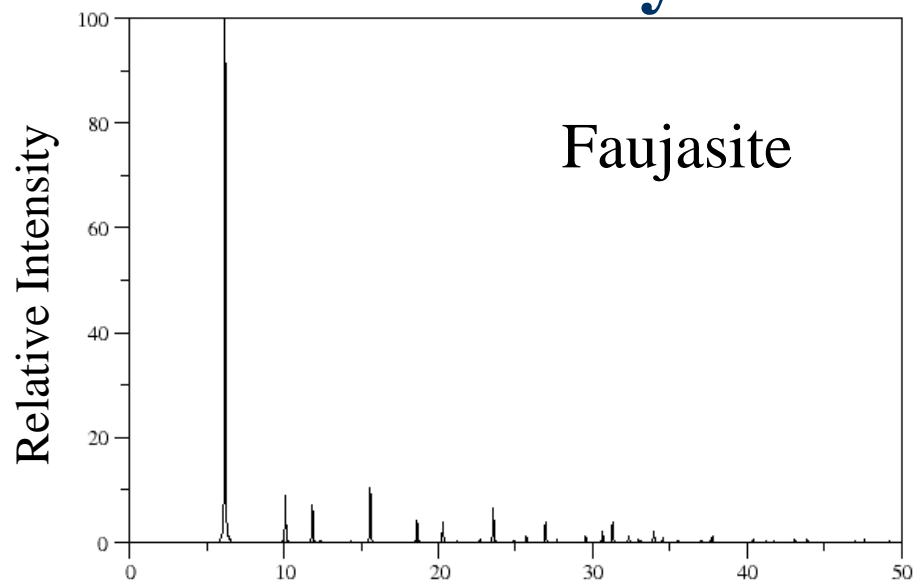
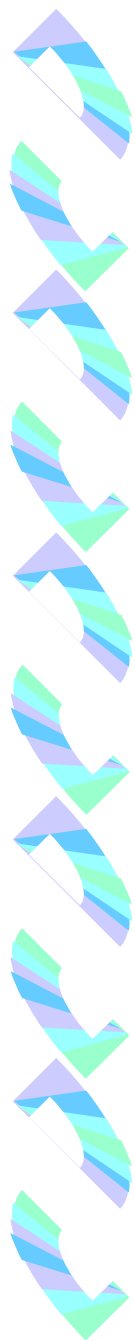
Structures & Structural characterization of Nano-porous materials



Techniques for characterization of nano-porous materials

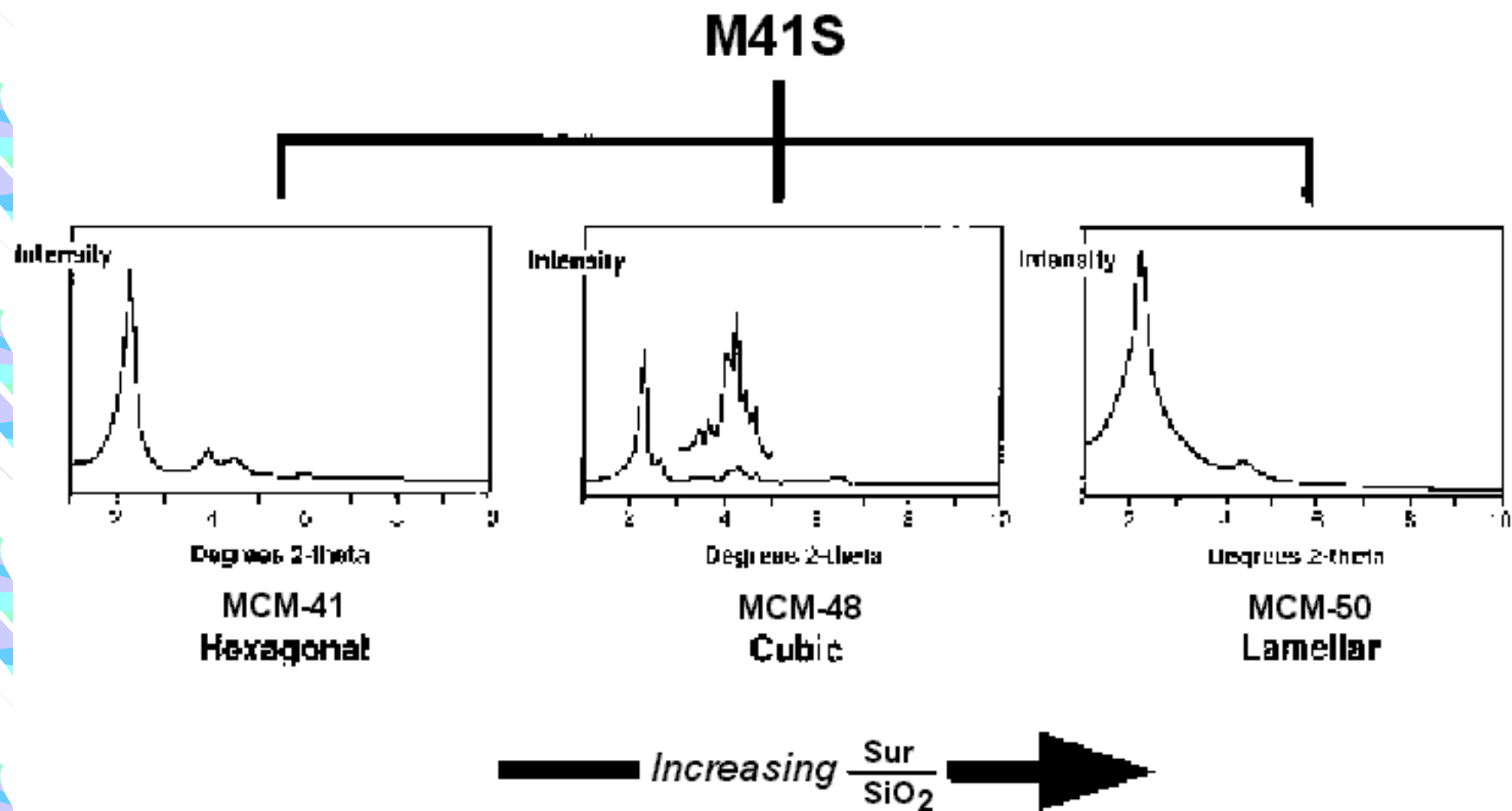
- ♦ **Crystalline structure**
 - Single crystal & Powder X-ray diffraction (XRD)
 - Electron crystallography
- ♦ **Oxidation state & Coordination**
 - X-ray absorption spectra
 - X-ray photoelectron spectra (XPS)
 - UV-Vis spectra
 - Solid state NMR (mainly coordination)
- ♦ **Elemental analysis- ICP-AES, XPS**
- ♦ **Surface area & Pore size- N₂ adsorption-desorption isotherm**
- ♦ **Morphology- SEM**
- ♦ **Pore structure- TEM**

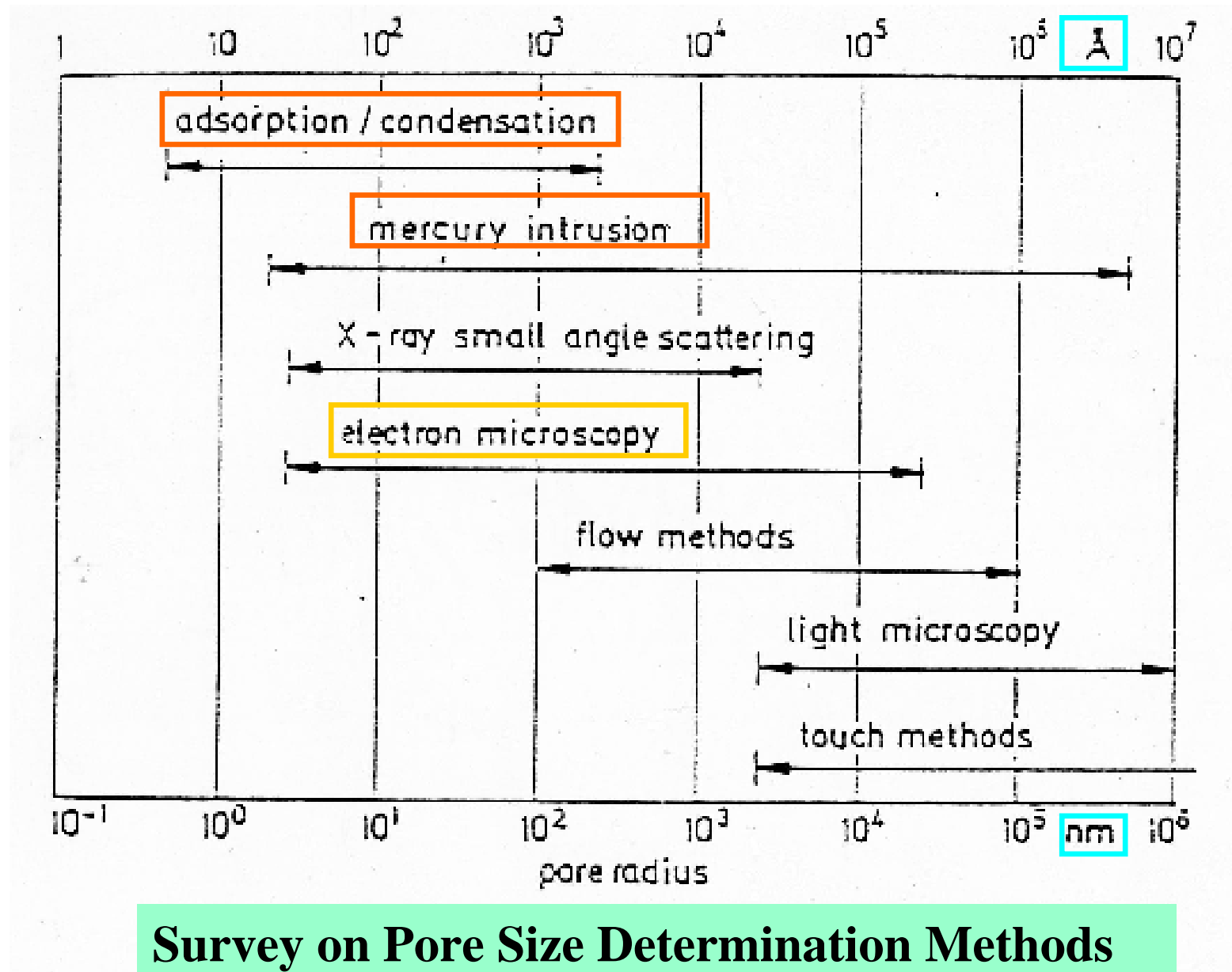
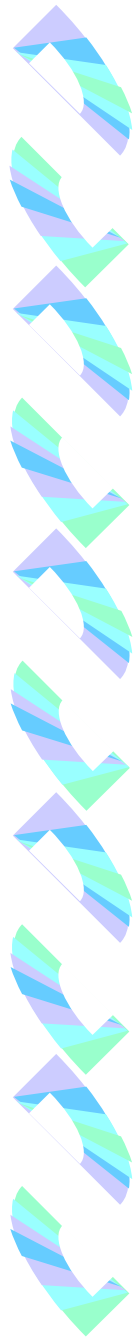
Powder X-ray diffraction (XRD)



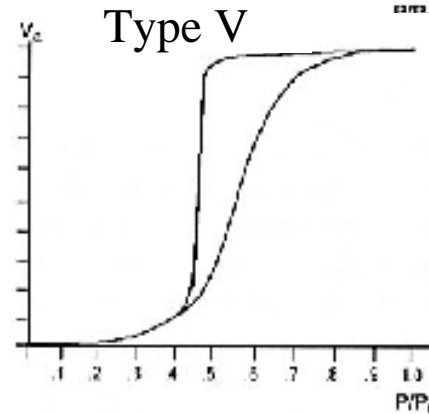
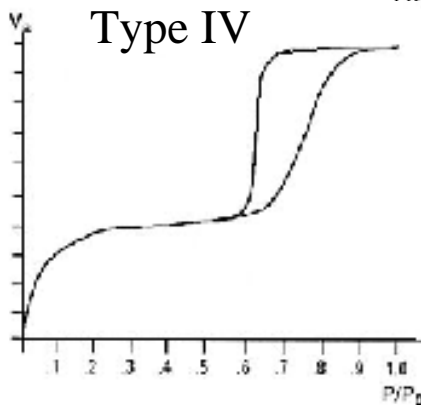
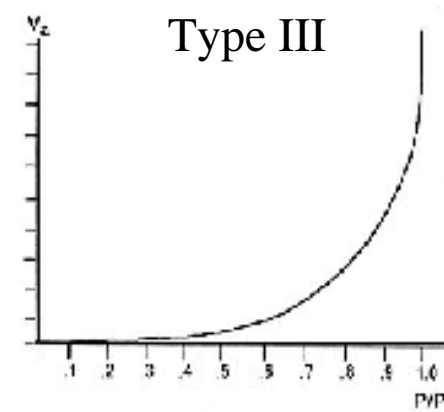
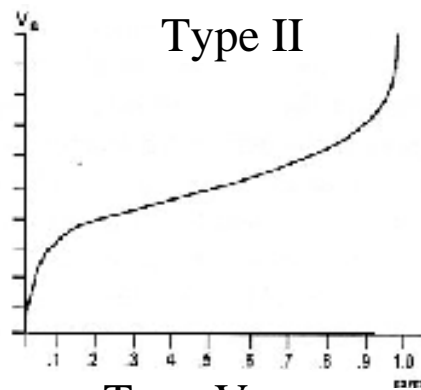
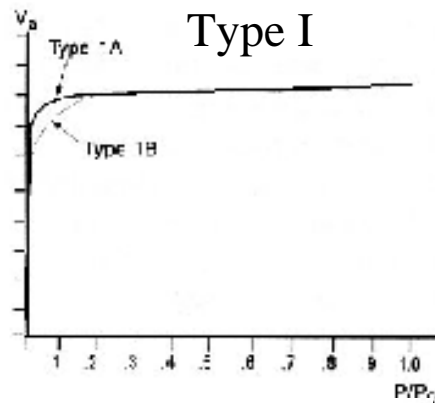
Discovery of M41S Family

C.T. Kresge et al., Nature, **1992**, 357, 710.





Physical Adsorption-Desorption Isotherms



BDDT classification (by Brunauer, Deming, Deming and Teller)

Type I . microporous – pore filling

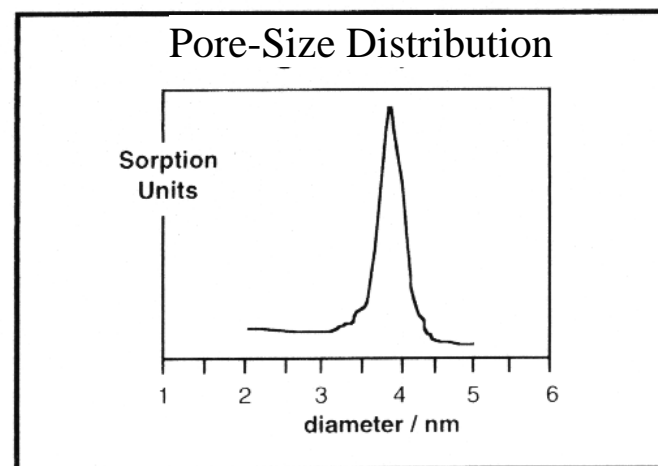
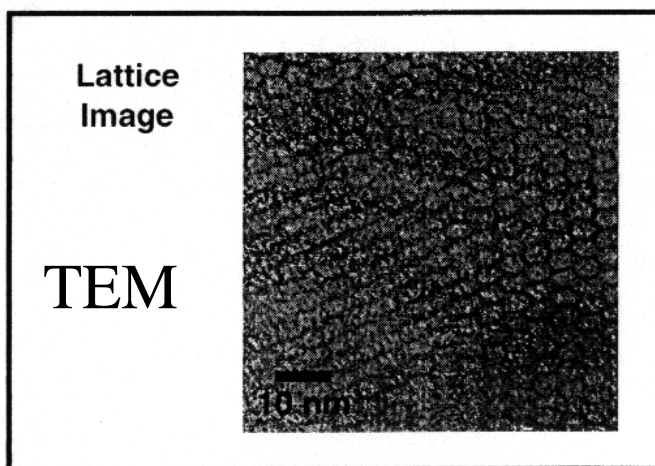
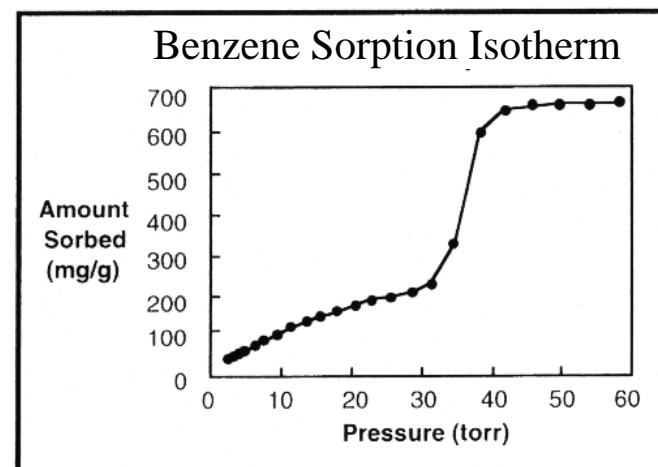
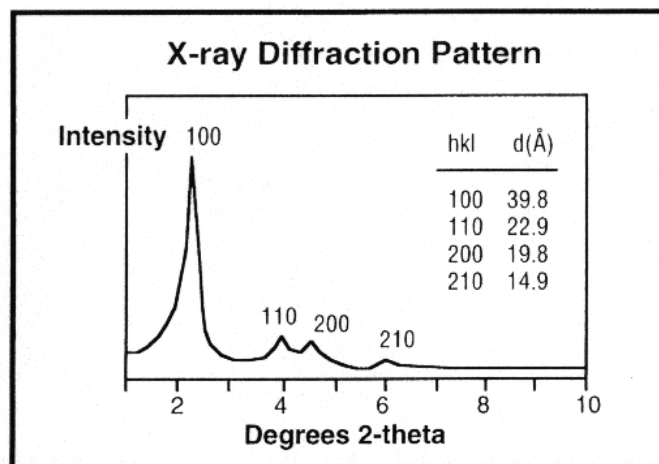
Type II . standard shape of non-porous

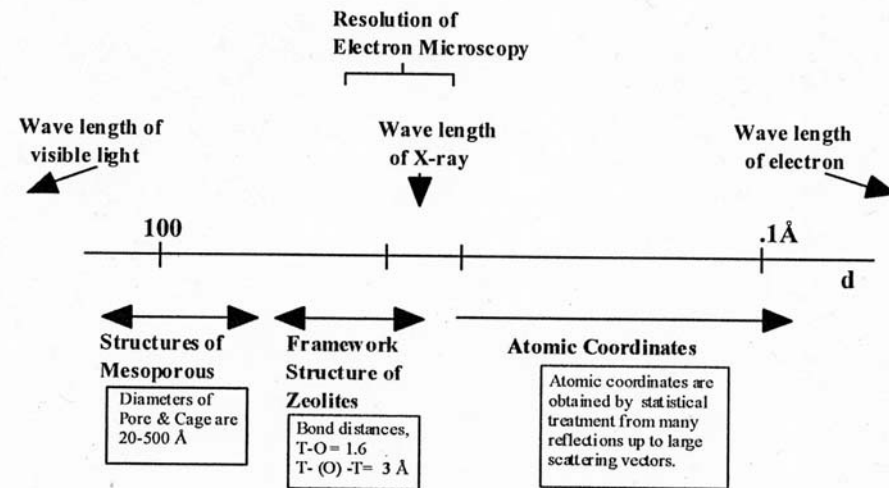
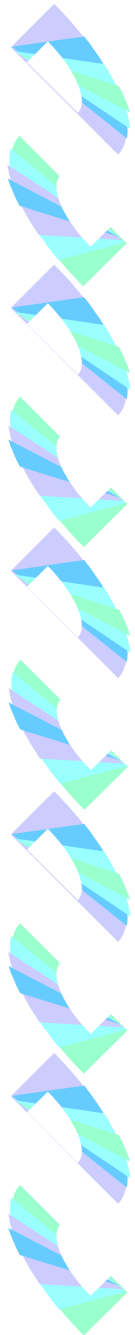
Type III . nonporous, unusually weak interaction between adsorbate and adsorbent

Type IV . mesoporous – capillary condensation

Type V . mesoporous, unusually weak interaction between adsorbate and adsorbent

Properties of Hexagonal MCM-41

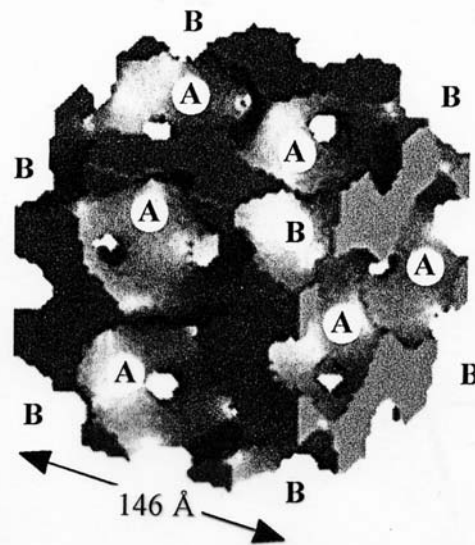




de Broglie relation

$$\lambda = h / mv$$

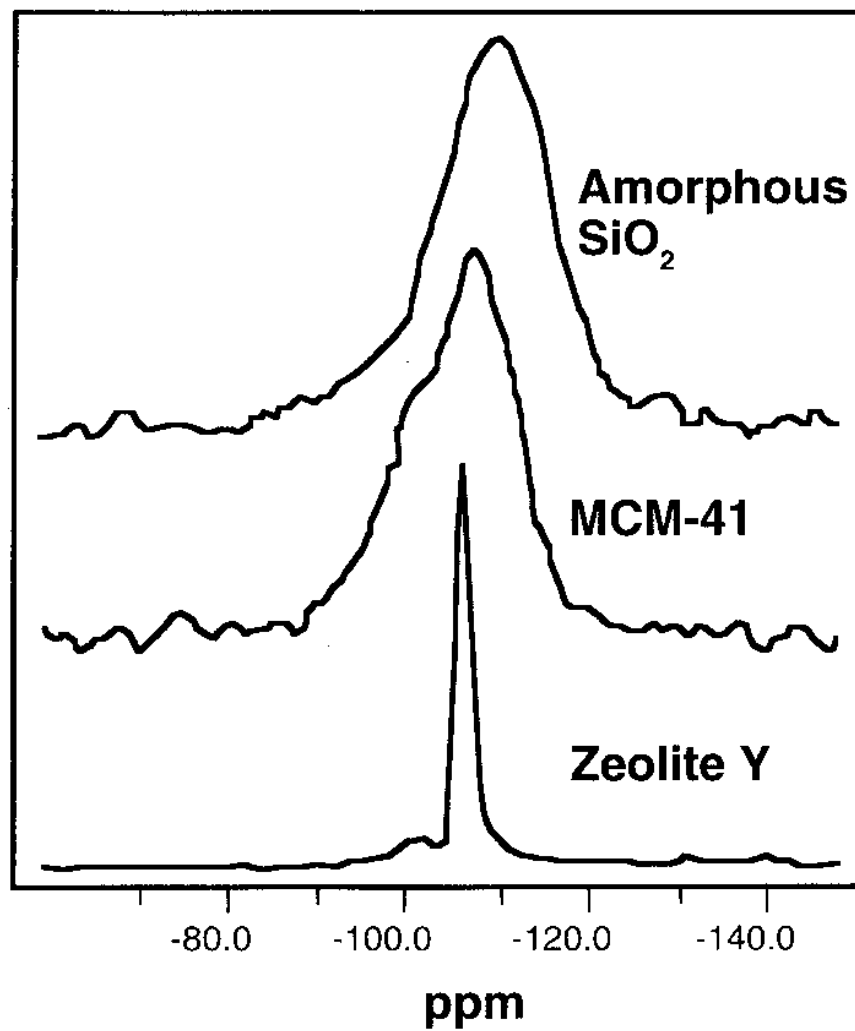
Fig. 1 Schematic Length Scale

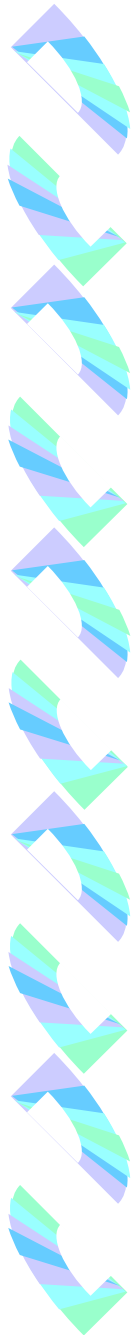


Electron diffraction
crystallography

Fig. 6 Structure solution of SBA-6. Pm-3n.

^{29}Si MAS NMR





Preparation of Nano-porous materials

Chemical bonds & Self-assembly



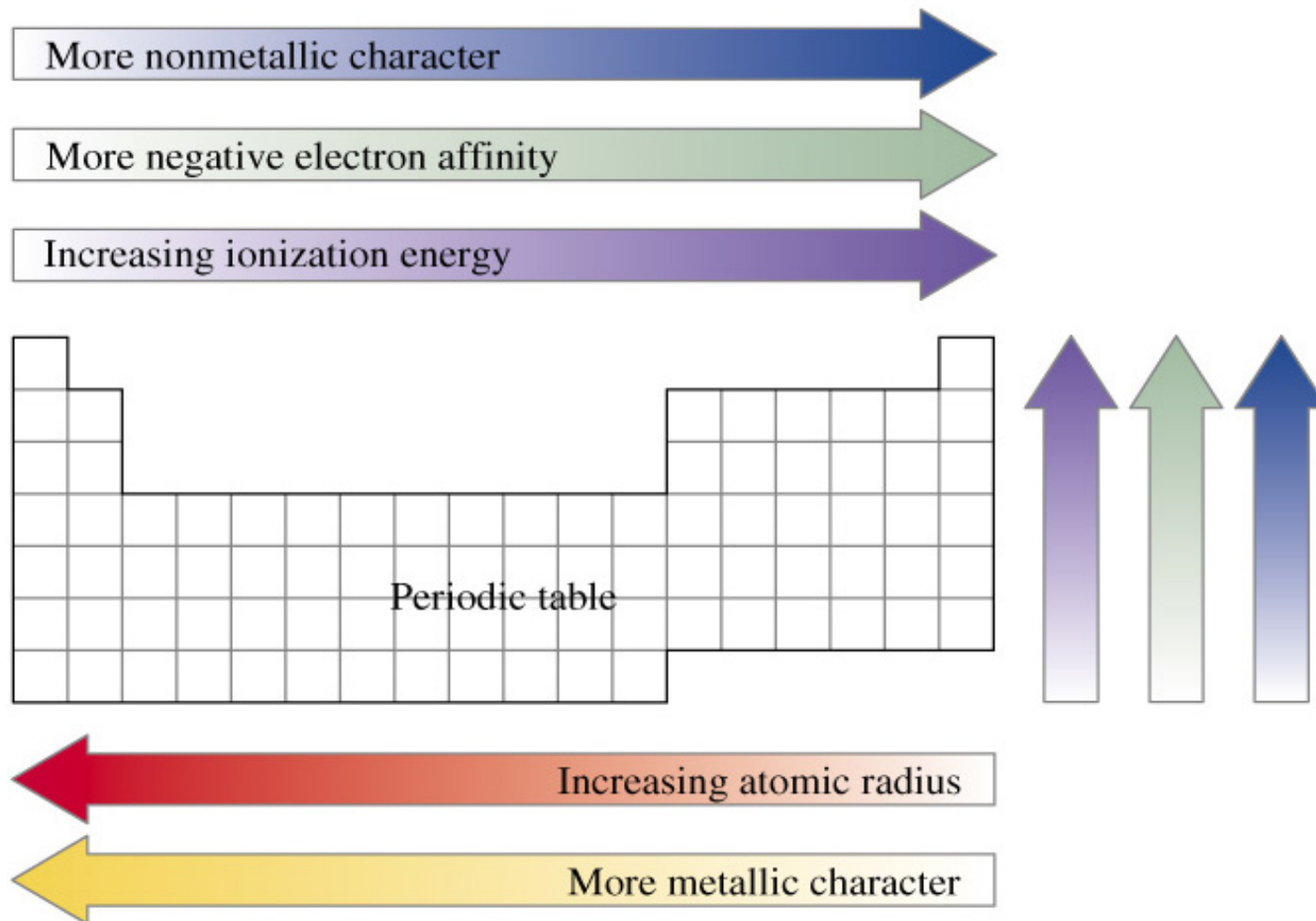
Periodic Table

	1A																	8A
1	H	2A																He
2	Li	Be											B	C	N	O	F	Ne
3	Na	Mg	3B	4B	5B	6B	7B	8B			1B	2B	Al	Si	P	S	Cl	Ar
4	K	Ca	Sc	Ti	V	Cr	Mn	Fe	Co	Ni	Cu	Zn	Ga	Ge	As	Se	Br	Kr
5	Rb	Sr	Y	Zr	Nb	Mo	Tc	Ru	Rh	Pd	Ag	Cd	In	Sn	Sb	Te	I	Xe
6	Cs	Ba	La*	Hf	Ta	W	Re	Os	Ir	Pt	Au	Hg	Tl	Pb	Bi	Po	At	Rn
7	Fr	Ra	Ac†	Rf	Db	Sg	Bh	Hs	Mt	**	**	**						

*Lanthanide series	Ce	Pr	Nd	Pm	Sm	Eu	Gd	Tb	Dy	Ho	Er	Tm	Yb	Lu
†Actinide series	Th	Pa	U	Np	Pu	Am	Cm	Bk	Cf	Es	Fm	Md	No	Lr

** Not yet named

A Summary of Trends





Electronegativity

- ♦ **Electronegativity (EN, expressed as χ)**, is a measure of the ability of an atom to attract bonding electrons to itself **when the atom is in a molecule**.

- ♦ **Mulliken's EN**

$$\text{Absolute EN, } \chi = (\text{IE} + \text{EA})/2$$

- ♦ **Pauling's EN**

$$\text{define } \chi_{\text{H}} = 2.2$$

$$\Delta \chi = \chi_{\text{A}} - \chi_{\text{B}} = [\Delta_{\text{AB}}(\text{kJ})/96.49]^{1/2} = [\Delta_{\text{AB}}(\text{kcal})/23.06]^{1/2}$$

$$\Delta_{\text{AB}} = D(\text{A-B}) - [D(\text{A-A}) \times D(\text{B-B})]^{1/2}$$

↖
Bond dissociation energy of A-B

Pauling's Electronegativities

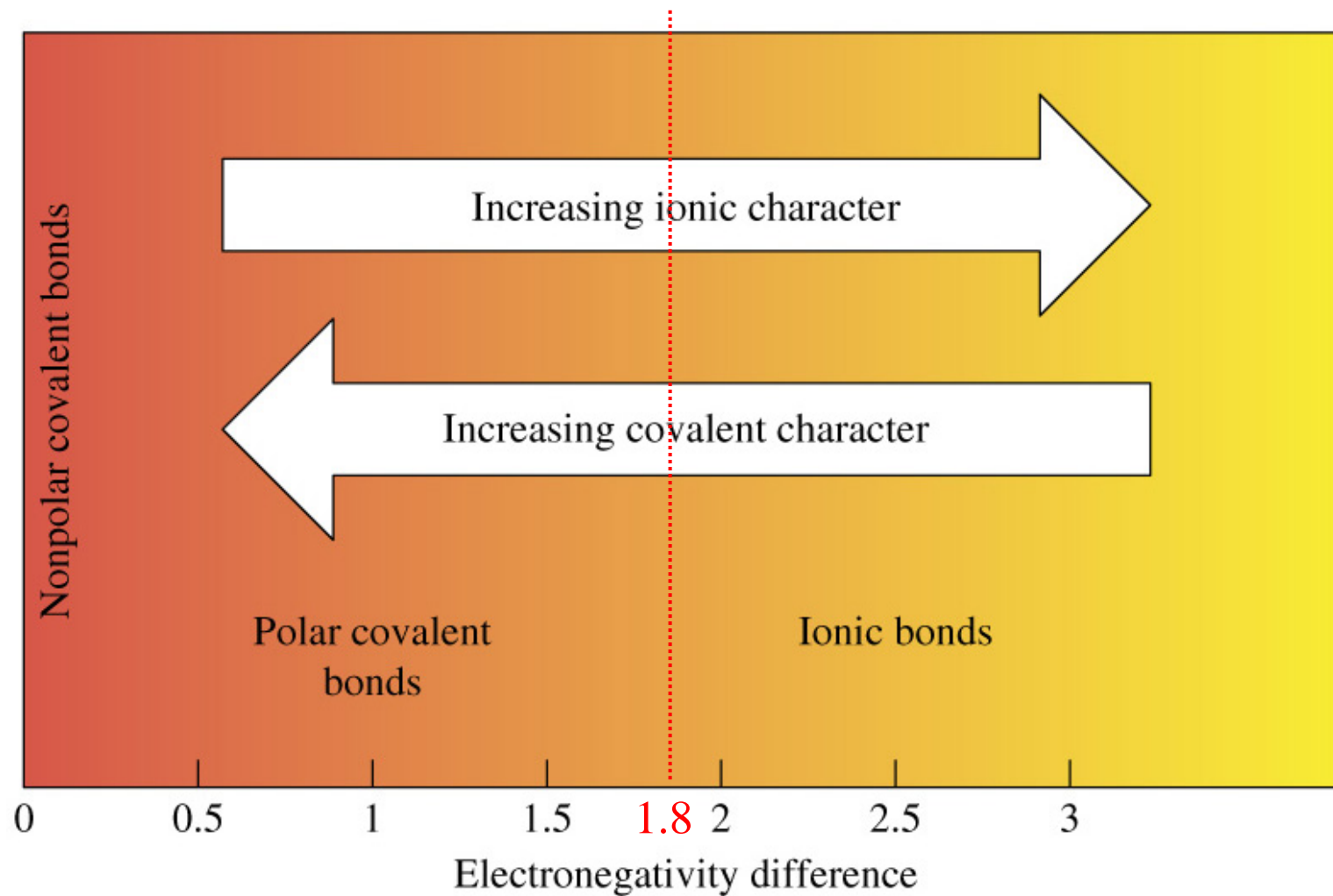
		<div><div><div></div><div>Below 1.0</div></div><div><div></div><div>1.0–1.4</div></div><div><div></div><div>1.5–1.9</div></div><div><div></div><div>2.0–2.4</div></div><div><div></div><div>2.5–2.9</div></div><div><div></div><div>3.0–4.0</div></div></div>																
												3A	4A	5A	6A	7A		
1	1A	H 2.2																
2	2A	Li 1.0	Be 1.5											B 2.0	C 2.5	N 3.0	O 3.5	F 4.0
3		Na 0.9	Mg 1.2	3B	4B	5B	6B	7B	8B		1B	2B	Al 1.5	Si 1.8	P 2.1	S 2.5	Cl 3.0	
4		K 0.8	Ca 1.0	Sc 1.3	Ti 1.5	V 1.6	Cr 1.6	Mn 1.5	Fe 1.8	Co 1.8	Ni 1.8	Cu 1.9	Zn 1.7	Ga 1.6	Ge 1.8	As 2.0	Se 2.4	Br 2.8
5		Rb 0.8	Sr 1.0	Y 1.2	Zr 1.4	Nb 1.6	Mo 1.8	Tc 1.9	Ru 2.2	Rh 2.2	Pd 2.2	Ag 1.9	Cd 1.7	In 1.7	Sn 1.8	Sb 1.9	Te 2.1	I 2.5
6		Cs 0.7	Ba 0.9	La* 1.1	Hf 1.3	Ta 1.5	W 1.7	Re 1.9	Os 2.2	Ir 2.2	Pt 2.2	Au 2.4	Hg 1.9	Tl 1.8	Pb 1.8	Bi 1.9	Po 2.0	At 2.2
7		Fr 0.7	Ra 0.9	Ac† 1.1	*Lanthanides: 1.1–1.3 †Actinides: 1.3–1.5													



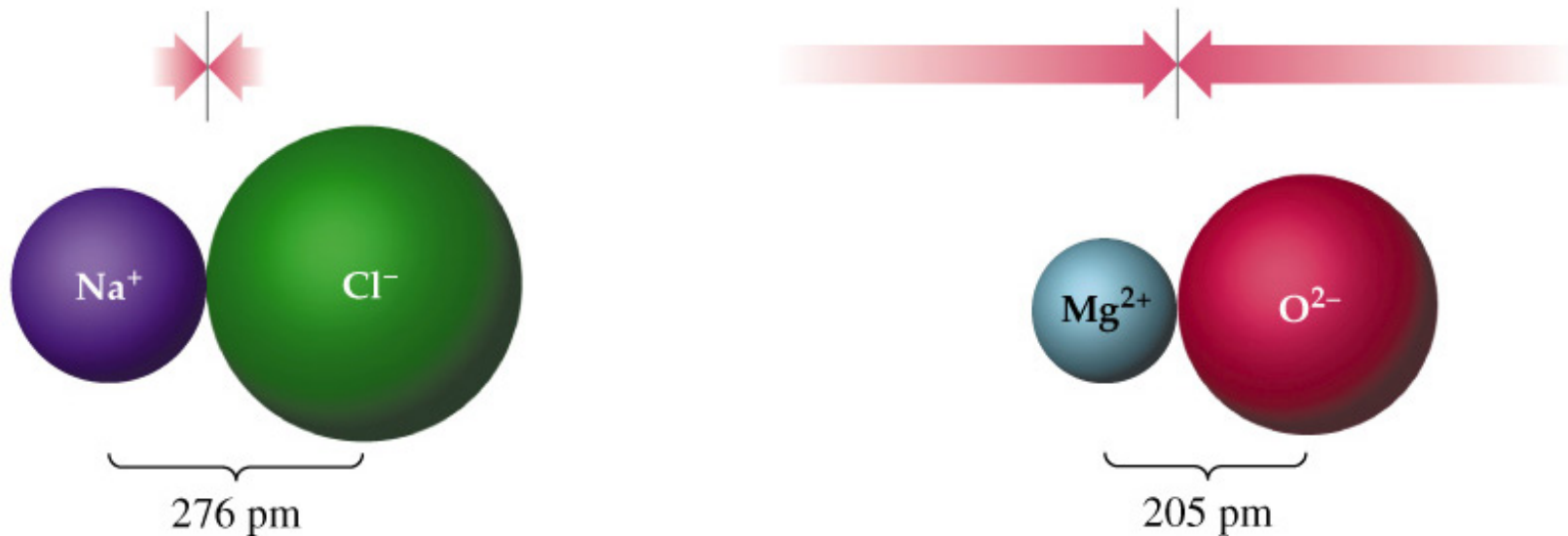
Electronegativity Difference and Bond Type

- ◆ Two identical atoms have the same electronegativity and share a bonding electron pair equally. This is called a **non-polar covalent bond**. (For $\chi_A \sim \chi_B$, or $|\chi_A - \chi_B| < 0.3$)
- ◆ In covalent bonds between atoms with somewhat larger electronegativity differences ($0.3 < |\chi_A - \chi_B| < 1.8$), electron pairs are shared unequally. The electrons are drawn closer to the atom of higher electronegativity, and the bond is called a **polar covalent bond**.
- ◆ With still larger differences in electronegativity ($|\chi_A - \chi_B| > 1.8$), electrons may be completely transferred from metal to nonmetal atoms to form **ionic bonds**.

Electronegativity and Bond Type



Interionic Forces of Attraction



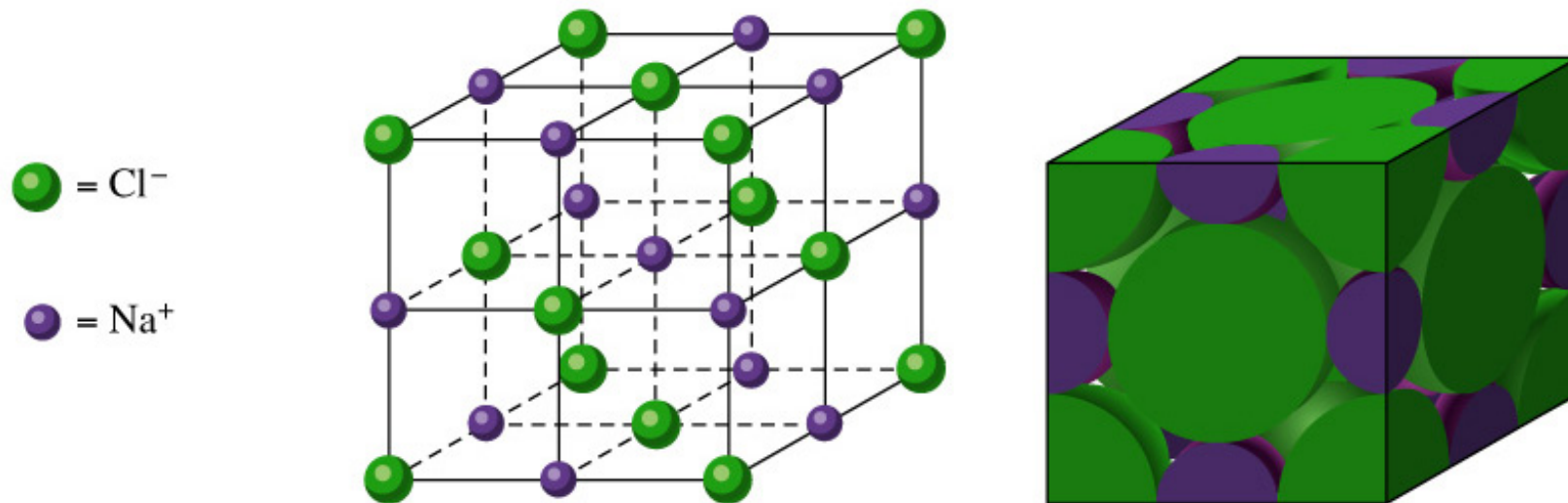
$$E = (Z^+Z^-)/4\pi\epsilon r$$

$\epsilon = 1$ in vacuum

$\epsilon = 80$ in water

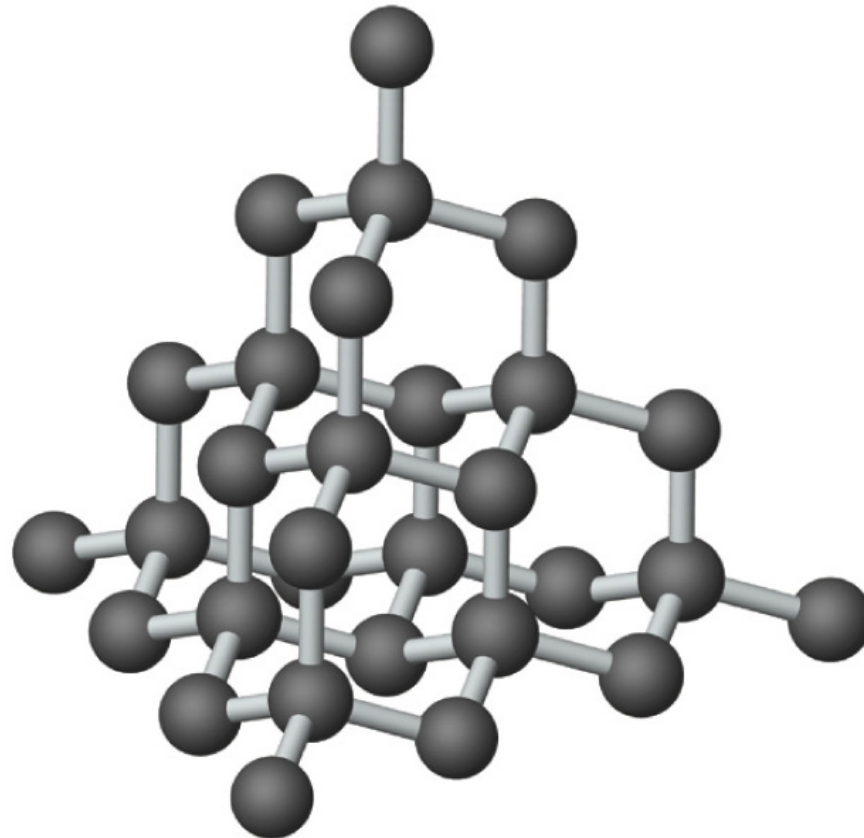
Dielectric constant

Unit Cell of Sodium Chloride

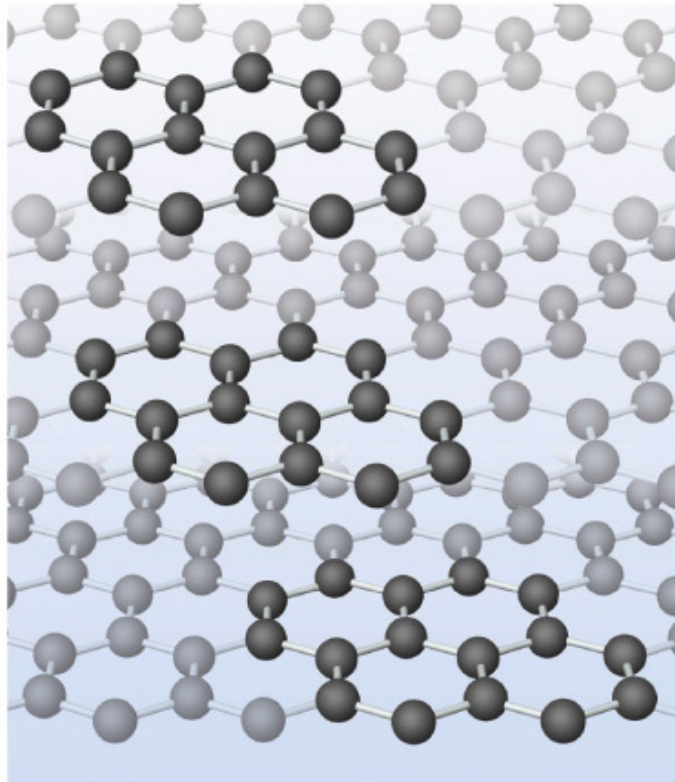


Covalent Bond

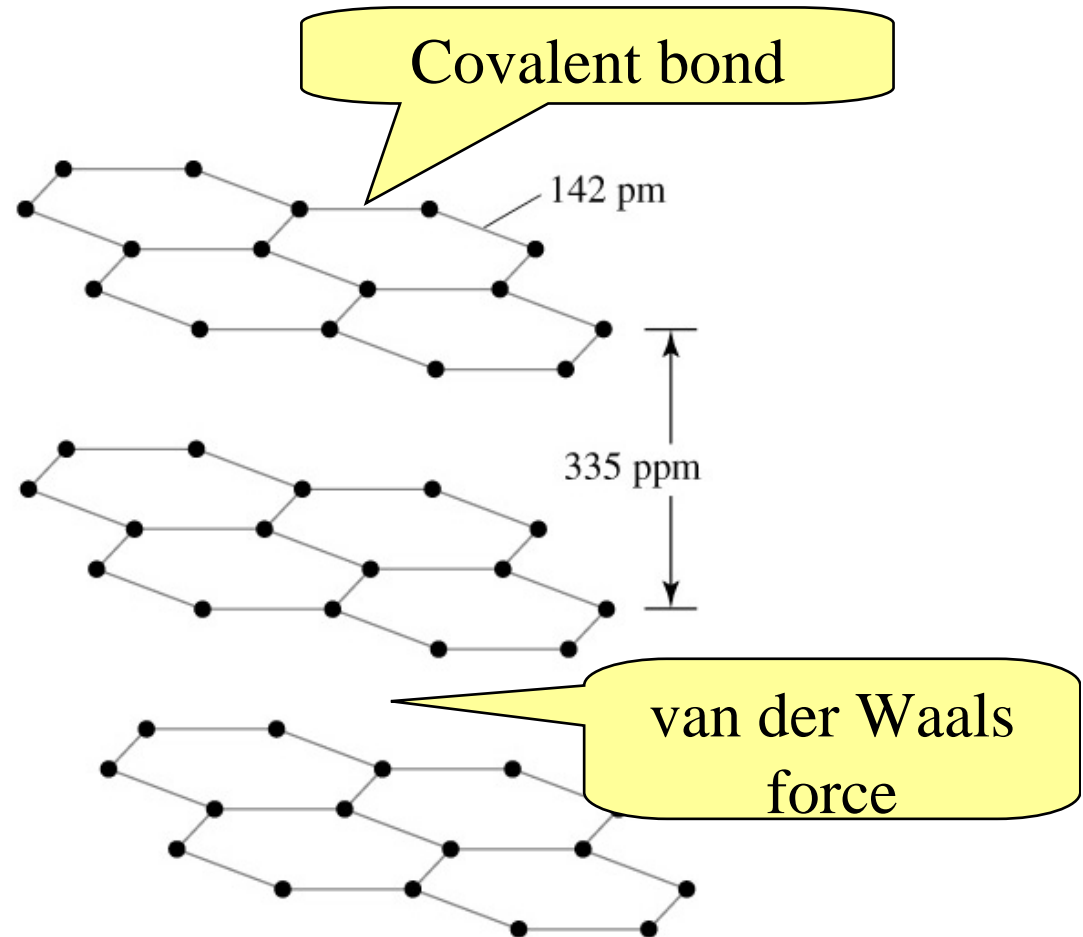
Crystal Structure of Diamond



Crystal Structure of Graphite

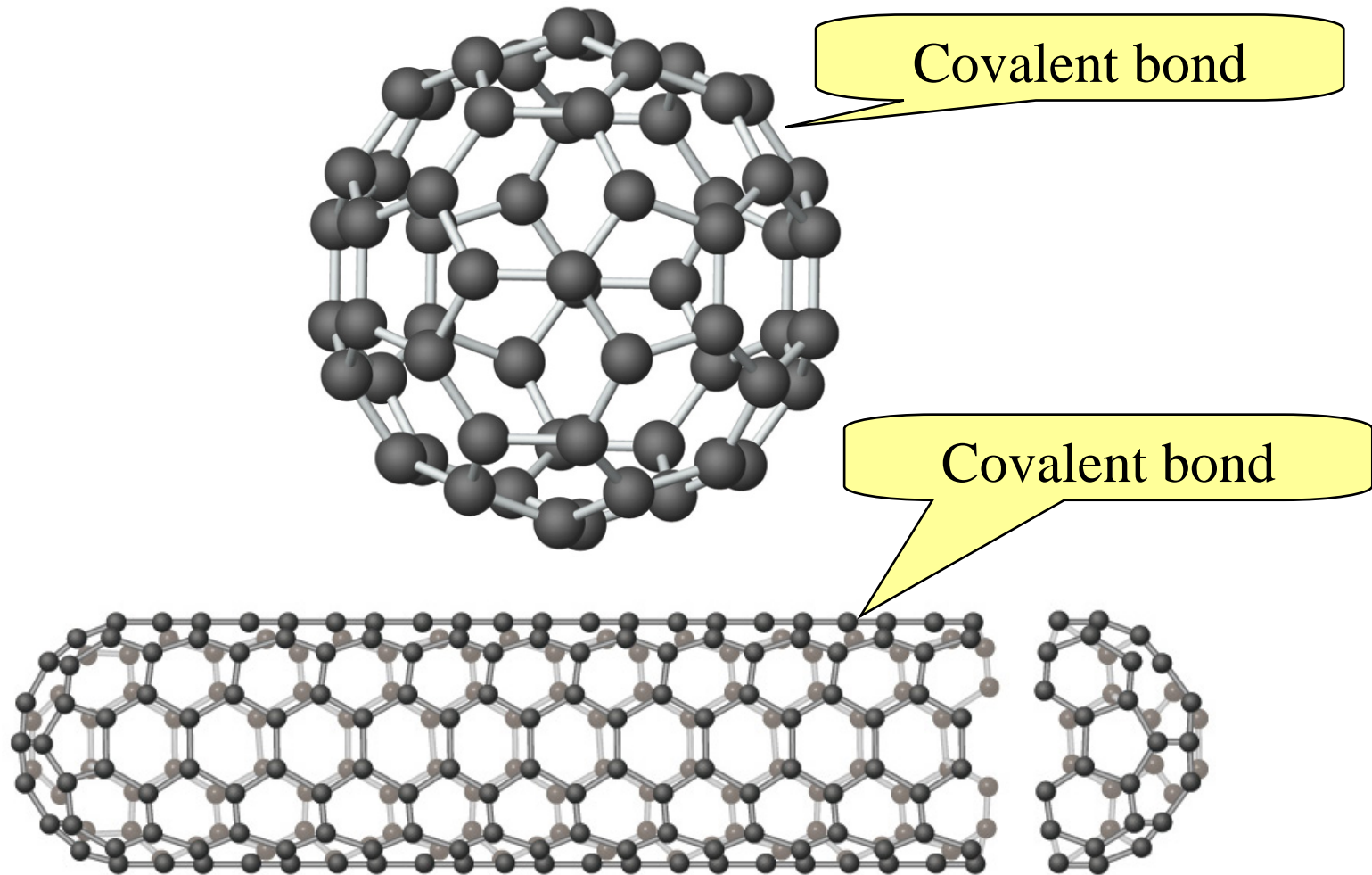


(a)

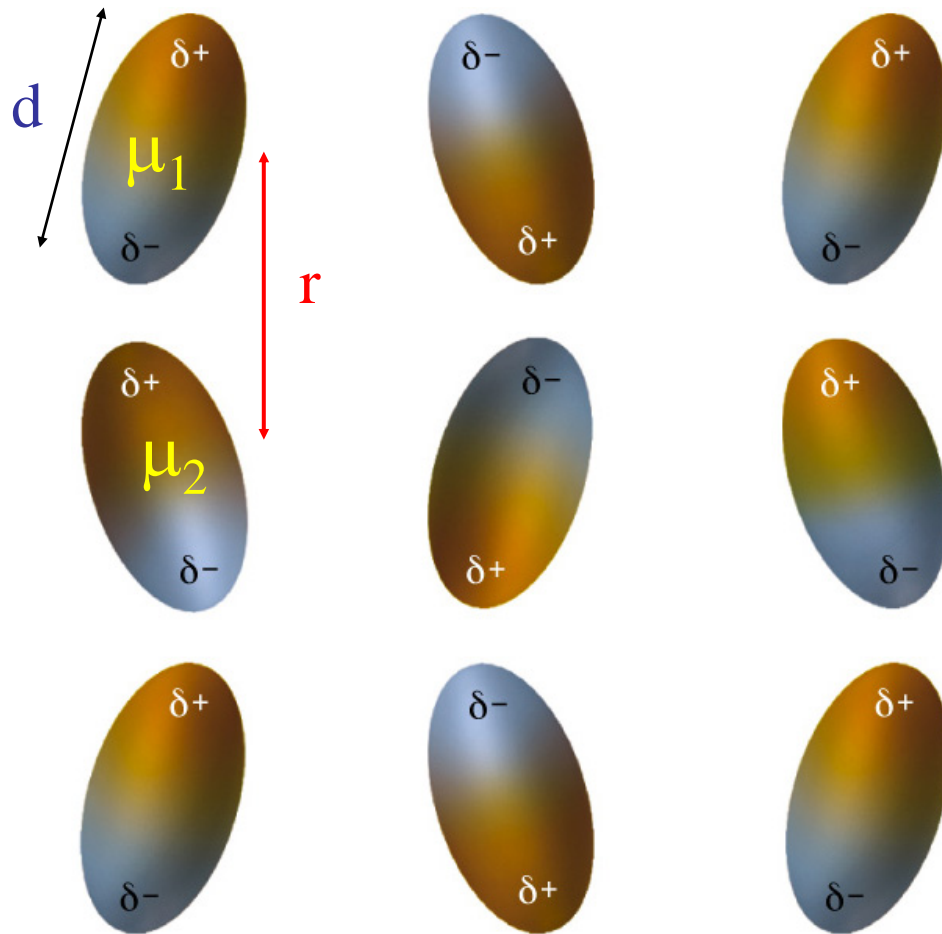


(b)

Structure of a Buckyball & a Nanotube



Dipole-Dipole Interactions



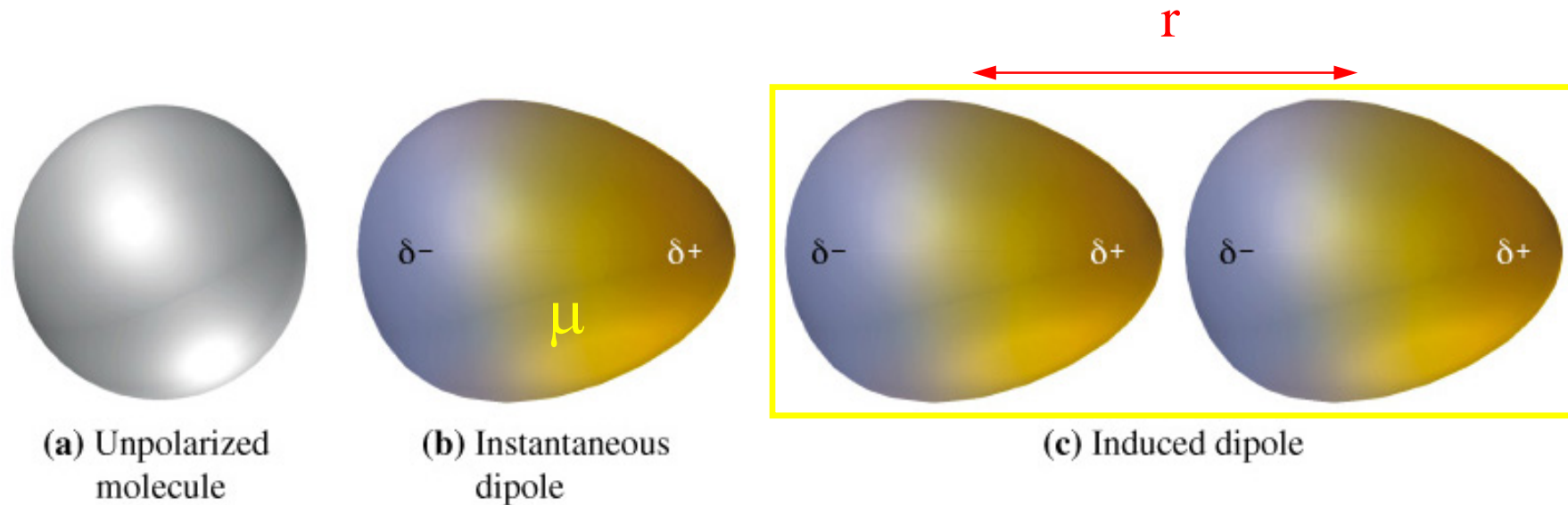
Dipole moment
 $\mu = \delta \cdot d$

$$E = - 2(\mu_1 \cdot \mu_2)/4\pi\epsilon r^3$$

Dispersion Forces

- ◆ A **dispersion force** is the force of attraction between an instantaneous dipole and an induced dipole.
- ◆ Also called a *London force* after Fritz London who offered a theoretical explanation of these forces in 1928.
- ◆ The **polarizability** of an atom or molecule is a measure of the ease with which electron charge density is distorted by an external electrical field.
- ◆ The greater the polarizability of molecules, the stronger the intermolecular forces between them.

Dispersion Forces Illustrated



$$E = - 2(\bar{\mu}^2 \cdot \alpha) / r^6$$

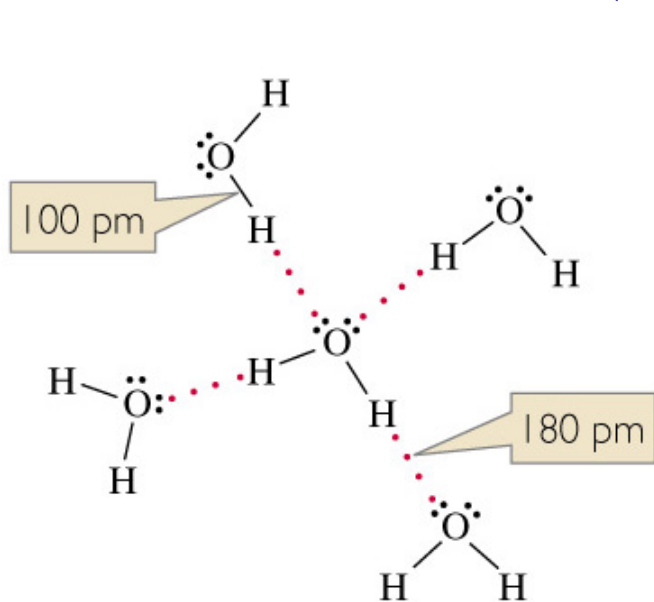
Mean instantaneous
dipole

polarizability

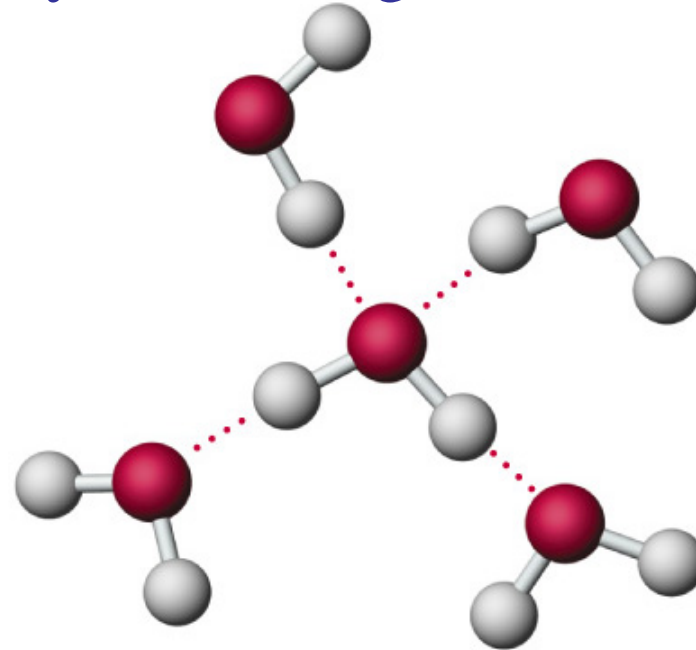
Hydrogen Bonds



X, Y = F, O, N, Cl, S (highly electronegative elements)



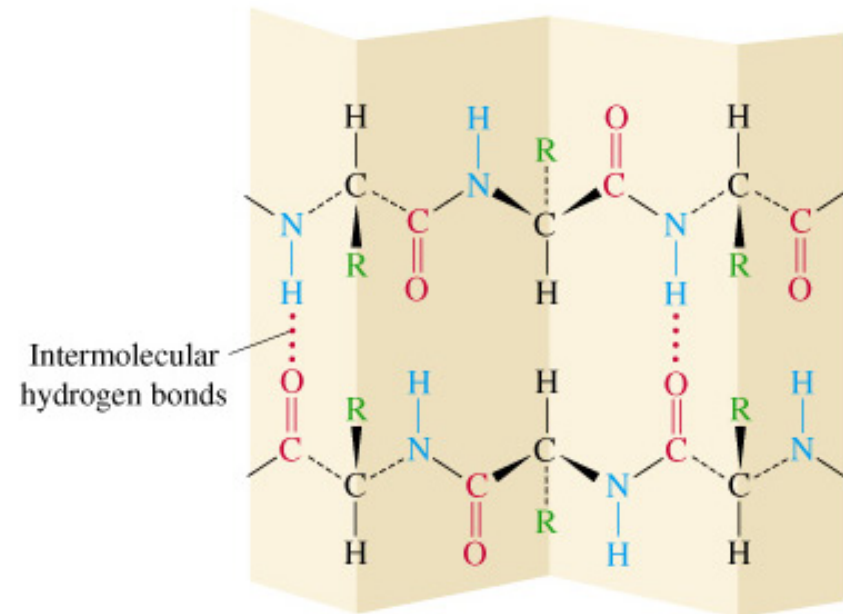
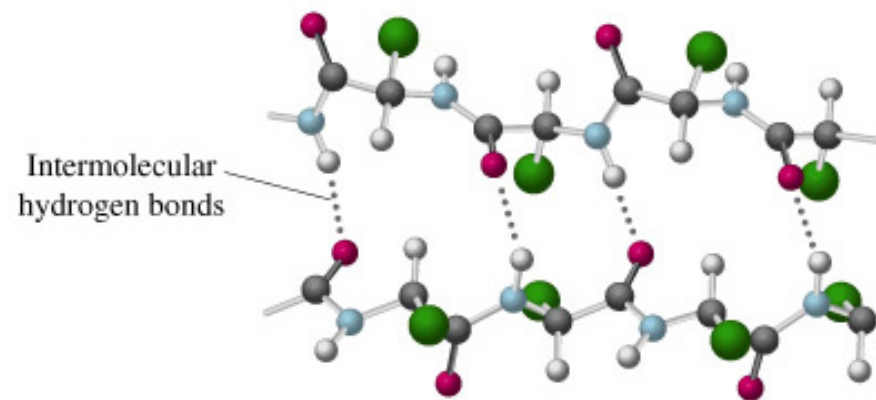
(a)



(b)

Hydrogen Bonds in Water

Intermolecular Hydrogen Bonds



(a)

*Intra*molecular Hydrogen Bonds

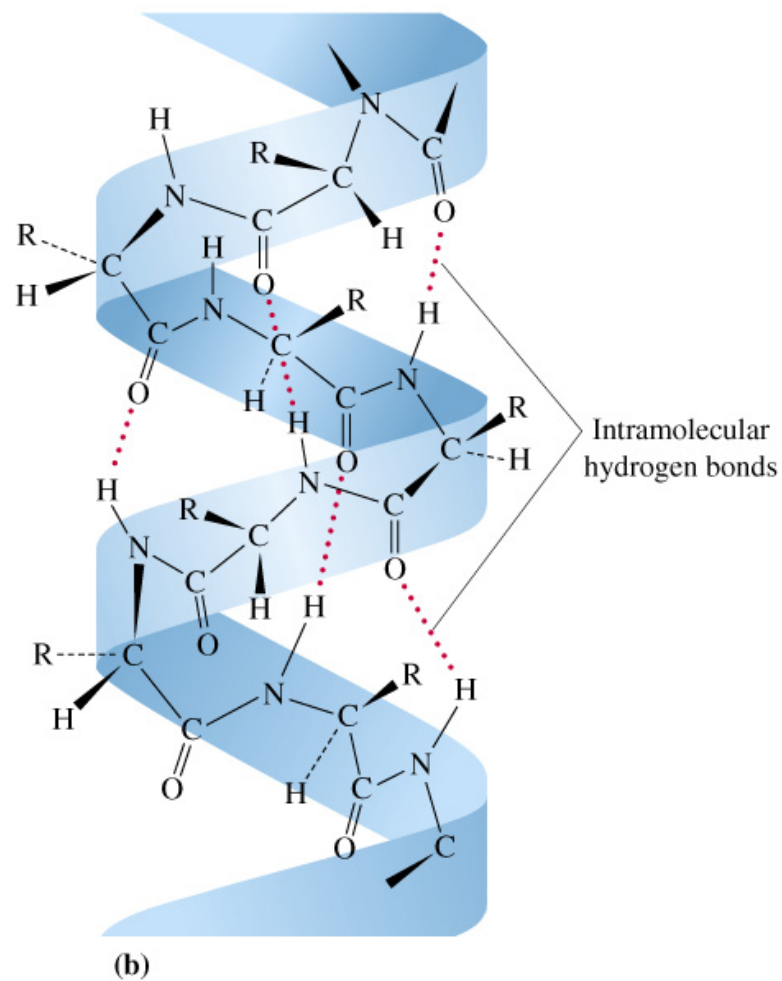
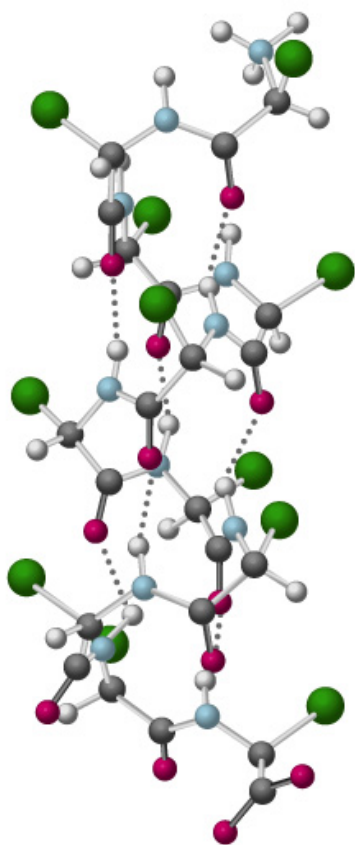
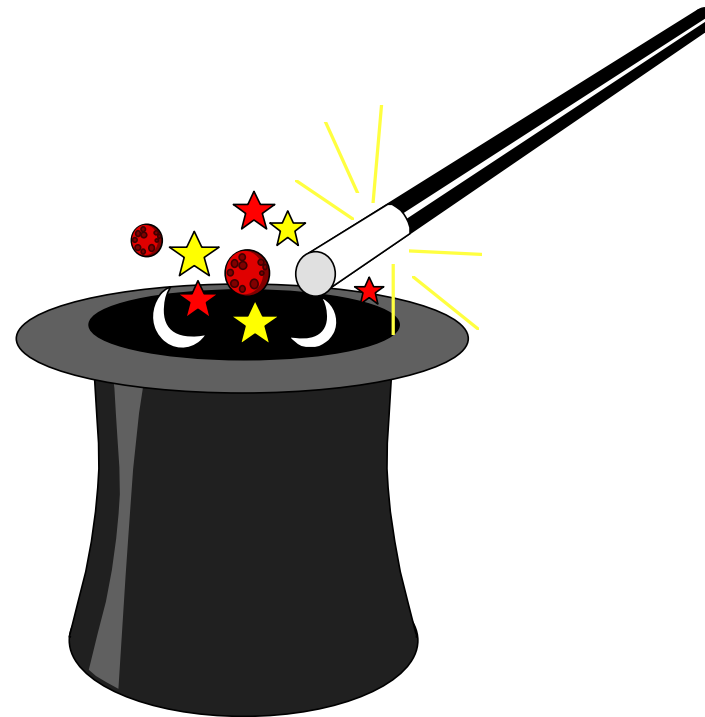
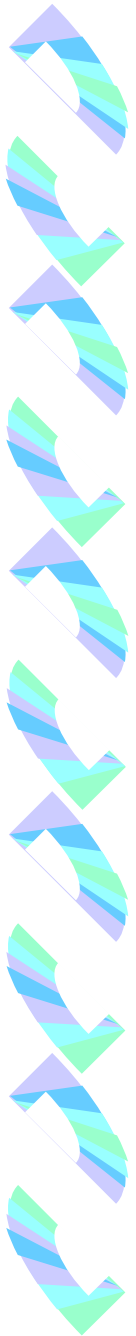


Table 2.11 Comparison of intermolecular and intramolecular interactions

<i>Type of interaction</i>	<i>Example</i>	<i>Energy of interaction between molecules or units</i>
Dispersion (Instantaneous dipole–induced dipole)	H ₂ (bp 20 K) CH ₄ (bp 112 K) CCl ₄ (bp 350 K) CF ₄ (bp 112 K) <i>n</i> -C ₂₈ H ₅₈ (mp 336 K)	~0.1–5 kJ/mol or ~10 (T _{bp} K) J/mol
Dipole–induced dipole	Xe(H ₂ O) _x solvation of noble gases or hydrocarbons (see text)	
Ion–induced dipole	Ions in a molecular matrix (see text)	
Dipole–dipole	NF ₃ —NF ₃ (bp 144 K) BrF—BrF (bp 293 K)	5–20 kJ/mol
Ion–Dipole	K(OH ₂) ₆ ⁺ Ions in aqueous solution and solid hydrates	67 kJ/mol (energy per bond)
Hydrogen bond	(H ₂ O) _x , (HF) _x , (NH ₃) _x alcohols, amines HF ₂ [−]	4–50 kJ/mol for neutral molecules
Cation–anion	NaCl, CaO	400–500 kJ/mol of MX “molecules”
Covalent bond	H ₂ F ₂ Cl ₂ Li ₂	432.08 kJ/mol 154.6 kJ/mol 239.32 kJ/mol 100.9 kJ/mol

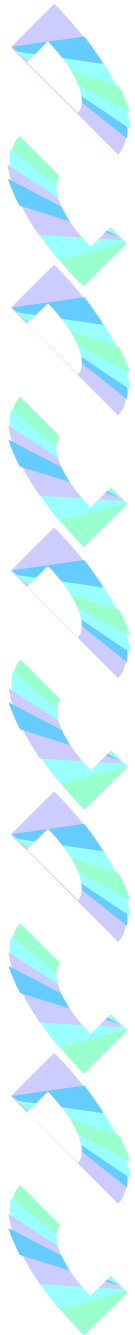
Experimental Procedures of Producing Nanoporous Materials





Methods of preparing solid materials

- **Precipitation** from aqueous or non-aqueous solution
- **Solid state reaction** (high temperature)
- **Sol-gel method** (commonly by hydrolysis in alcohols)
- **Hydrothermal** (or, Solvothermal) **reaction** in a sealed container



Geological exploration of Zeolite Formation

- Crystals resulting from **hydrothermal reactions** or **hot-spring activity** between solutions and basaltic lava flows.
- Deposits from **volcanic sediments** in closed alkaline and saline lake-system.
- Deposits from open freshwater-lake or groundwater systems acting on **volcanic sediments**.
- Deposits from **volcanic materials** in alkaline soils.
- Deposits from **hydrothermal** or low-temperature alteration of **marine sediments**.
- Results of low-grade burial metamorphism.

TABLE 9

Likely relations between pH, temperature and occurrence of some hydrothermally formed minerals⁽⁹⁶⁾

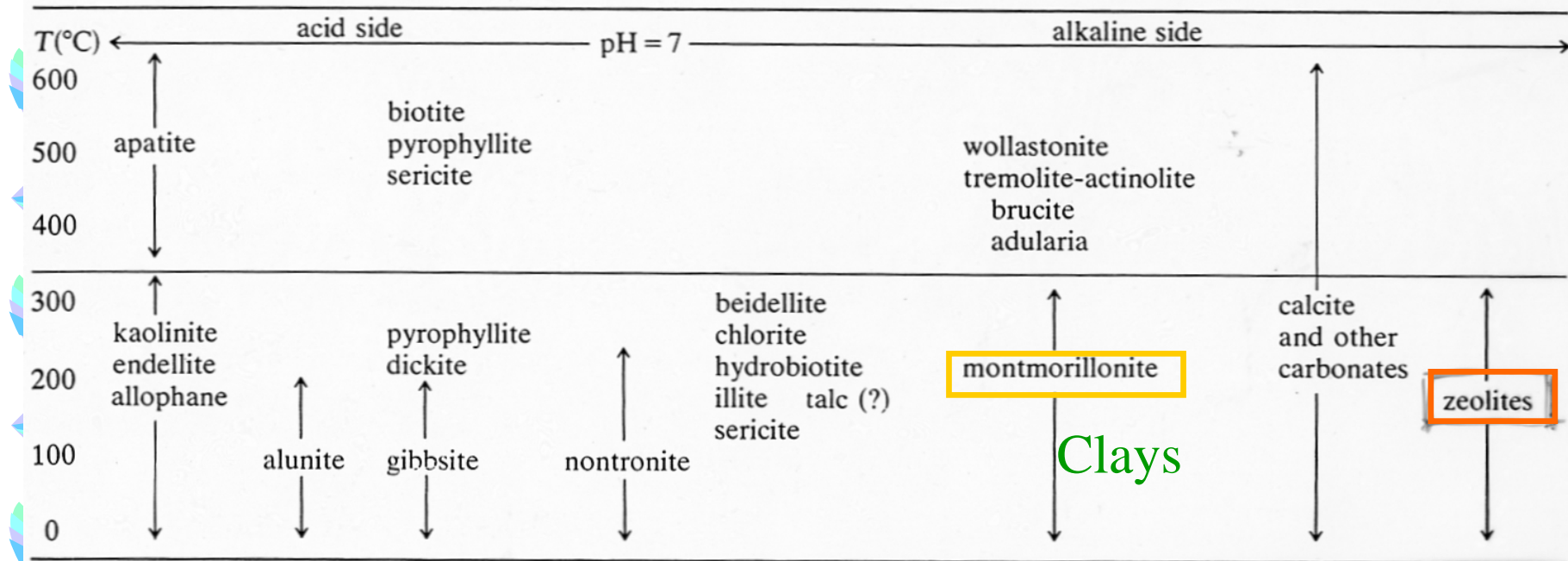
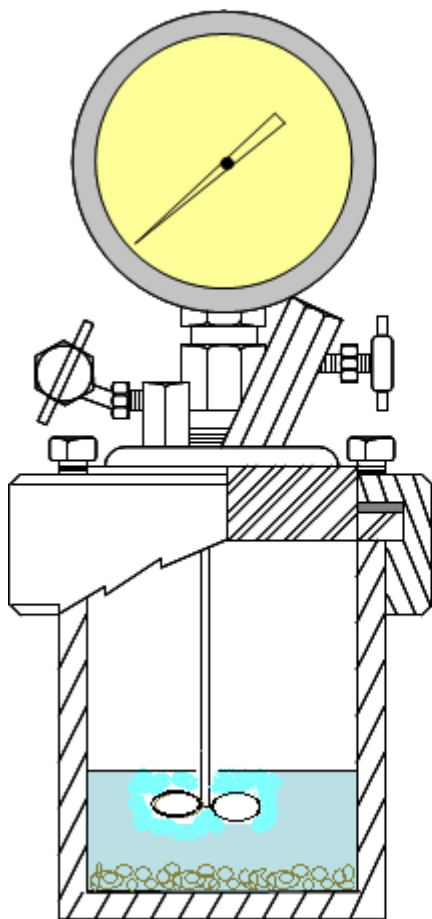


TABLE 6(b)
Solubilities in water⁽⁷⁶⁾ (g/100 g)

Substance	100°C	150°C	200°C	250°C	300°C	350°C	374°C	Refs.
ZnS	—	—	5×10^{-5}	—	1×10^{-4}	—	—	(77, 78)
AgI	—	—	—	—	1.9×10^{-3}	5.4×10^{-3}	—	(79)
AgBr	3.7×10^{-4}	1.9×10^{-3}	6.0×10^{-3}	1.1×10^{-2}	1.5×10^{-2}	2.5×10^{-2}	—	(79)
SiO ₂ (quartz)	—	3.0×10^{-3}	2.4×10^{-2}	4.9×10^{-2}	6.8×10^{-2}	7.0×10^{-2}	2.3×10^{-2}	(80)
AgCl	2.2×10^{-2}	6.4×10^{-3}	1.3×10^{-2}	2.5×10^{-2}	3.1×10^{-2}	5.0×10^{-2}	—	(79)
CaCO ₃ (1 atm of CO ₂)	2.2×10^{-2}	9.2×10^{-3}	3.9×10^{-3}	1.5×10^{-3}	6.8×10^{-4}	—	—	(81)
CuI	—	—	12×10^{-2}	4.4×10^{-2}	9.3×10^{-2}	1.9×10^{-1}	—	(77)
SiO ₂ (amorphous)	3.8×10^{-2}	6.2×10^{-2}	9×10^{-2}	1.26×10^{-1}	1.68×10^{-1}	2.3×10^{-1}	—	(80)
CuBr	—	—	2.2×10^{-1}	5.9×10^{-1}	1.18	1.8	—	(79)
CuCl	—	3.6×10^{-1}	9.5×10^{-1}	1.7	3.5	6.2	—	(79)
NaPO ₃	6.05×10^{-1}	7.05×10^{-1}	7.5×10^{-1}	7.9×10^{-1}	8.4×10^{-1}	9.2×10^{-1}	9.25×10^{-1}	(82)
La ₂ (SO ₄) ₃	9×10^{-1}	$< 1 \times 10^{-1}$	—	—	—	—	—	(83)
Y ₂ (SO ₄) ₃	5.1	2.4	1×10^{-1}	—	—	—	—	(83)
ZnSO ₄	—	—	26.5	10.0	< 0.1	—	—	(83)
B ₂ O ₃	15.6	34.0	77.0	83.5	87.4	91.5	—	(84)
Na ₂ SO ₄	29.4	29.7	30.7	30.6	19.9	2.3	$< 2 \times 10^{-1}$	(85, 86)
Na ₂ CO ₃	30.6	28.4	23.3	17.2	8.4	1.9	$< 2 \times 10^{-2}$	(85, 86)
KCl	36.0	40.2	44.5	48.4	53.5	58.2	—	(85, 86)
NaCl	—	—	31.3	34.0	37.4	42.0	44.3	(85, 86)
CdSO ₄	41	19	1.5	—	—	—	—	(83)
NaBr	54.8	57.2	60.0	63.0	66.1	69.8	—	(85, 88)
Cs ₂ SO ₄	68.2	71	73.5	74.7	75.5	—	—	(83)
NaI	—	78.3	81.7	84.7	87.4	89.7	90.7	(85, 86)

Autoclave Bomb Reactor

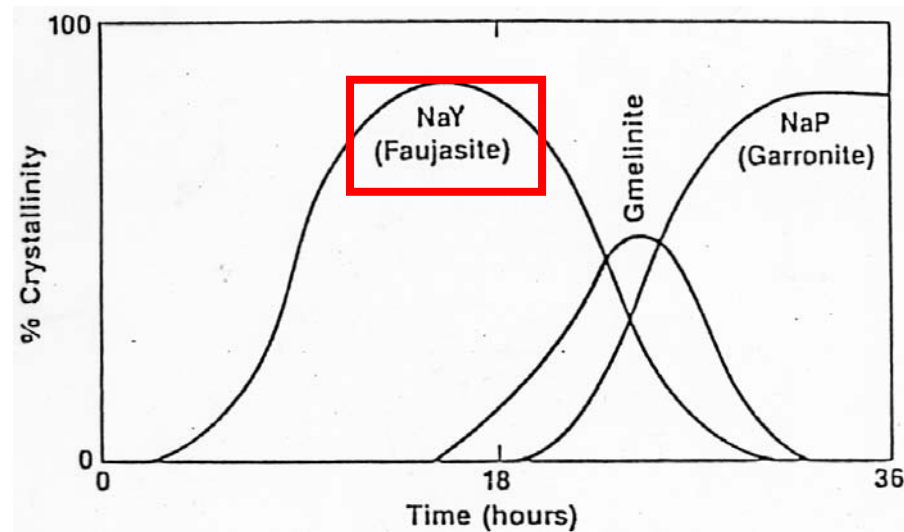
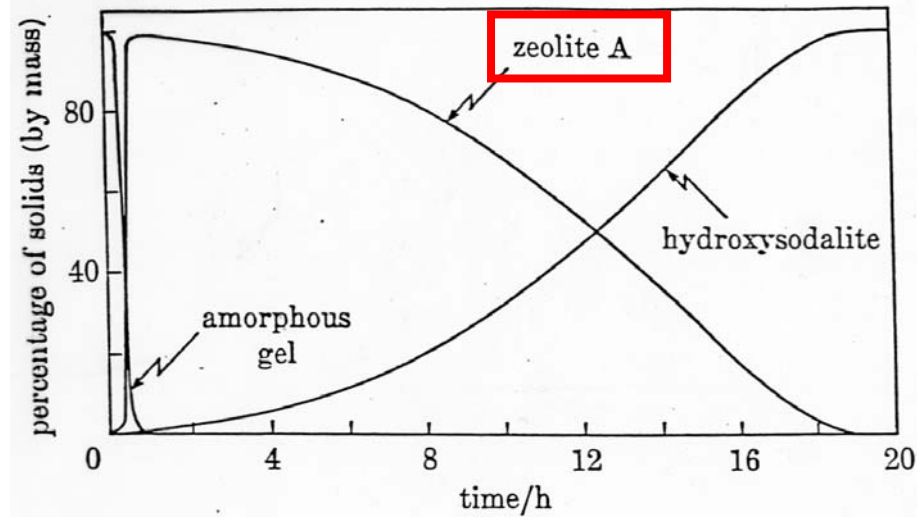


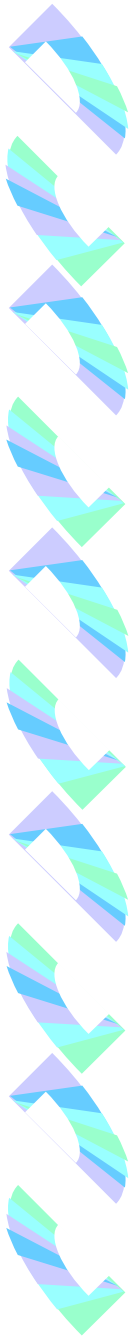
with stirrer and pressure gauge



static

Zeolites are Meta-stable Phases





Pore-directing Agents

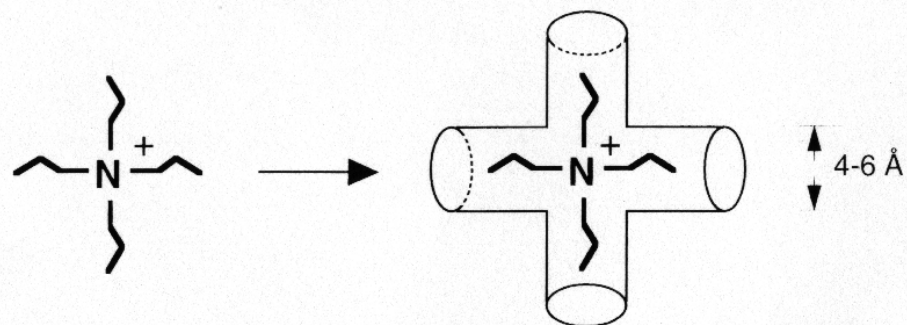
Ionic

- Solvated alkali and alkaline earth ions.
- Tetra-alkyl ammonium ions
- ionic surfactants
- ionic polymers
- metallocenes

Non-ionic

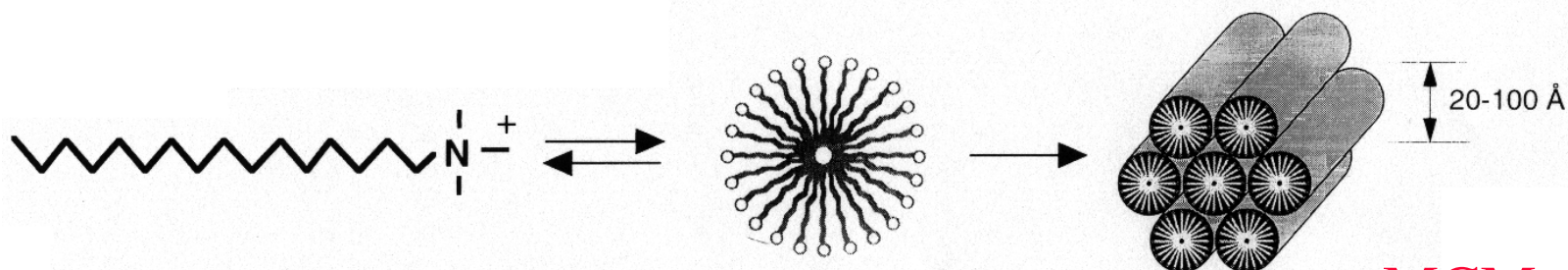
- alkylamines
- non-ionic surfactants
- tri-block co-polymers

The Role of Quaternary Directing Agents



zeolites

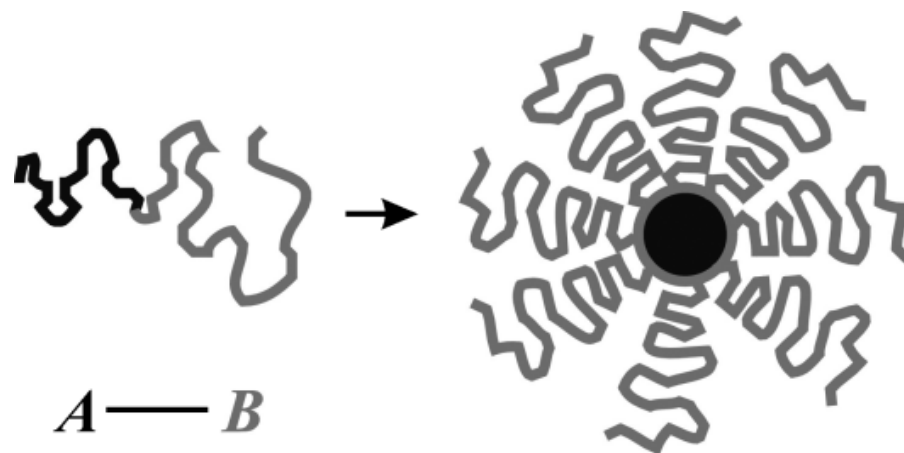
**Individual Small Alkyl Chain Length Quaternary Directing Agents
Generate the Formation of Microporous Molecular Sieves**



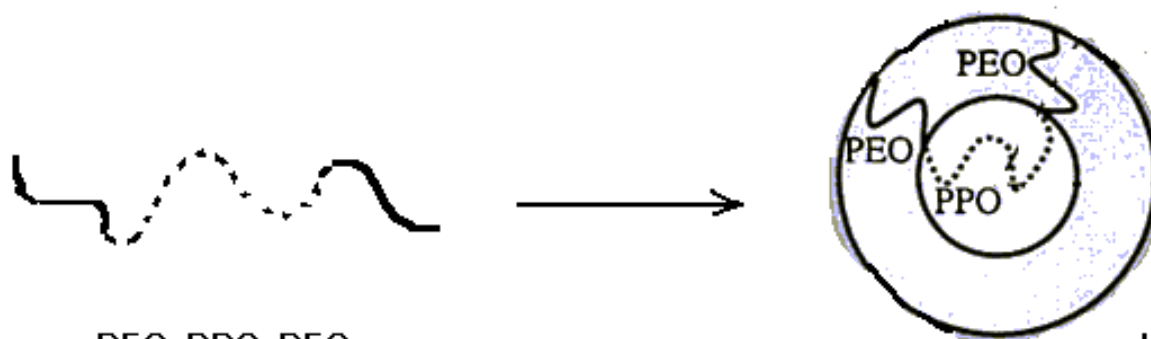
MCM-41

**Long Alkyl Chain Length Quaternary Directing Agents Self-Assemble to
Supramolecular Species Which Can Generate the Formation of Mesoporous Molecular
Sieves**

Micelles formed by Block- Copolymers



Diblock- Copolymers



PEO-PPO-PEO
Triblock-copolymer

hydrophilic media

Micelle

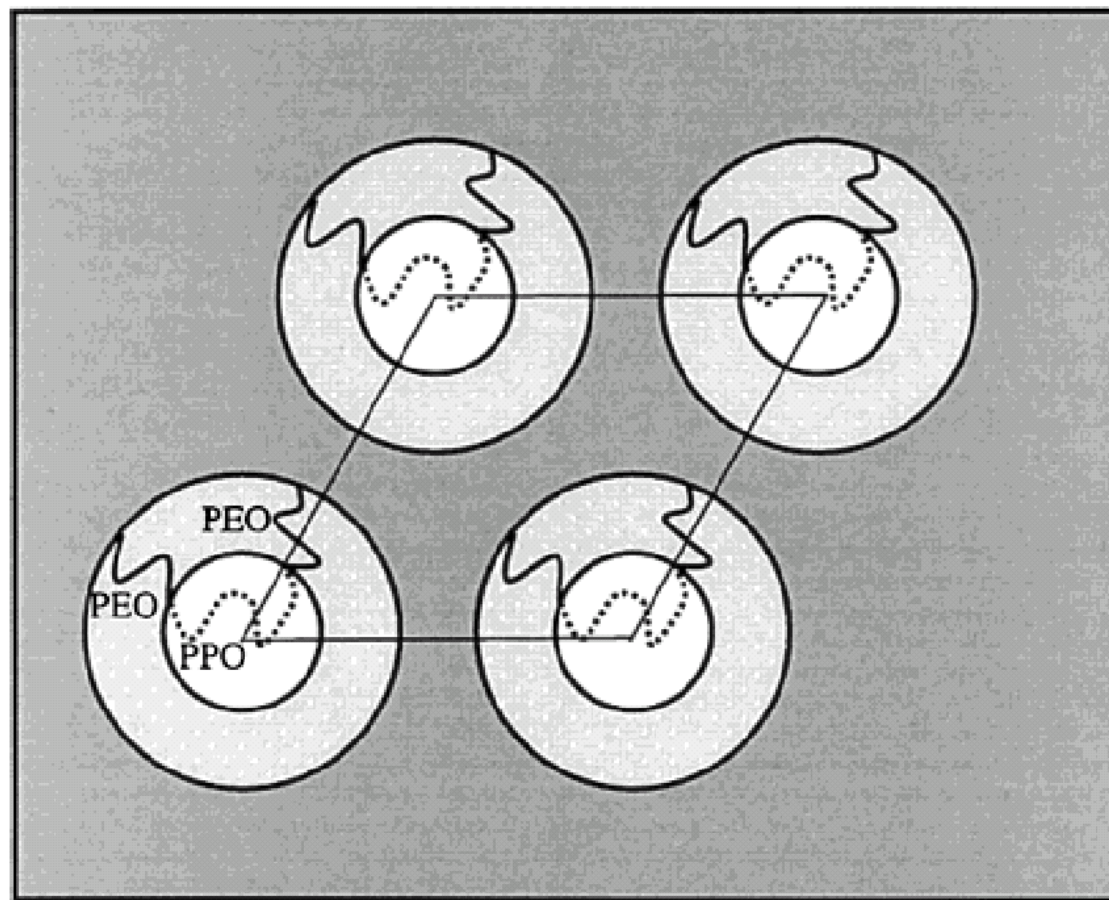
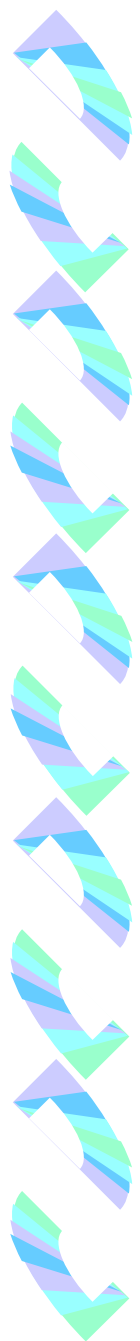


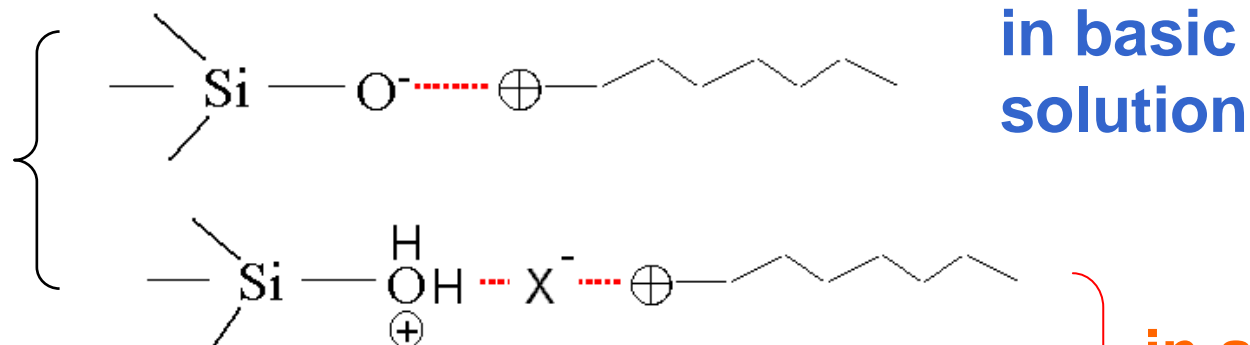
Figure 1. Schematic picture of the organization of uncalcined SBA-15 materials.



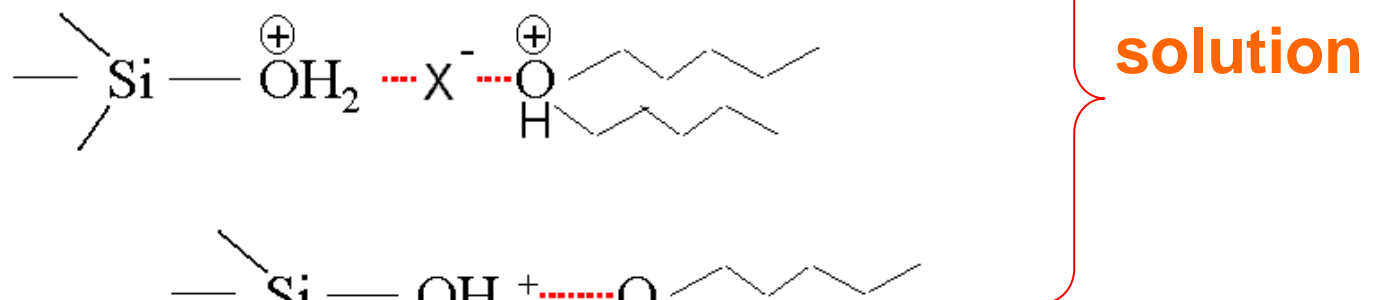
Interaction between Pore-Direction Agent and Silica

Coulombic force

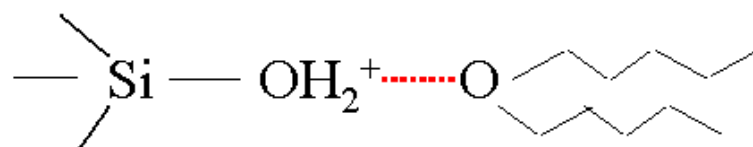
Cationic
template



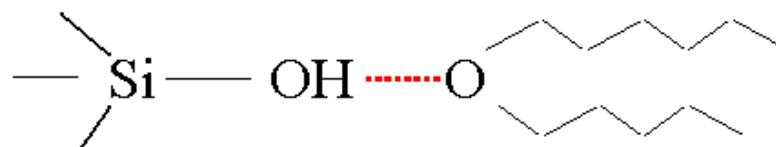
Neutral
template



Ion-dipole interaction



H-bond



Packing parameter vs. Micelle structure

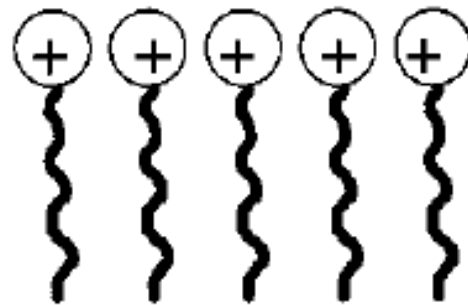
$$g = V/a_0 l$$

g : packing parameter

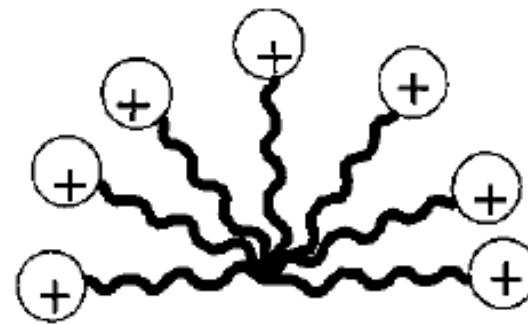
a_0 : area of head group

l : chain length

The curvature of micelle increases when the g value decreases.



$$g > 2/3$$



$$g \sim 1/2$$

Discovery of M41S Family

C.T. Kresge et al., Nature, **1992**, 357, 710.

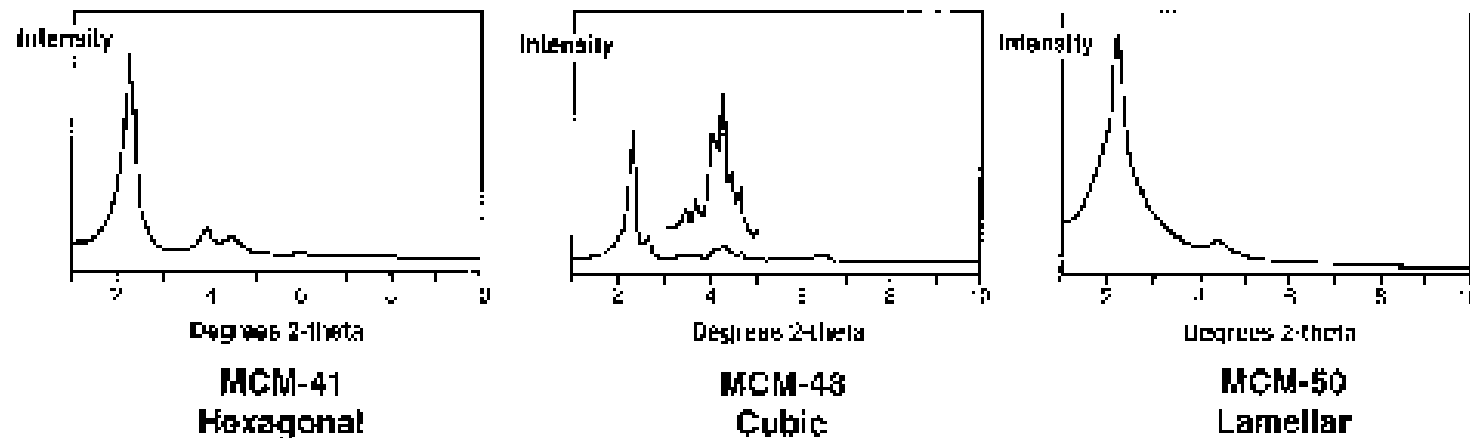
Si source: **sodium silicate**

Pore-directing agent: **cetyltrimethylammonium (CTMA) ion**

Acidity pH ~10

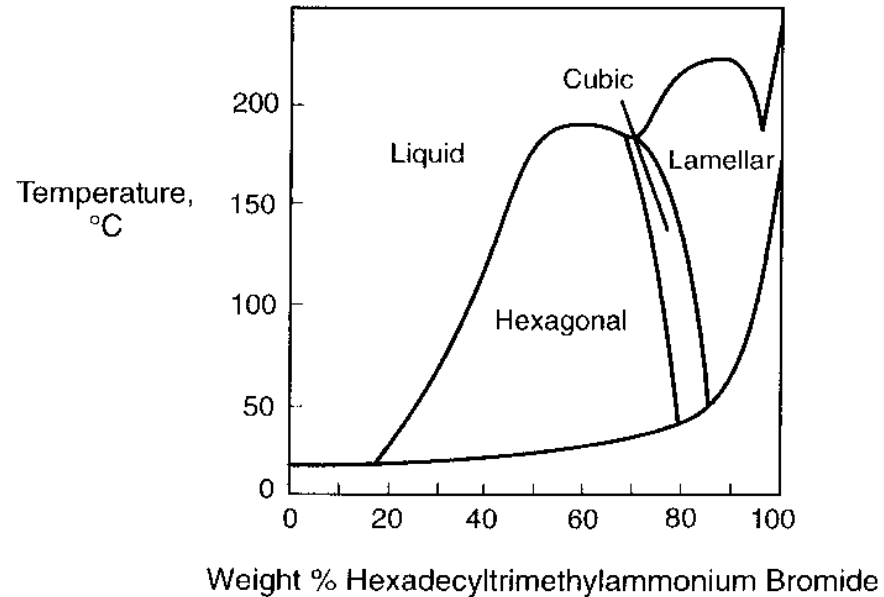
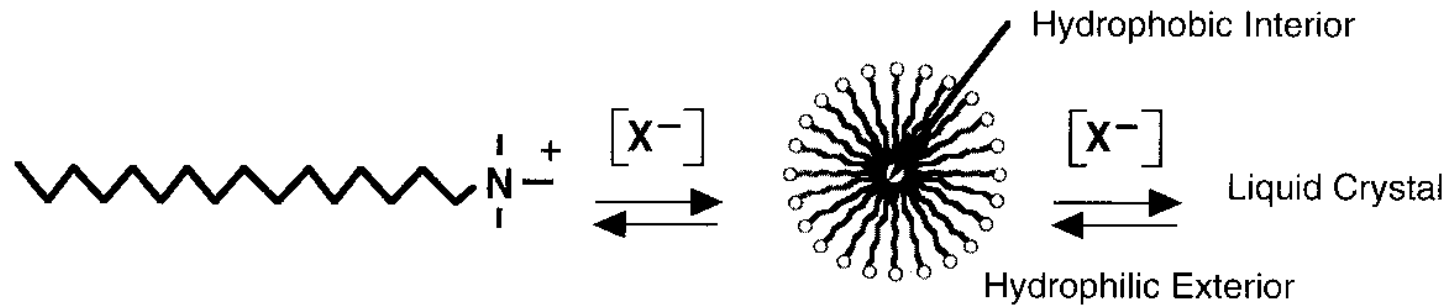
Temp. ~ 100°C

M41S

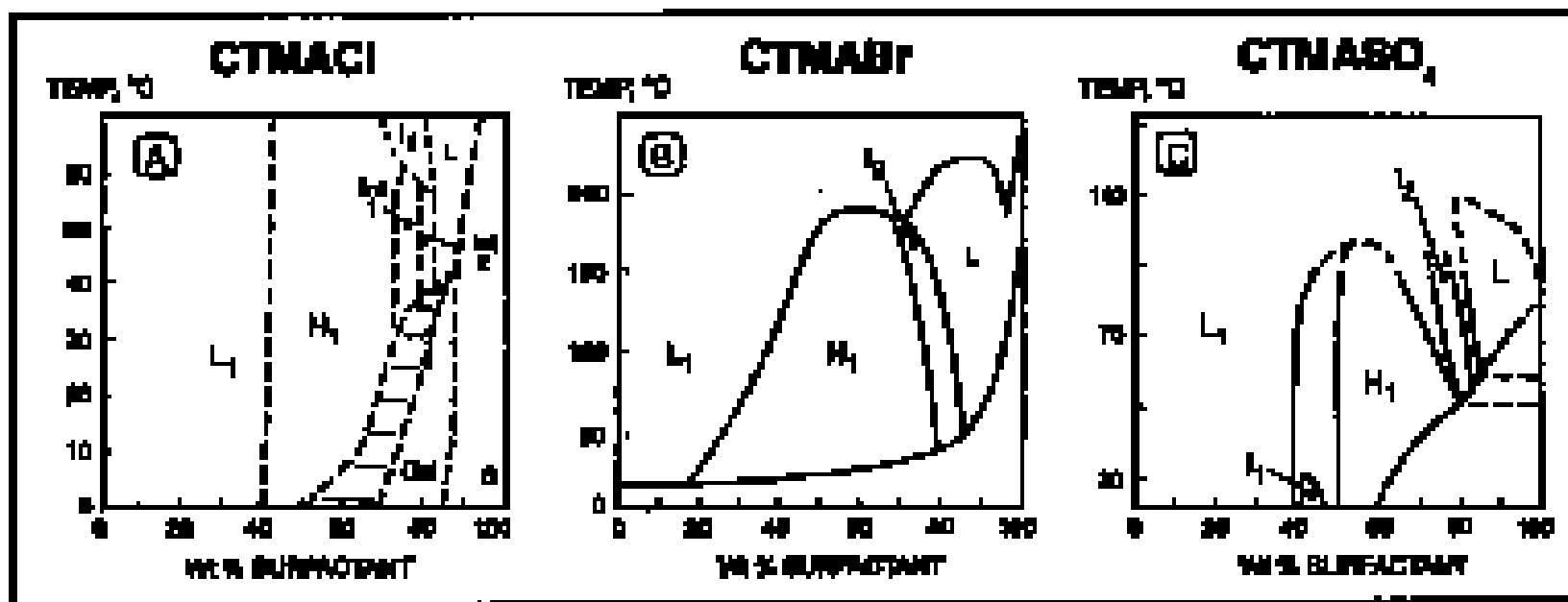


Increasing $\frac{\text{Sur}}{\text{SiO}_2}$ →

Organization of Surfactant Cations



Effect of Anion on Crystal Phase Diagram

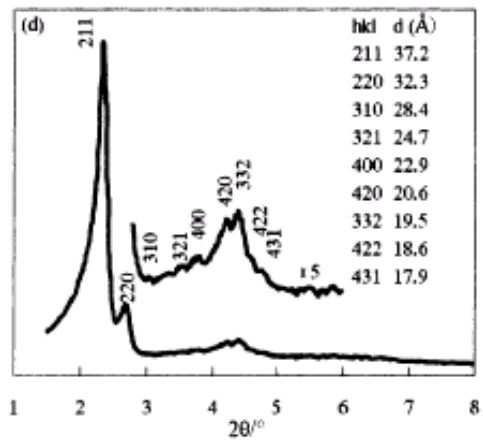
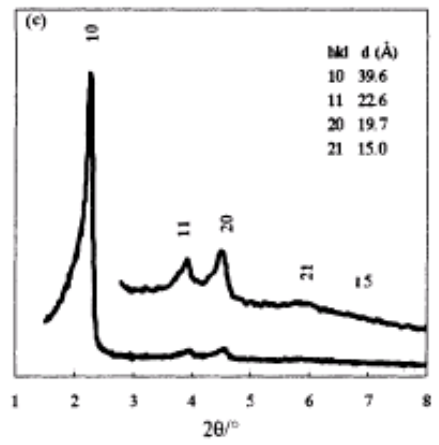
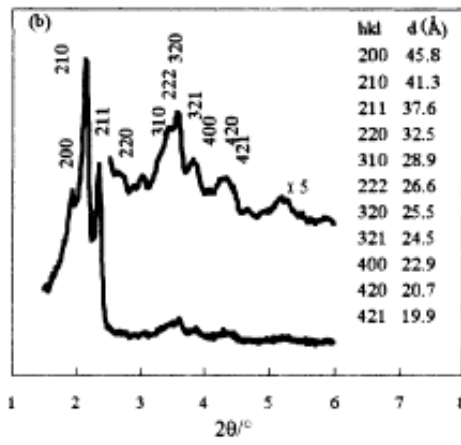
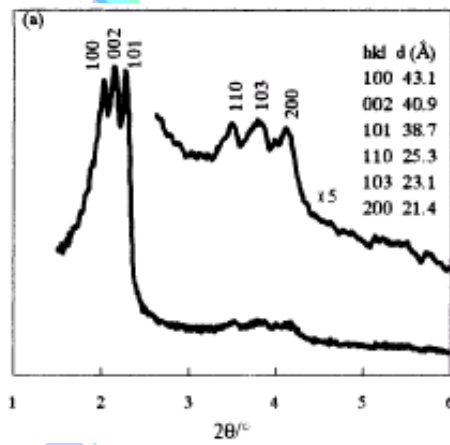
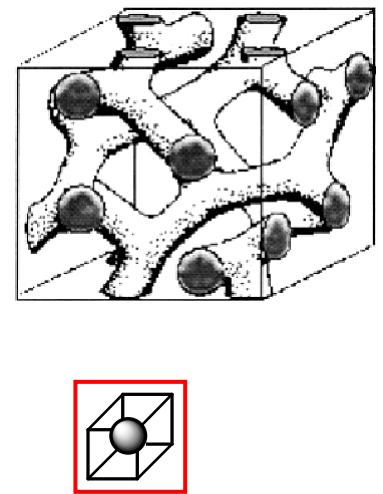
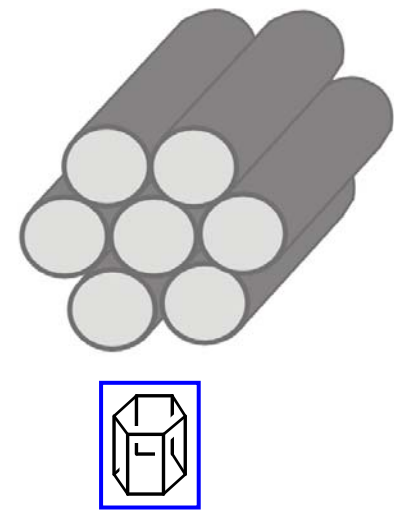
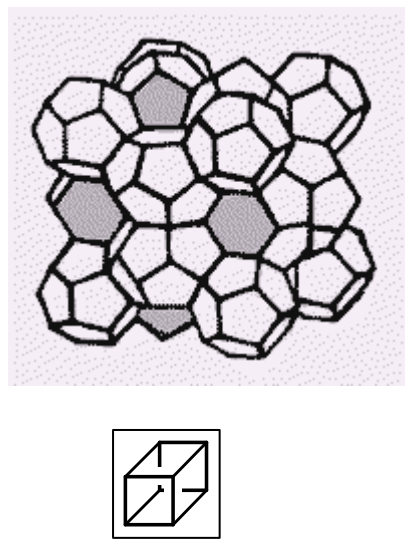
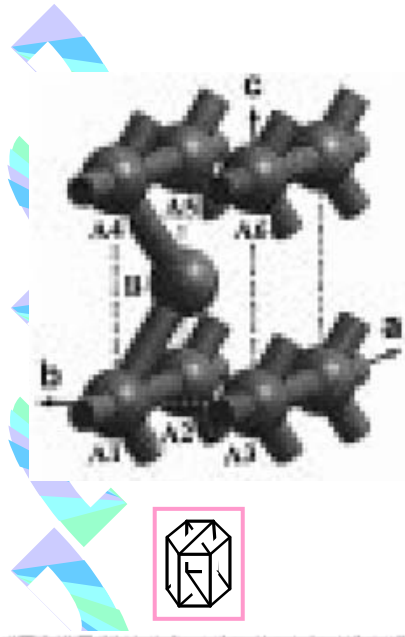


H₁ – Hexagonal, I – Cubic, L – Lamellar, L₁ – Solution

(A) J. Phys. Chem., **86**, 3894 (1992).

(B) Progress in Colloid & Polymer Science, **73**, 174 (1987).

(C) Progress in Colloid & Polymer Science, **73**, 174 (1987).



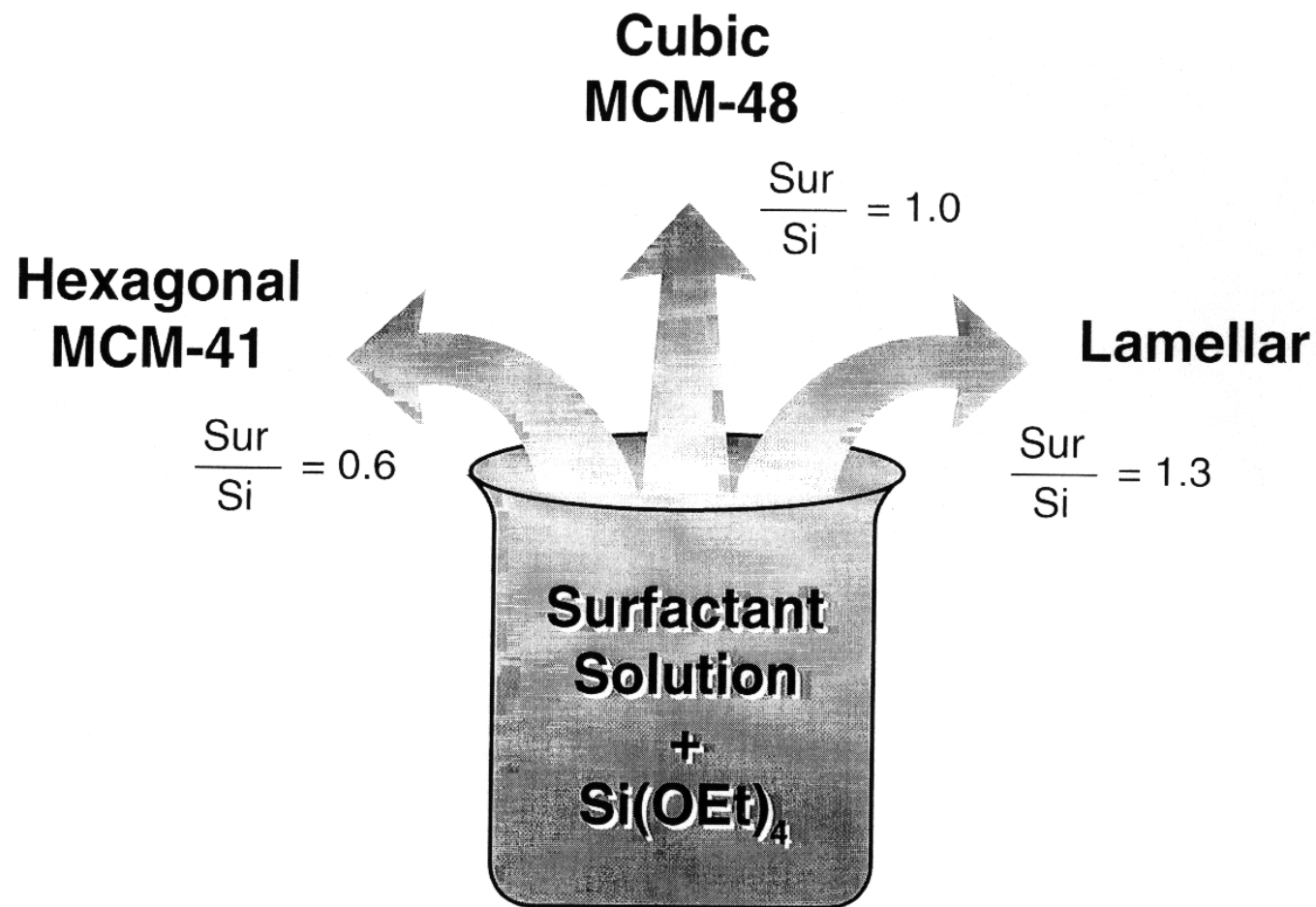
3D-Hexagonal
(P6₃/mmc)
 $g < 1/3$

Cubic (*Pm3n*)
 $g = 1/3$

2D-Hexagonal
(P6m)
 $g = 1/2$

Cubic (*Ia3d*)
 $g = 1/2 - 2/3$

Effect of Surfactant/Silica Ratio



Discovery of SBA-15

D. Zhao et al. Science, 1998, 279, 548.

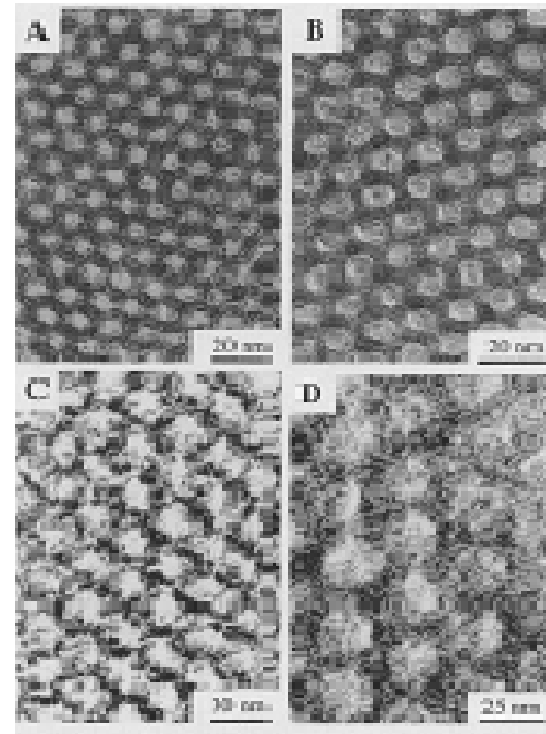
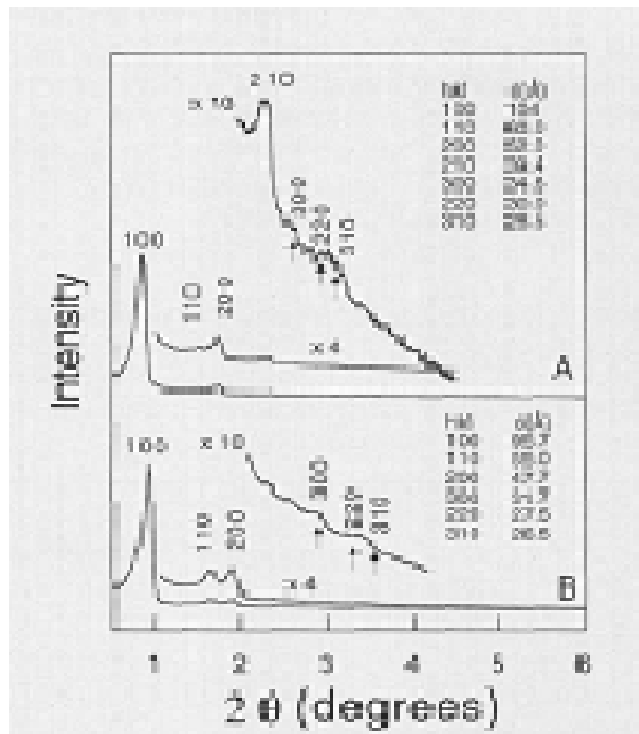
Si source: **TEOS**

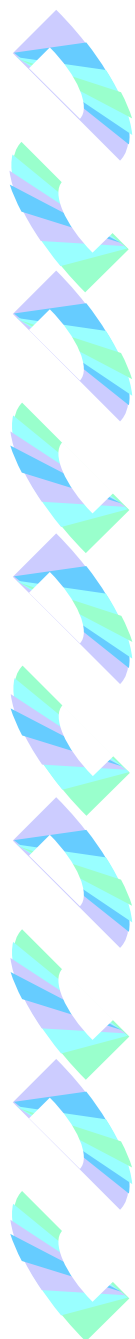
Pore-directing agent: Amphiphilic triblock copolymers

e.g.: Pluronic P-123, $(EO)_{20}(PO)_{70}(EO)_{20}$, 0.5~6wt%,

Acidity > 0.1M HCl

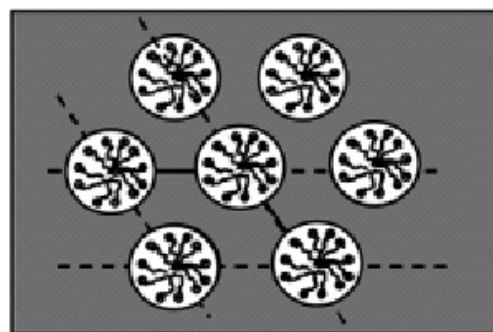
Temp. 35~ 80°C



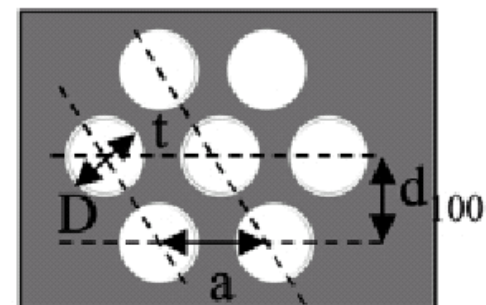


MCM-41

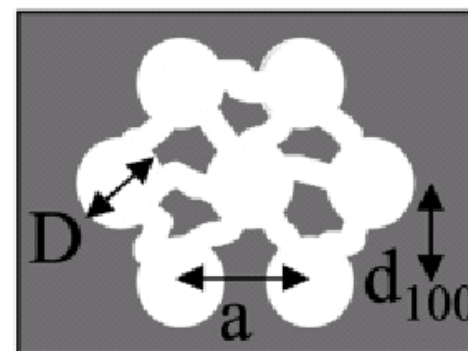
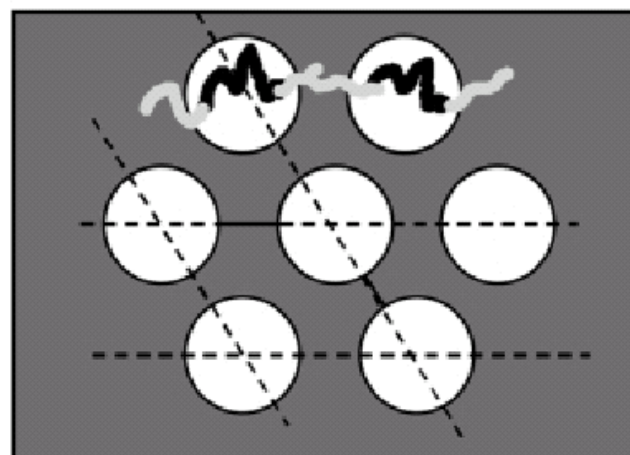
HYBRID
(surfactant-containing)



CALCINED
(surfactant-free)



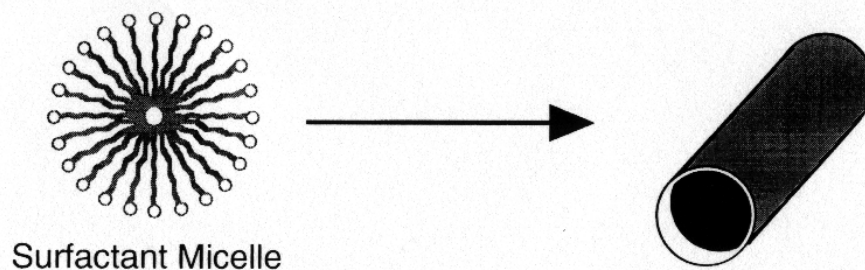
**SBA-15
Model 1**



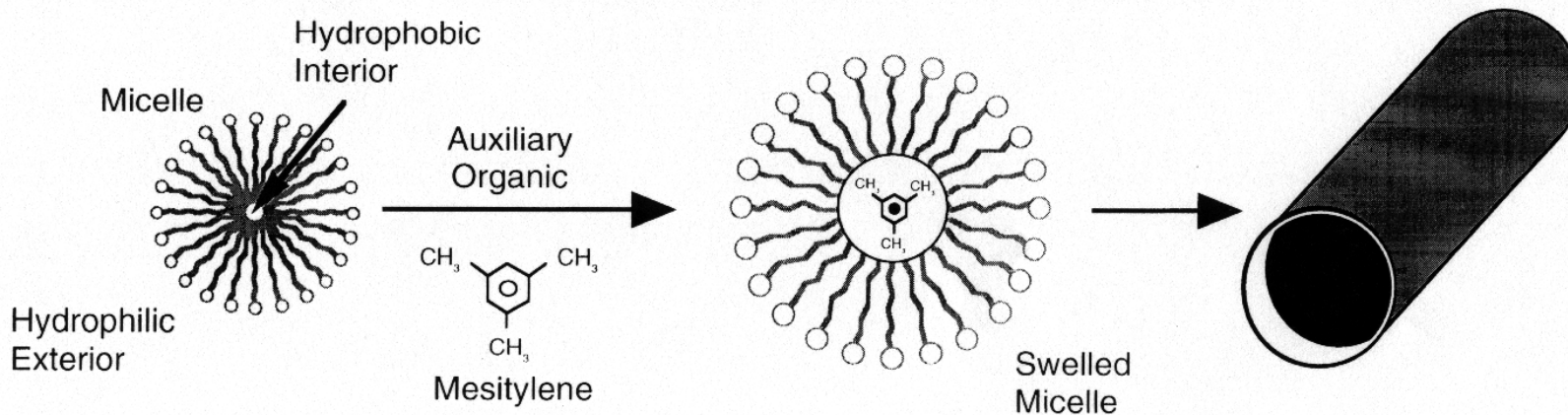
Davidson A. *Current Opinion in Colloid & Interface Science* **2002**

Methods to Change Pore Diameter

- Length of Surfactant Alkyl Chain Determines Pore Diameter



- Addition of Solubilization Agents Increases Pore Diameter



Microemulsion Templating of Siliceous Mesostructured Cellular Foams with Well-Defined Ultralarge Mesopores

Patrick Schmidt-Winkel,^{†,‡} Wayne W. Lukens,
David I. Margolese,[†] John S. Lettow,[§] Jackie Y. Ying,

Chem. Mater. 2000, 12, 686–696

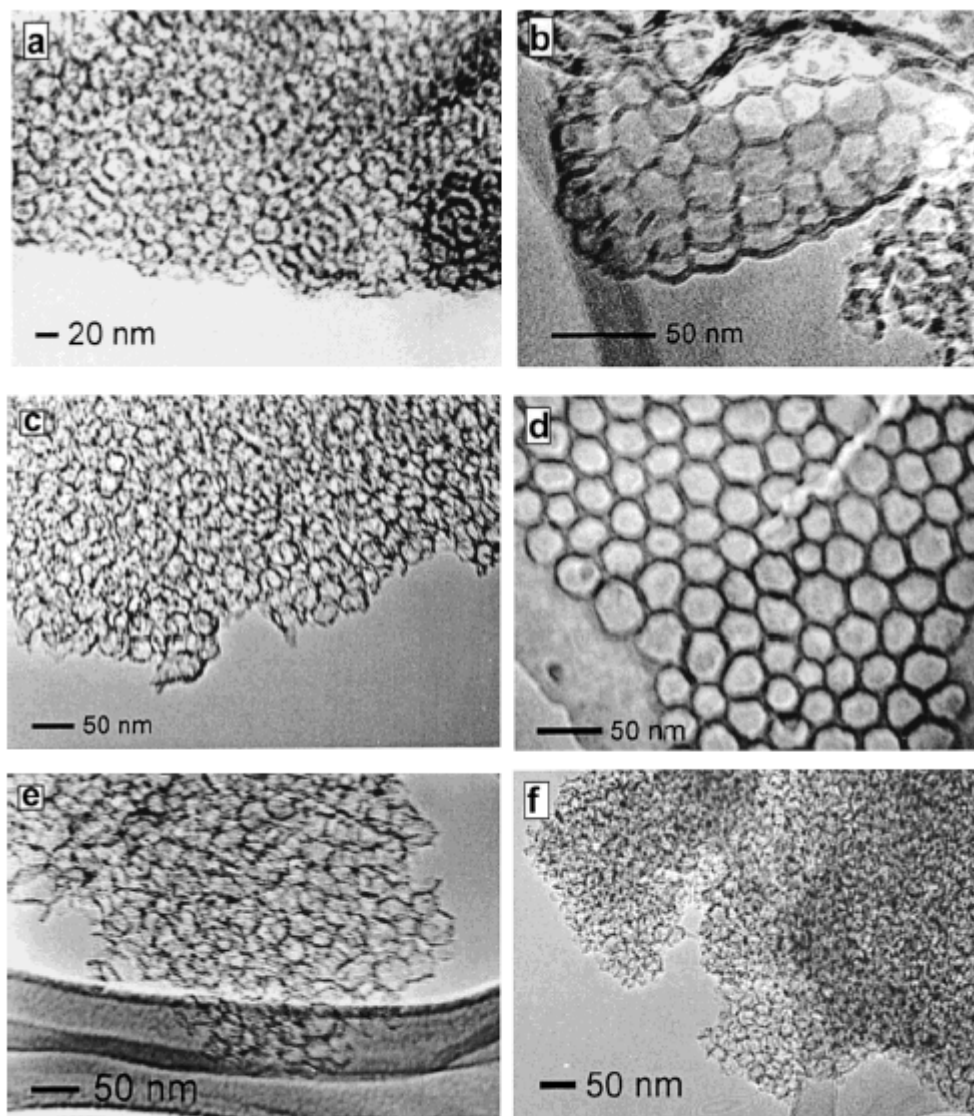


Figure 5. TEM images of MCFs prepared under different synthesis conditions reflecting the strutlike structure that is reminiscent of aerogels: (a) MCF 1-F prepared with TMB/P123 = 0.3 in the presence of NH_4F , TEM cell size ~ 25 nm; (b) MCF 2 prepared with TMB/P123 = 0.4, TEM cell size ~ 26 –28 nm; (c) MCF 5 prepared with TMB/P123 = 0.75, TEM cell size ~ 30 nm; (d) higher magnification image of MCF 5 prepared with TMB/P123 = 0.75, TEM cell size ~ 29 –34 nm; (e) MCF 8 prepared with TMB/P123 = 1.5, TEM cell size ~ 35 nm; (f) MCF 8-F prepared with TMB/P123 = 1.5 in the presence of NH_4F , TEM cell size ~ 33 nm. Wall thickness estimate ~ 4 –6 nm.

Mesoporous Silica Nanoparticles (MSNs)



- Unlike polymer nanoparticles, the silica frameworks that comprise MSNs are inherently immune to hydrolysis and enzymatic degradation, and enable extraordinarily large loadings of drugs.
- The narrow confines of the MSN nanochannels provide a physical barrier to enzyme entry, as most enzymatic proteins have diameters considerably greater than those of the MSN pores.
- Drugs conjugated to the inner walls of the MSN nanochannels are largely protected from in vivo hydrolysis and premature release.

Stöber method

a one-pot synthesis that is carried out at room temperature under alkaline conditions in **ethanol:water mixtures** and avoids the use of potentially toxic organic solvents and surfactants.

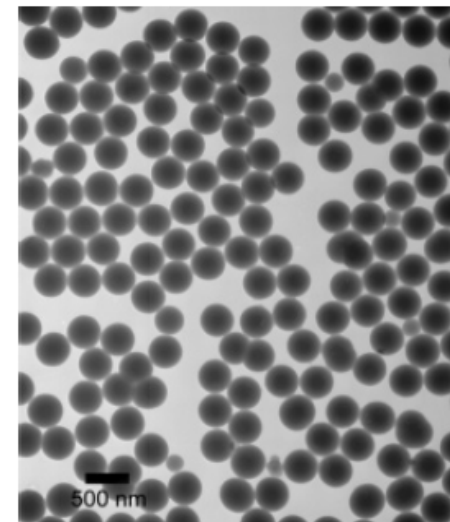


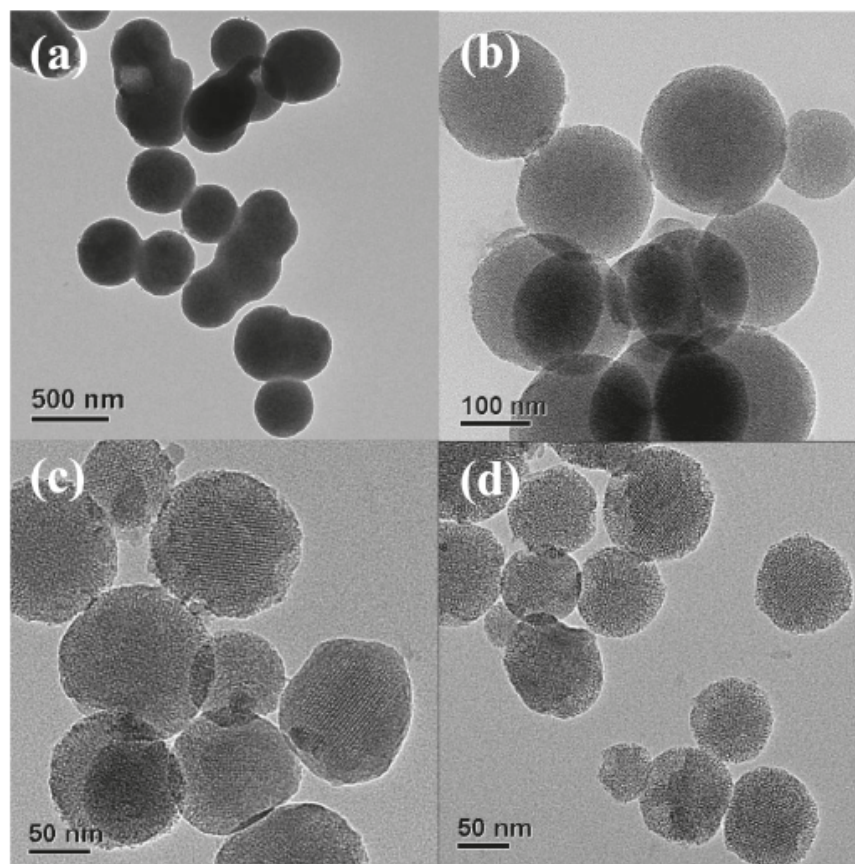
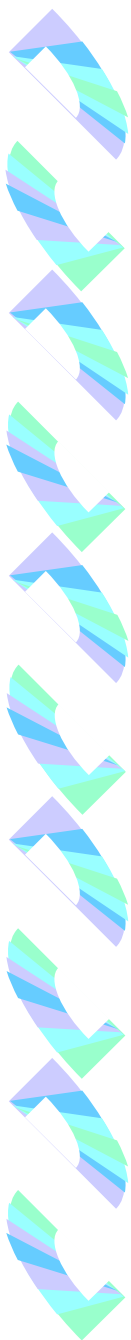
Table 1. Reagents and Quantities Used in the Preparation of Fluorescent Silica Nanospheres

TEOS	NH ₄ OH (30%)	[Ru(phen) ₃]Cl ₂ (0.5 mg/mL)	ethanol	product weight	mean diameter (from TEM images)
1.3 mL	3 mL	3 mL	22.7 mL	0.30 g	800 ± 20 nm
1.3 mL	7 mL	3 mL	18.7 mL	0.30 g	440 ± 18 nm
2 mL	1.5 mL	0.5 mL	25 mL	0.50 g	65 ± 8 nm



Preparation of MCM-48 MSN

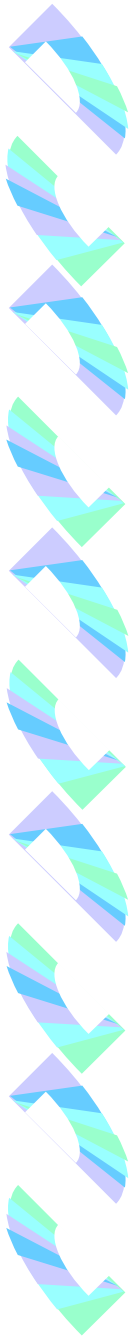
- The preparation of MCM-48 ordered mesoporous silica nanoparticles was based on the modified Stöber method.
- The MCM-48-type MSNs were synthesized under various synthetic conditions using a mixture of **cetyltrimethylammonium bromide (CTAB)** and ethanol as a structure-directing mixture.
- Tetraethyl orthosilicate (TEOS) and **triblock copolymer F127 (Pluronic F127, PO₁₀₆PO₇₀EO₁₀₆)** were applied as a silica source and a **particle dispersion agent**, respectively.
- The molar composition of the reaction mixture was varied in the range of TEOS: CTAB: NH₃: EtOH: H₂O: F127 = x: 0.4: 12.5y: 54y: 417y: z, with x = 1-4.25, y = 1-9, and z = 0-0.094.



TEM images for calcined *cubic Ia3d* MCM-48 mesoporous silica nanoparticles with different amounts of the F127 under diluted CTAB concentration. F127 (in molar ratio)=(a) 0, (b) 0.047, (c) 0.078, and (d) 0.094.

Applications ?





Applications of Nano-porous Materials

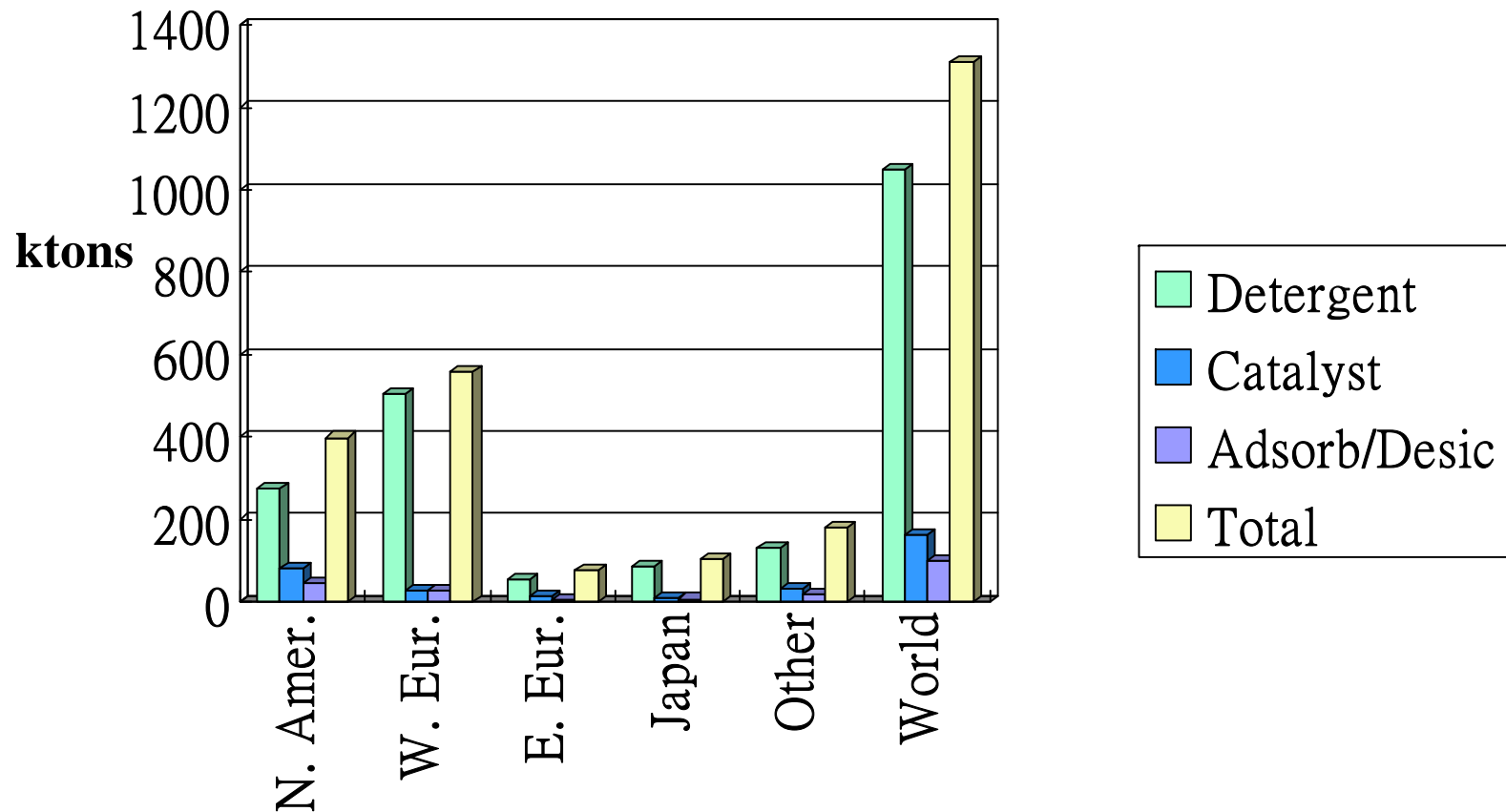
- ◆ **Adsorbents & Ion-exchangers**
- ◆ **Catalysis**
- ◆ **Nano-reactor**
quantum lines & dots, engineering polymers
- ◆ **Guest-Host interaction**
immobilized homogeneous catalysts, enzymes,
nonlinear optics, - - -, etc.
- ◆ **Low dielectric constant mediate**
- ◆ **Biomedical**

Zeolites:

Main field of application and market

1998 consumption

1.3 Mton Synthetic + 0.3 Mton (~18%) Natural zeolites





Catalysis Applications

World catalysts

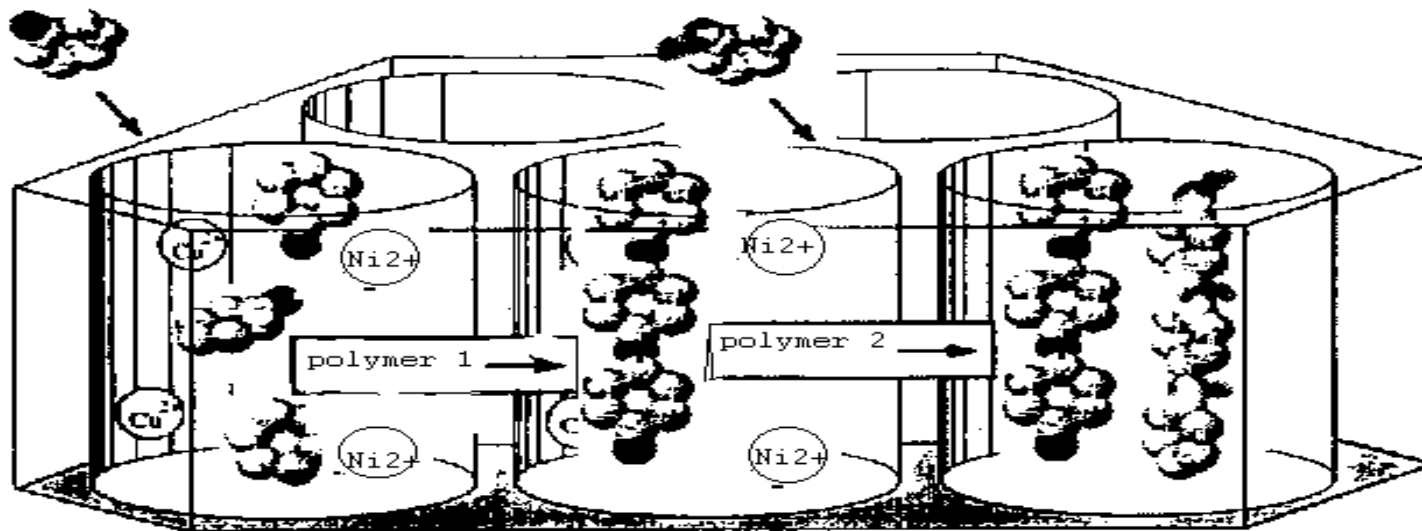
- ♦ 9 G\$ business in 1999
- ♦ 24% for Refining, 24% for Chemicals, 23% for Polymers, 29% for Environment

Zeolite market

- ♦ 160×10^3 tons in catalysis applications, 1998

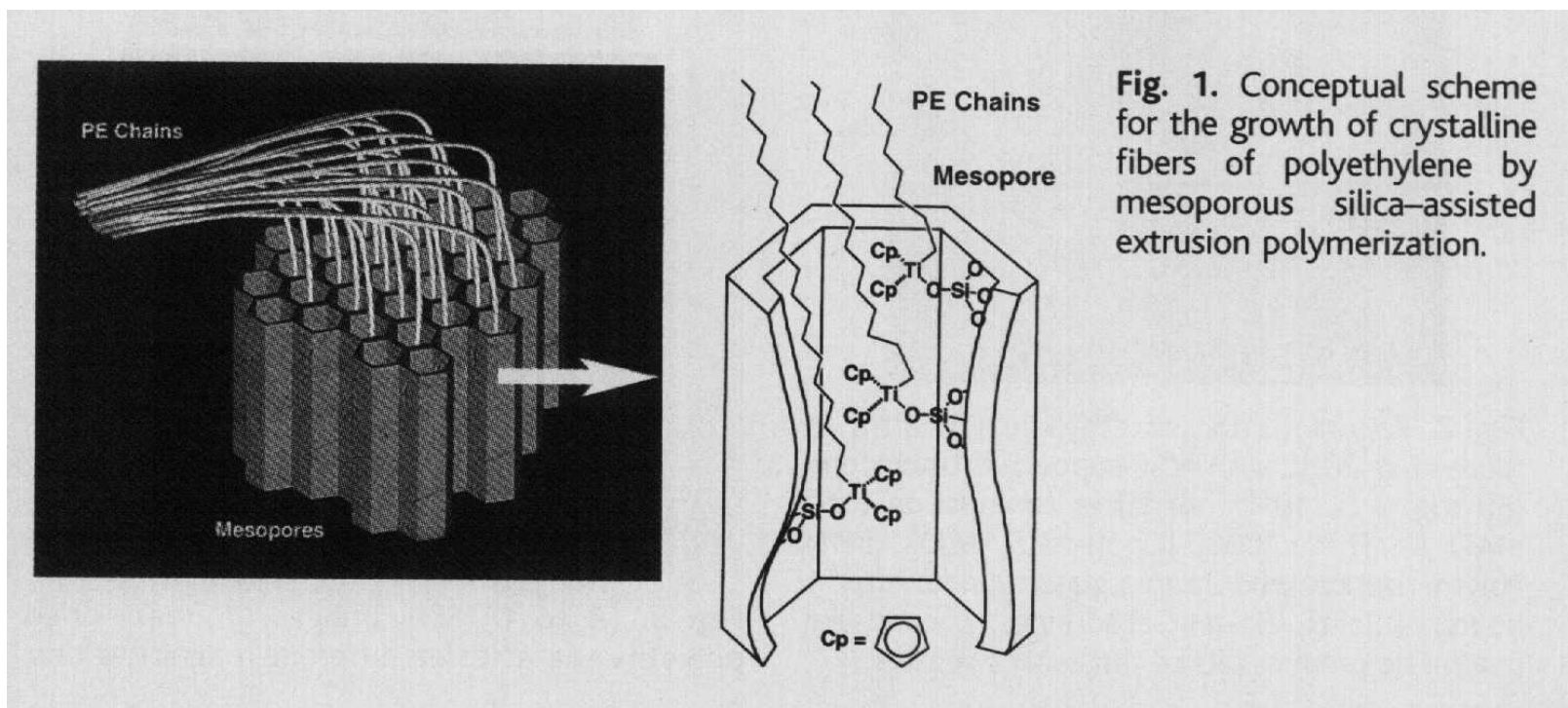
Polymerization in Confined Space

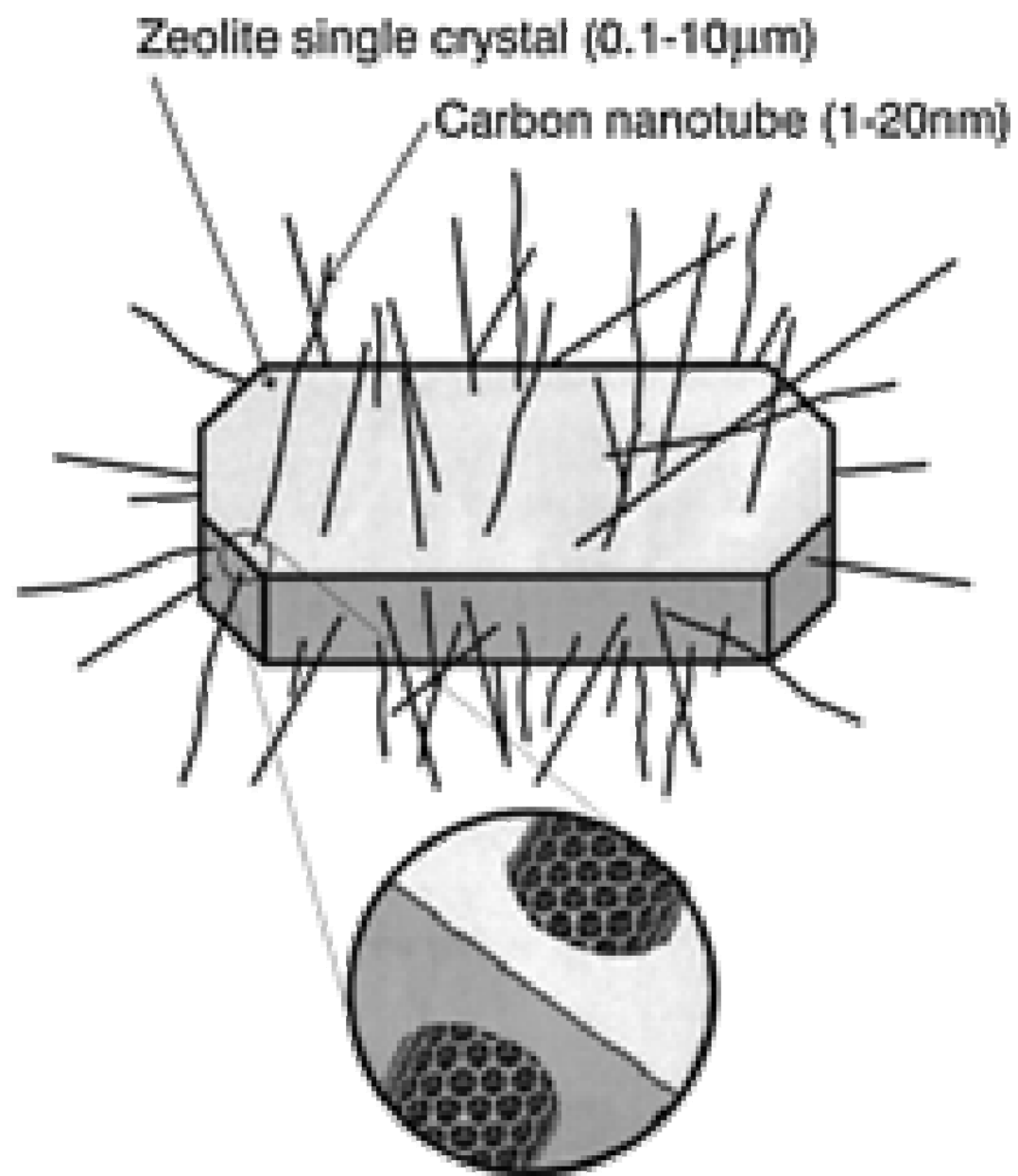
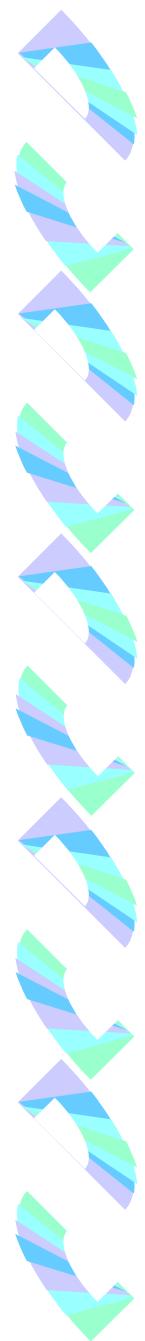
- Adsorption of Monomer in Vapor Phase
- Conducting Polymerization
- Control of Polymer Morphology and Physical Properties
- Molecular blending of different polymers



Extrusion polymerization: Catalyzed synthesis of crystalline linear polyethylene nanofibers within a mesoporous silica

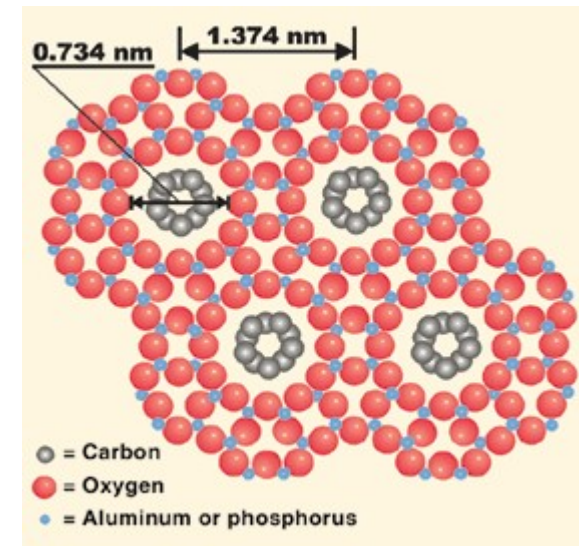
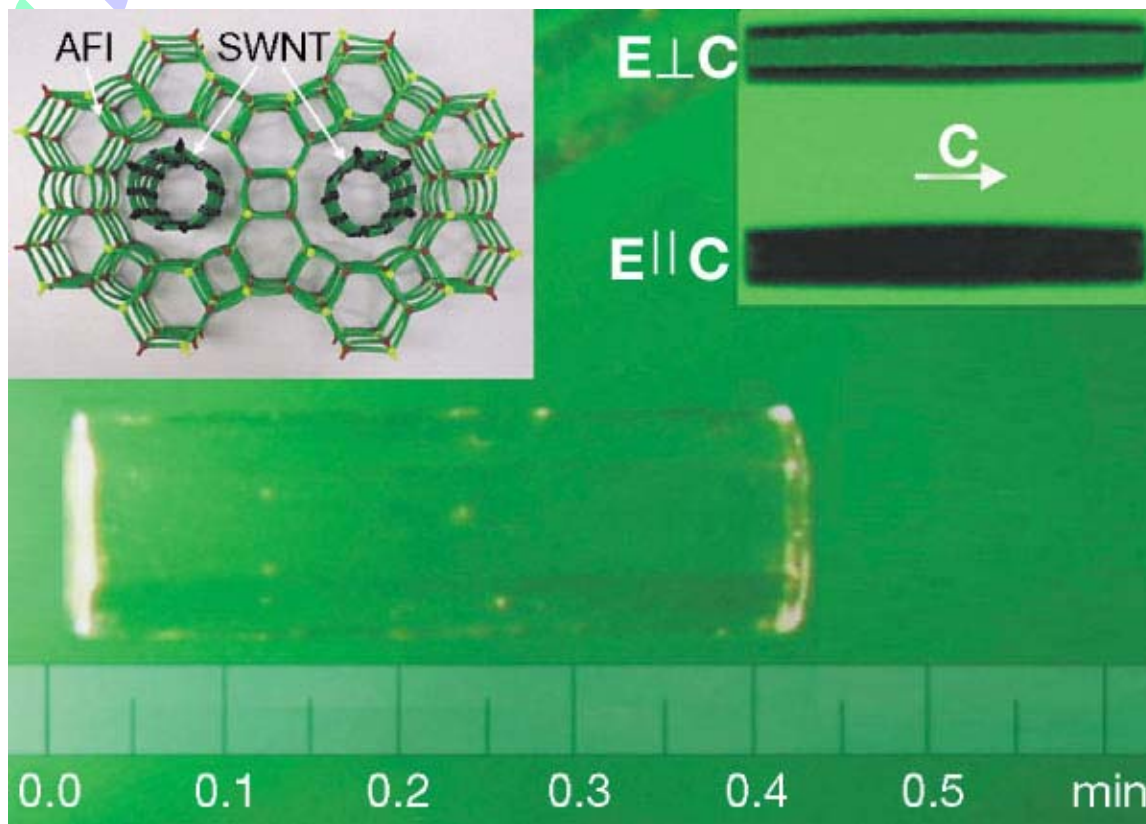
Keisuke Kageyama; Jun-ichi Tamazawa; Takuzo Aida
Science; 285 (1999) 2113.





The smallest carbon nanotubes possible in the channels of porous zeolite $\text{AlPO}_4\text{-5}$ (AFI) single crystals

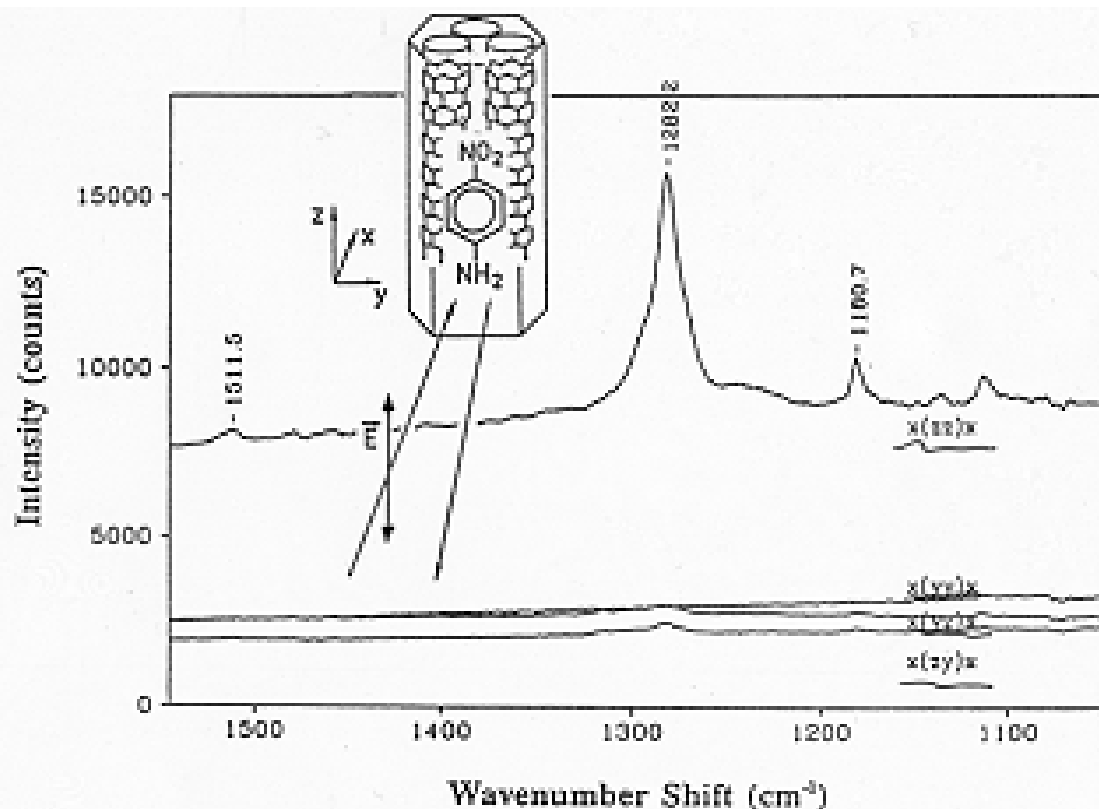
[*Nature* **408**, 50 - 51 (2000)]



Schematic drawing of 4Å single-walled carbon nanotubes formed in zeolite channels

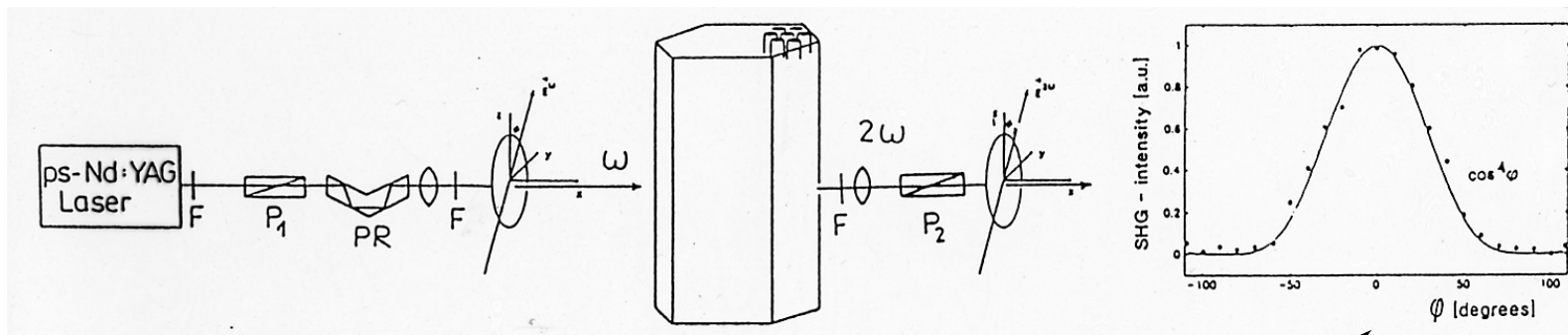
Self-assembled dipole molecules in molecular sieves

Figure 2. Raman spectra of pNA in $\text{AlPO}_4\text{-5}$ for different polarizations. As an example, the code $x(zz)x$ denotes a spectrum obtained for incident light in the x -direction (linearly polarized in z -direction) and the scattered wave in the x -direction (detection of the scattered wave in z -polarization) [13a].



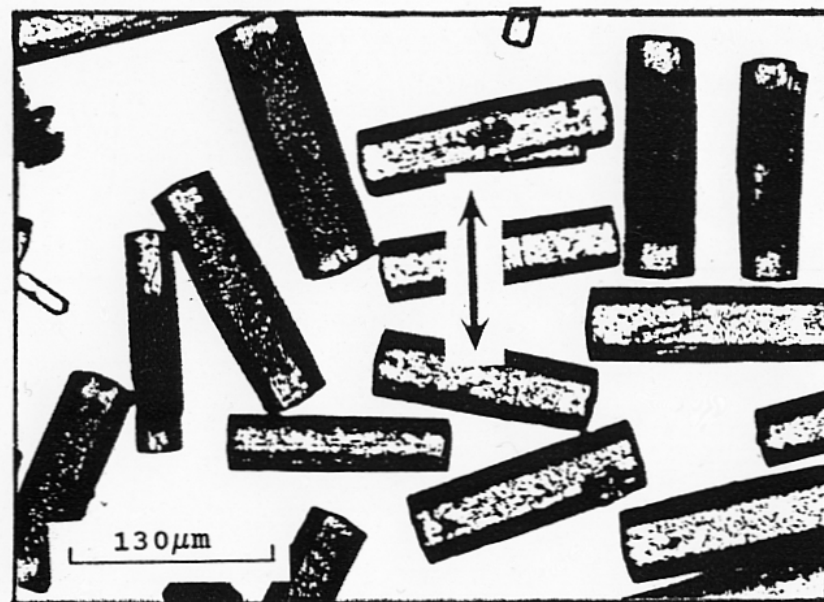
F. Marlow et al. Studies in Surface Science & Catalysis, **1994**, 84, 2277.

*Self-assembled polar molecules (pNA) in
 $AlPO_4-5$ molecular sieves*



*Polarization dependence of
the SHG*

Self-assembled polar molecules in molecular sieves



AlPO₄-5 molecular sieves crystals loaded with p-nitroaniline (pNA) in transmission of polarized light. The polarization plane is indicated by an arrow.

Studies in Surf. Science & Catal., 84, 2277 (1994)

Synthesis of Platinum Nanowires in Organic–Inorganic Mesoporous Silica Templates by Photoreduction: Formation Mechanism and Isolation

Yuzuru Sakamoto,[‡] Atsushi Fukuoka,^{*,†,‡} Takanori Higuchi,[‡] Noriyuki Shimomura,[‡] Shinji Inagaki,[§] and Masaru Ichikawa^{*,†,‡}

J. Phys. Chem. B 2004, 108, 853–858

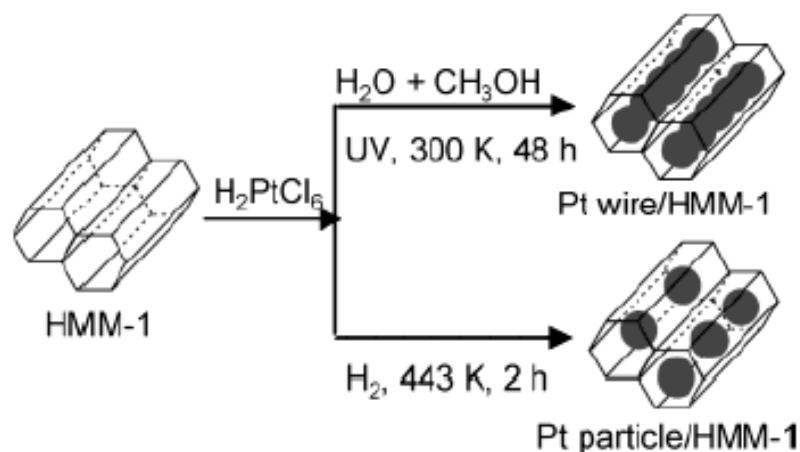


Figure 1. Schematic representation of the synthesis of Pt nanowires and nanoparticles in HMM-1.

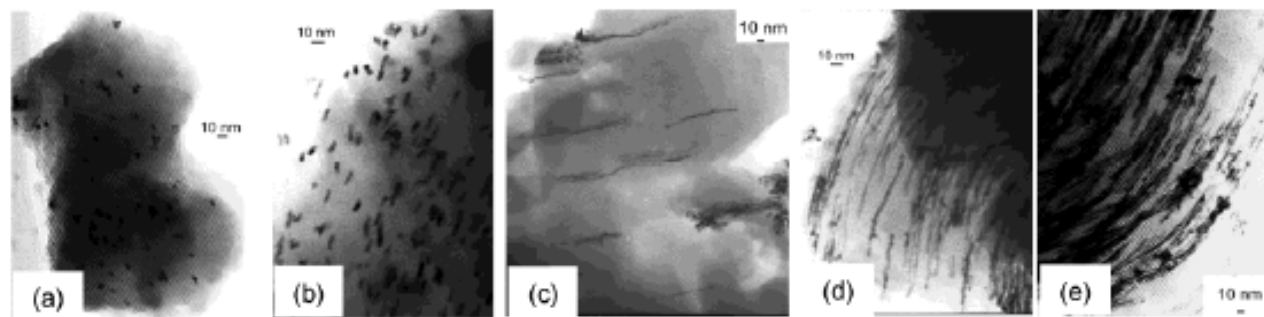


Figure 4. TEM images of Pt/HMM-1 after UV-irradiation for (a) 4, (b) 8, (c) 12, (d) 24, and (e) 48 h.

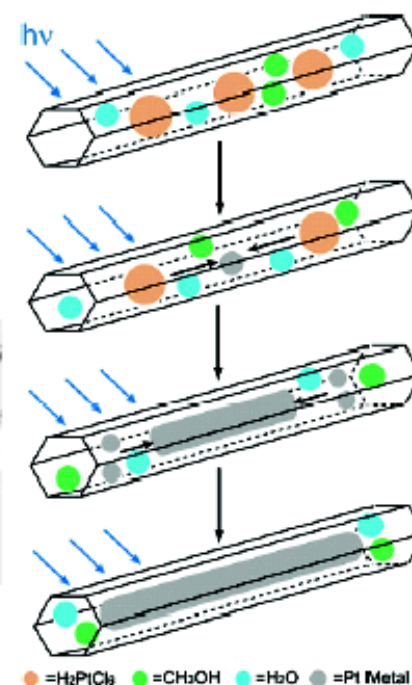
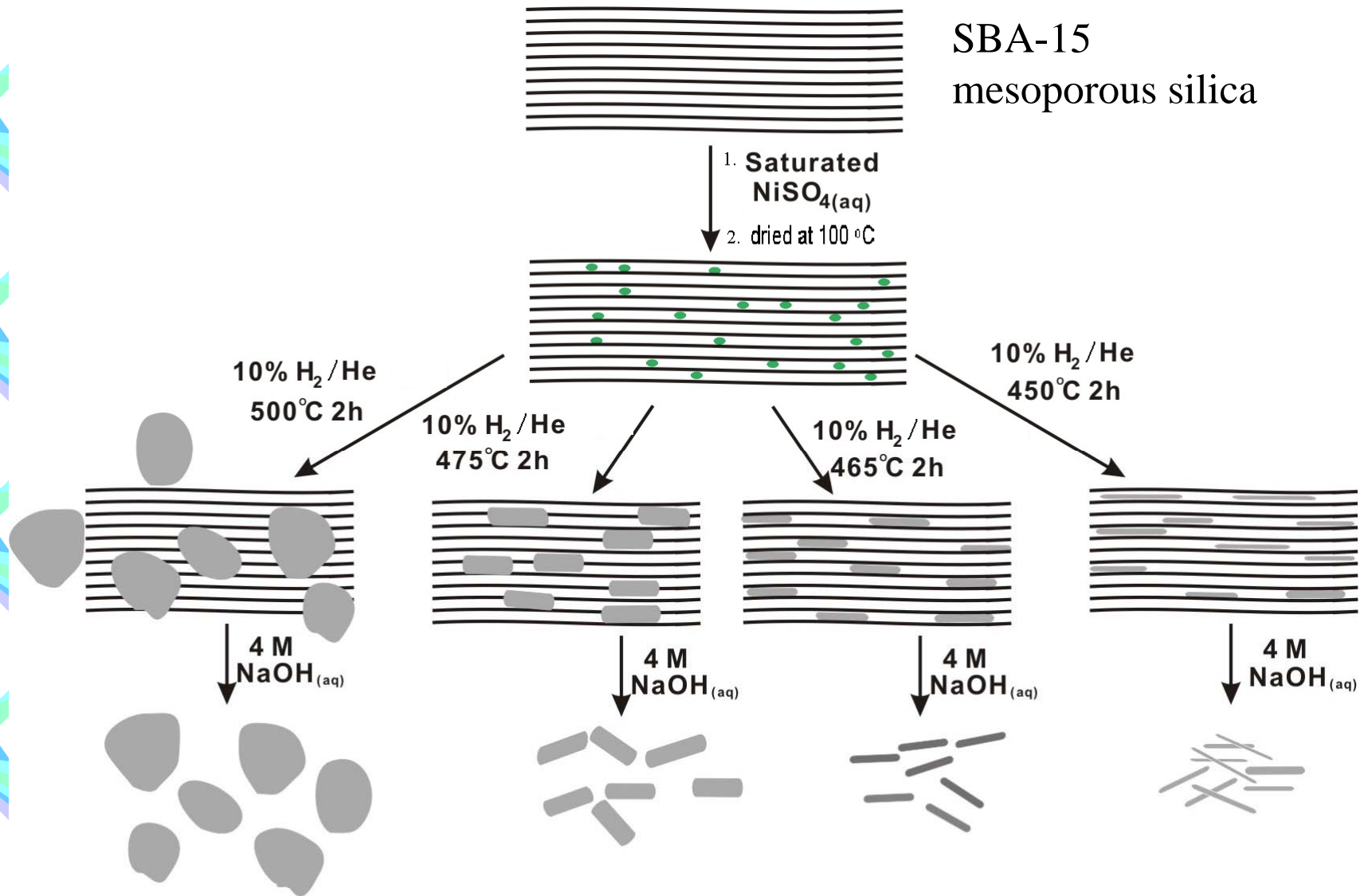
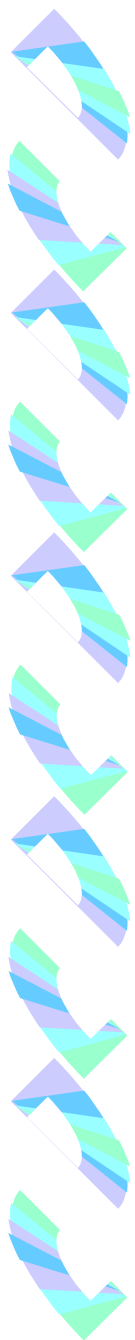


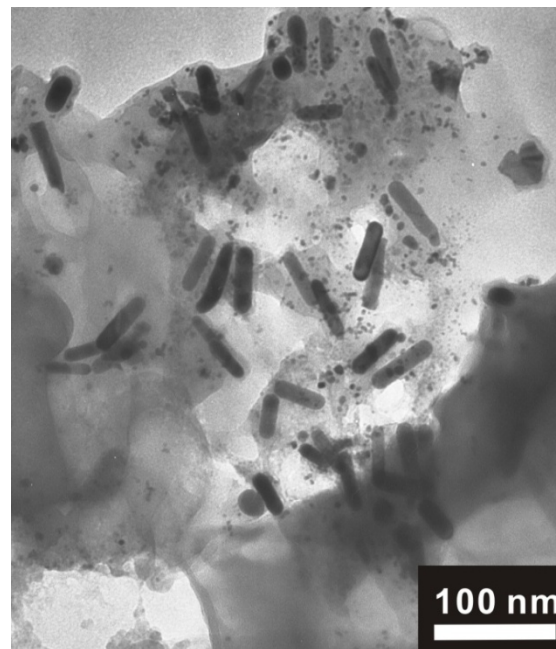
Figure 7. Proposed mechanism for the formation of Pt wires in HMM-1.

Preparation of Ni nanorods

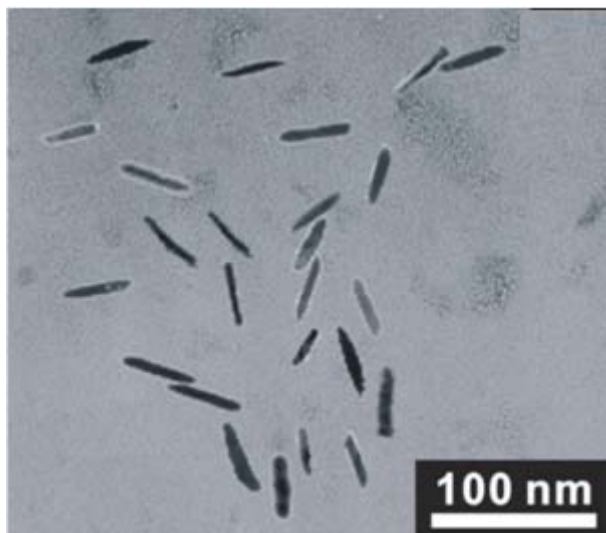




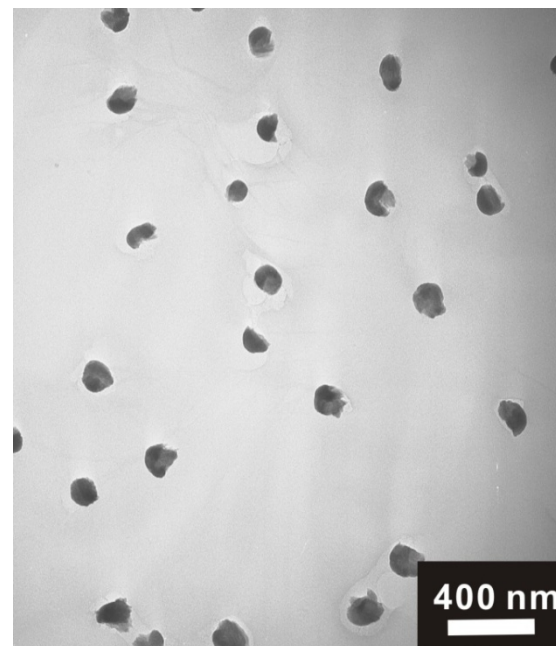
450°C



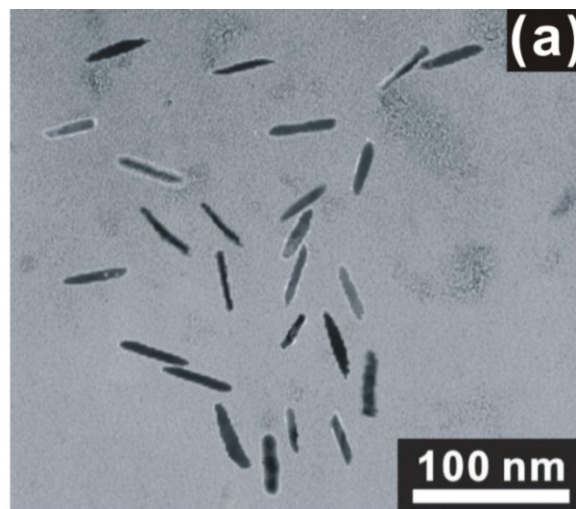
475°C



465°C



500°C



Reduction at 465°C

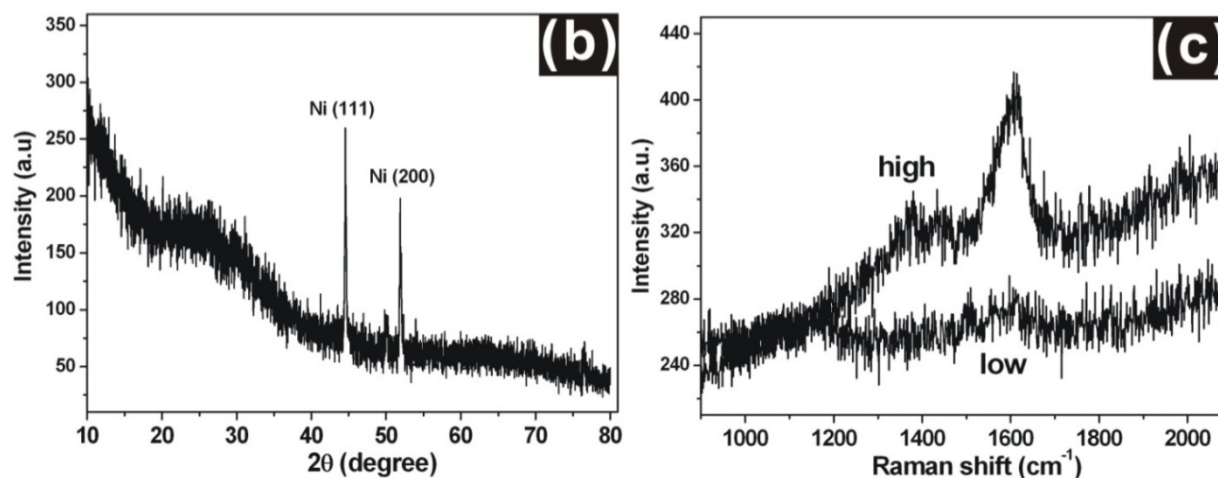
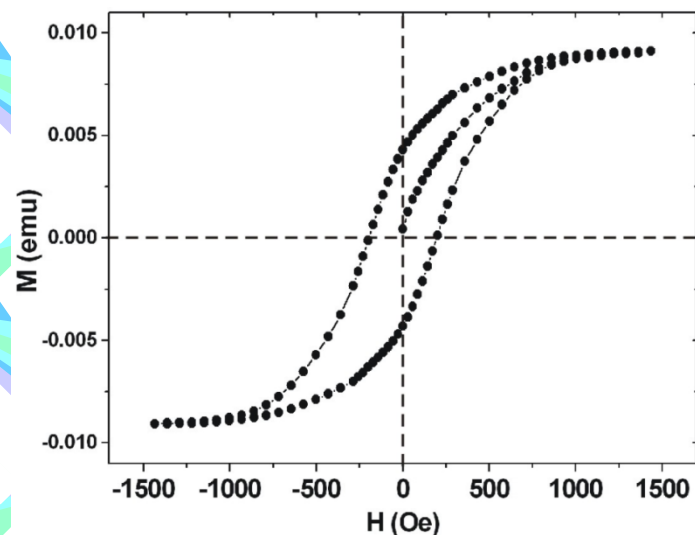
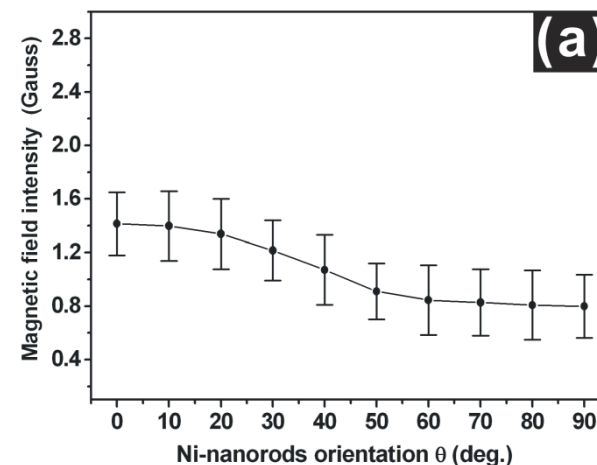
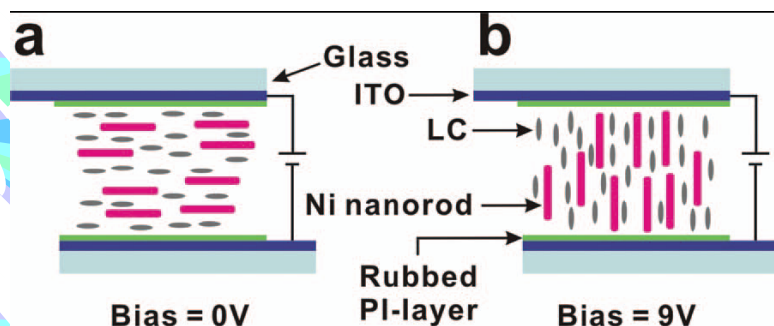


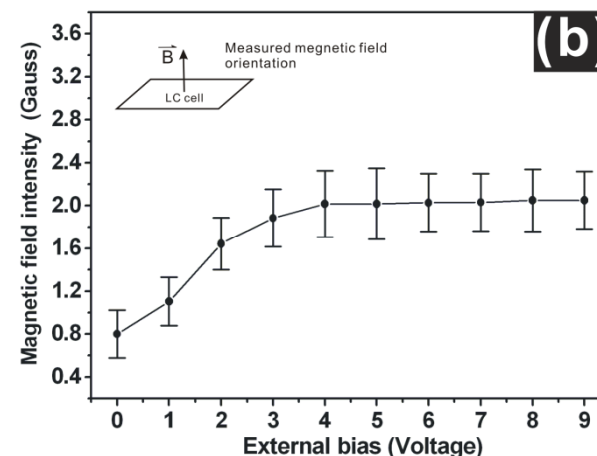
Figure 2. Transmission electron microscope (TEM), XRD pattern and Raman spectra of Ni nanorods investigated in this work. (a) TEM shows that the Ni nanorod has about 48 nm in length and 6 nm in diameter. (b) XRD pattern of Ni nanorods shows fcc structure of Ni nanorods. (c) Raman spectrum of the Ni nanorods in low concentration, and high concentration. The significant SERS enhancement on high concentrations might be attributed to nickel nanorods touching each other.



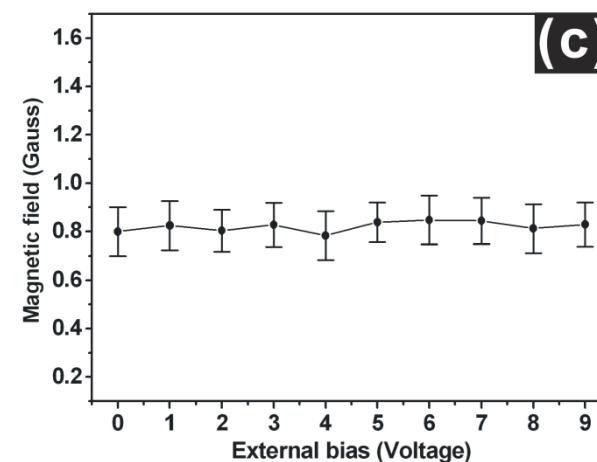
Magnetic hysteresis loop of Ni nanorods. The hysteresis curve (at 2 K) shows a coercive field measured of 191 Oe is much higher than nickel bulk. The high saturation magnetization demonstrates good surface magnetism of the nickel nanorods prepared using our method.



Ni nanorods oriented in **LC molecules** along the rubbed PI direction (0 deg.)

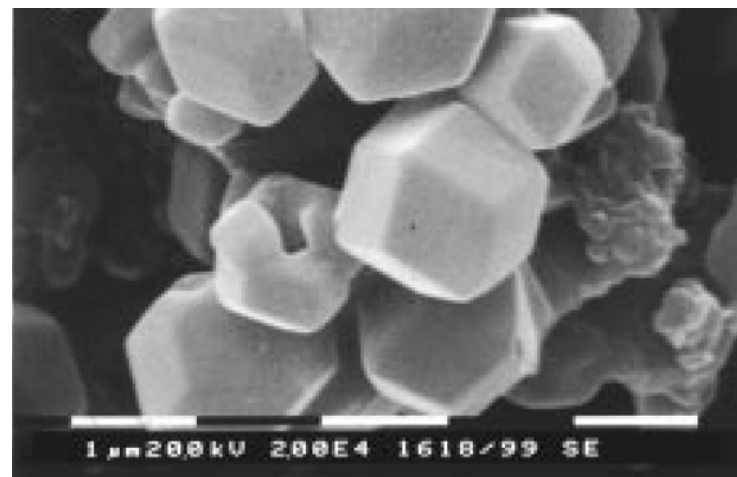
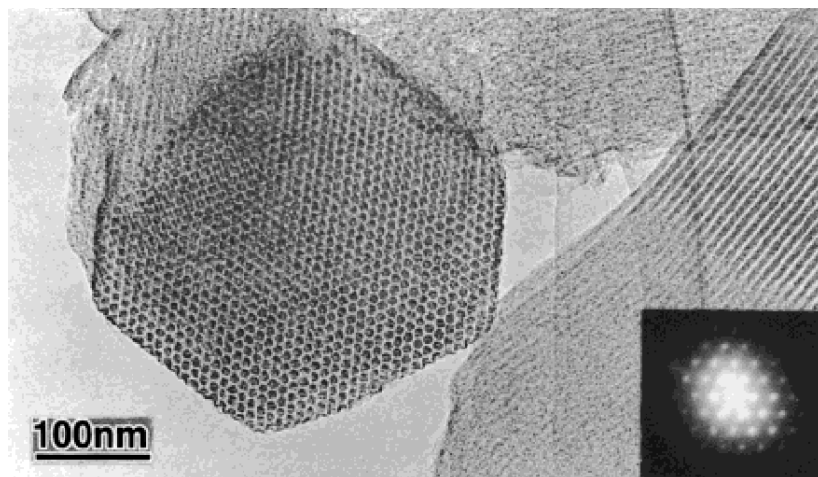


magnetic anisotropy changes gradually with external bias.



Ni nanorods mixed with **DI water**

Ordered Mesoporous Carbons



R. Ryoo* and S. H. Joo

Department of Chemistry (School of Molecular Science-BK21)
Korea Advanced Institute of Science and Technology, Taejon (Korea)

Dr. M. Kruk and Prof. M. Jaroniec

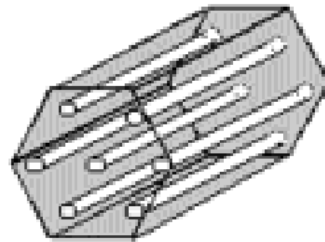
Department of Chemistry, Kent State University, Kent, (USA)

Advance Materials **13(9)**, 667 (2001).

Schematic Illustration of Formation of CMKs Materials

MCM-41

A

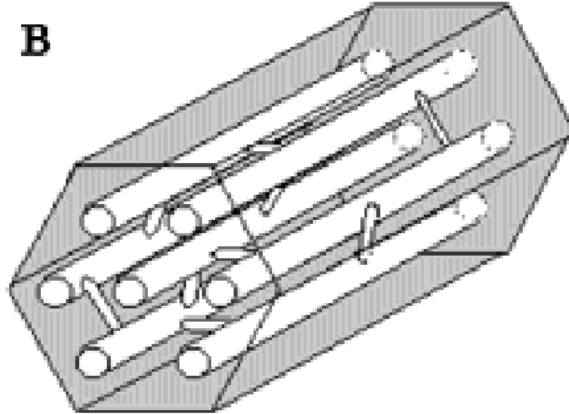


High-surface-area microporous carbon

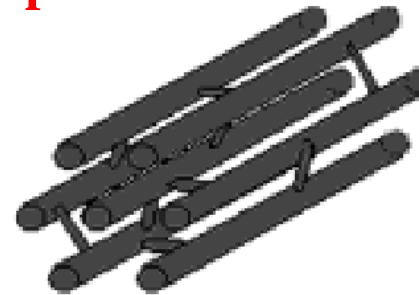


SBA-15

B



SBA-15 exists connecting micropores and small mesopores in the wall of large-pore channel.



Scheme 1. Schematic illustration of formation of A) disordered carbon using a template with disconnected pores (MCM-41, or alternatively SBA-15 calcined at temperatures of about 1243 K), and B) ordered CMK-3 carbon using a template with an interconnected pore system (for instance SBA-15 calcined at temperatures below about 1173 K).

Modify Pore Properties By:

- **One-pot synthesis**

Mixing silane with functional groups into the silica source

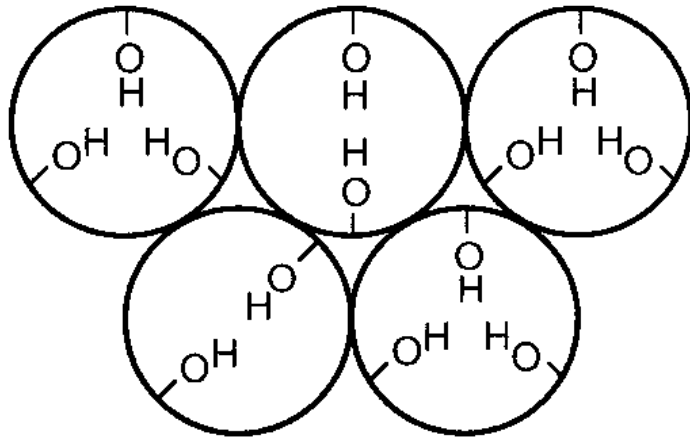
Mixing the reactive species with the silica source

- **Post Functionalization**

Silylation of functional groups (**grafting**)

Impregnation of reactive species such as metals, metal oxides

Functionalization of Surface Silanols

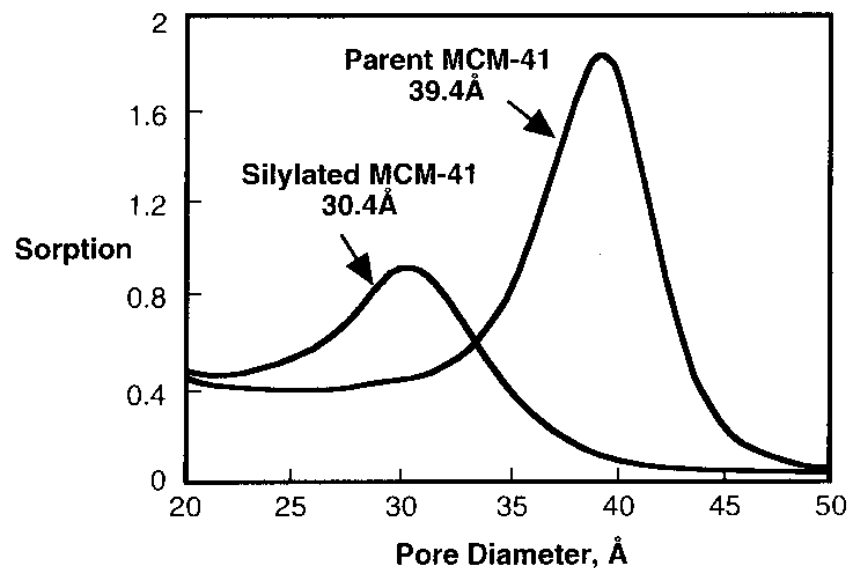
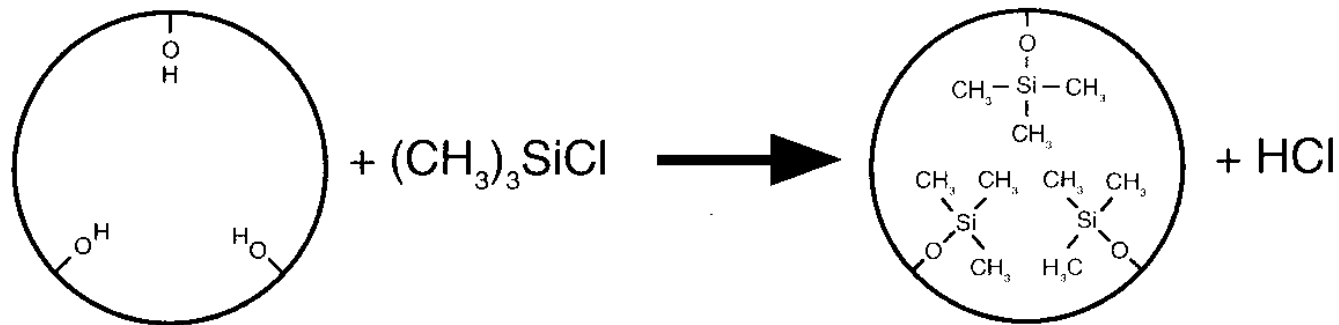


M41S Silanols react with a variety of compounds to:

- Change of Pore Size
- Change Hydrophilicity
- Anchor Catalytic Sites

**CP-MAS Si-NMR shows
20% of Si atoms are Si-OH**

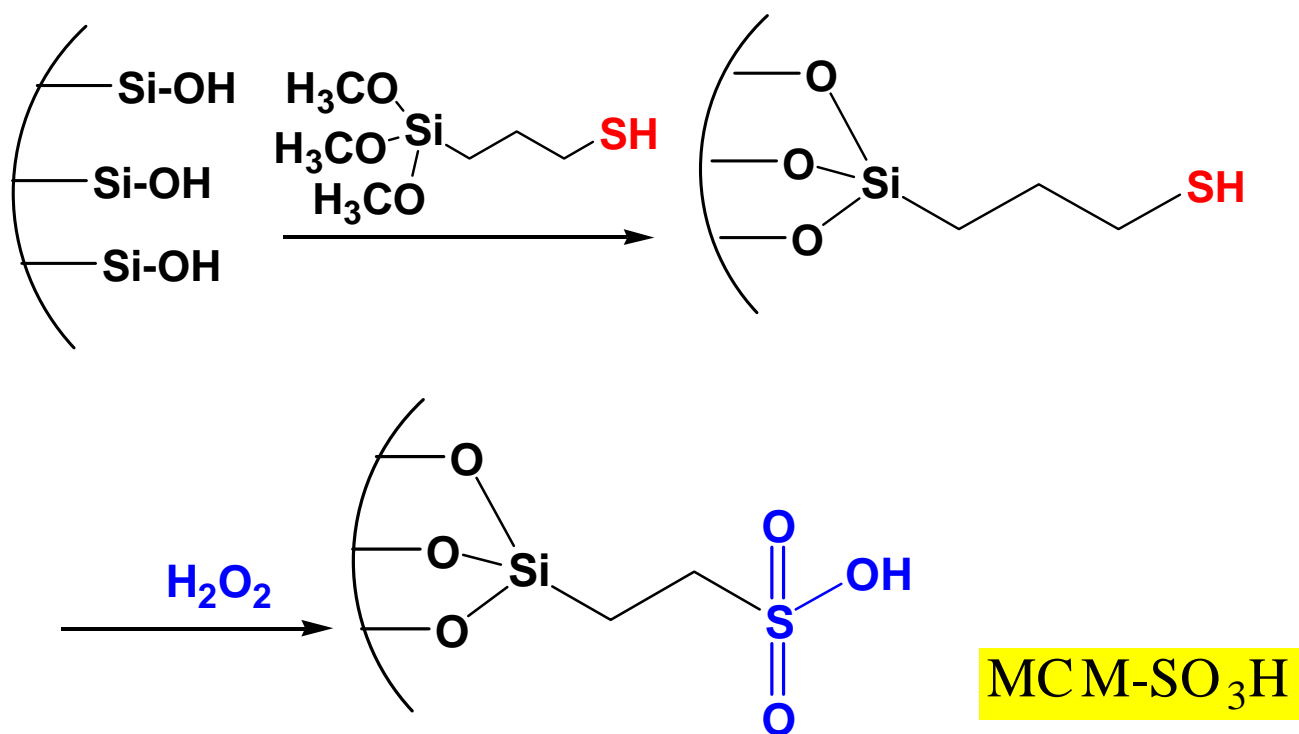
Functionalization of MCM-41 with Trimethylsilyl Chloride



- Pore Volume Decreased by 41%
- Pore Size Decreased from 39.4 Å to 30.4 Å

Experimental Methods

Grafting of Sulphonic Acid Groups on Nano-porous Materials



Shape-Selectivity: Catalytic reactions in Molecular Sieves

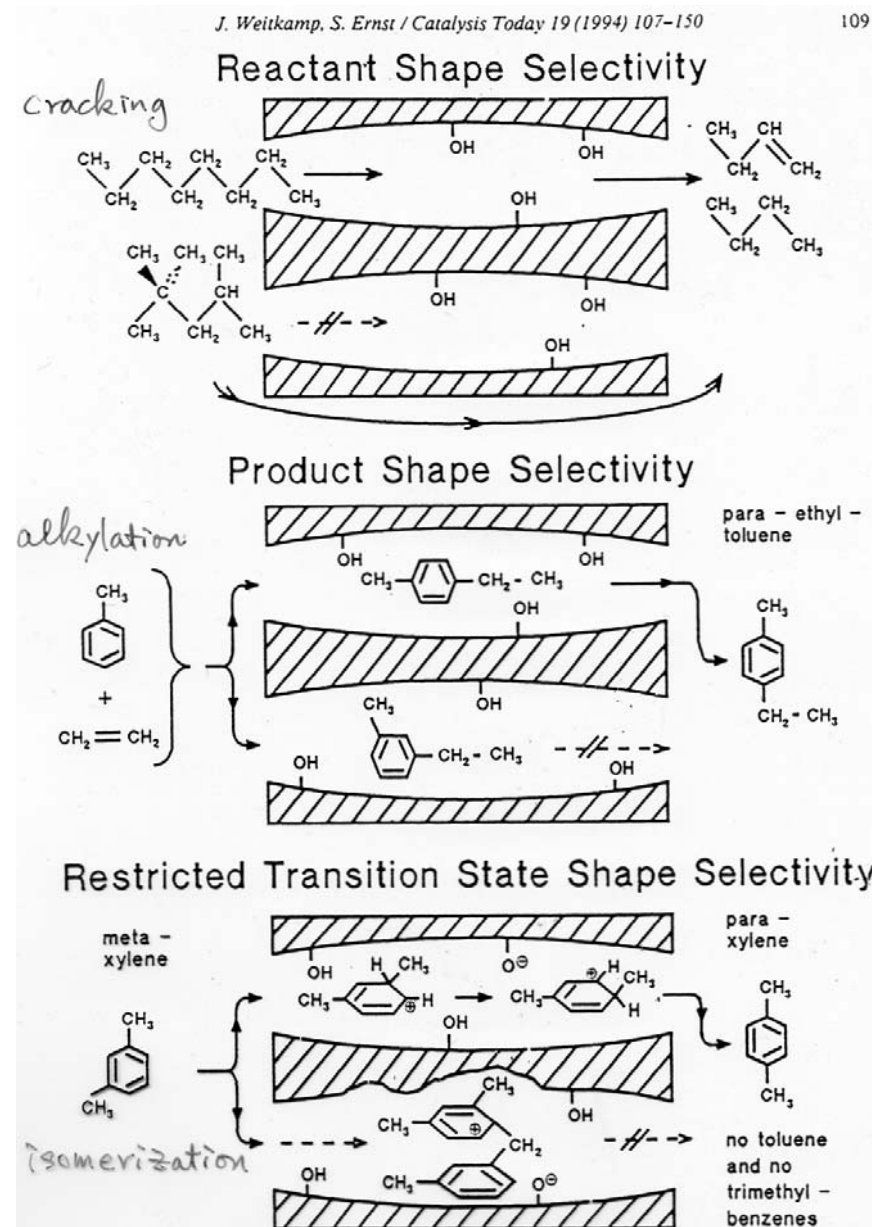


Fig. 1. Examples for the three classical types of shape selectivity after Weisz [27] and Csicsery [26,28,29].

Reactions- comparison of various catalysts in Bisphenol-A synthesis

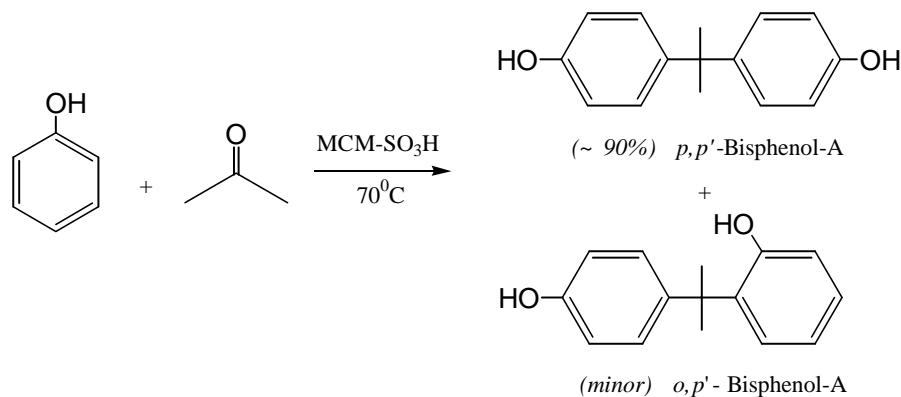


Table 1

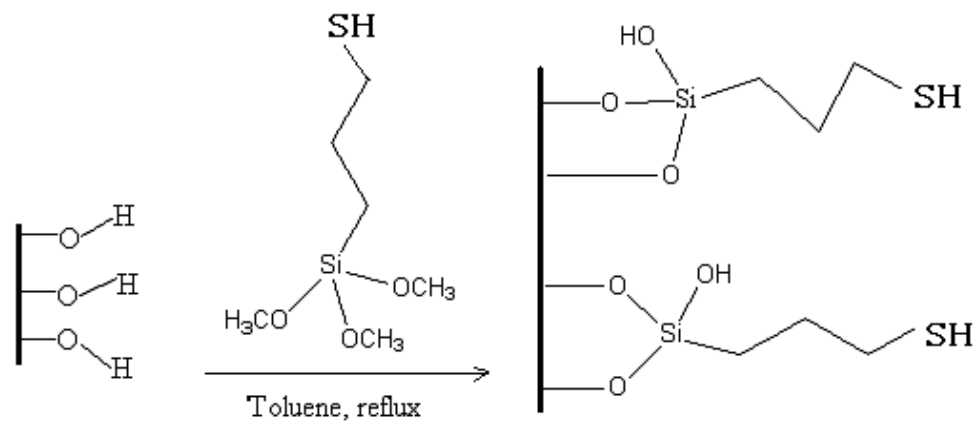
Synthesis of Bisphenol-A with sulphonic acid functionalized MCM-41 silicas

Entry	Catalyst	Phenol conversion (%)	Selectivity ^a (%)
1	---	0	--
2	H-beta ^b	5	55
3	HY ^c	7	--
4	HZSM-5 ^d	<5	10
5	MCM-SO ₃ H	30	92
6	MCM-SO ₃ H ^e	17	90

Phenol 4.7 g, acetone 0.58 g, (molar ratio = 5 :1) Catalyst 50 mg, 70°C, 24 h

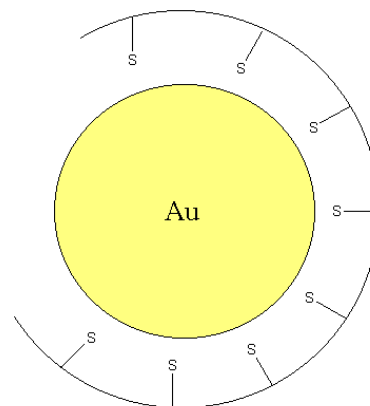
^a Selectivity to *p,p'*-Bisphenol-A, ^b Si/Al = 50, ^c Si/Al = 10.6, ^d Si/Al = 80, ^e incomplete oxidation (from XANES)

Experimental Methods

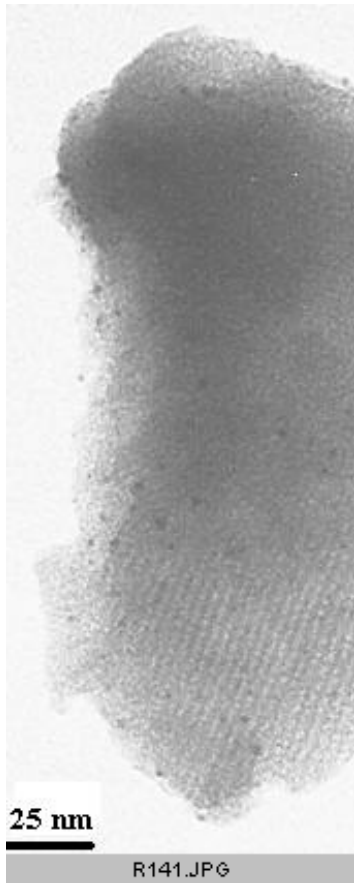


H₂O Refluxed MCM-41

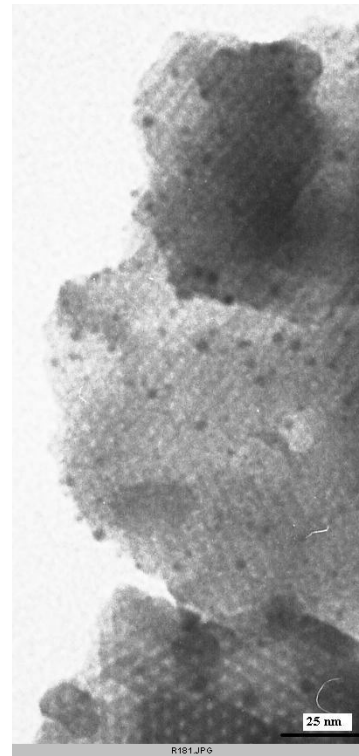
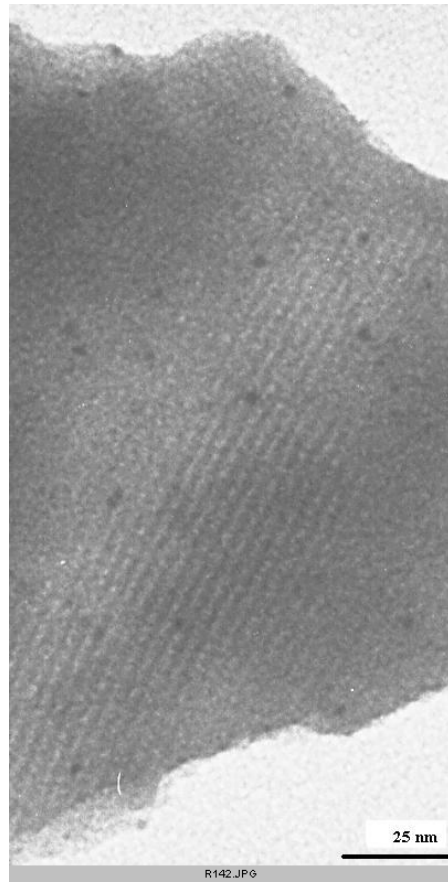
- ↓
1. Sorption of HAuCl_4 soln
 2. Reduxtion with NaBH_4



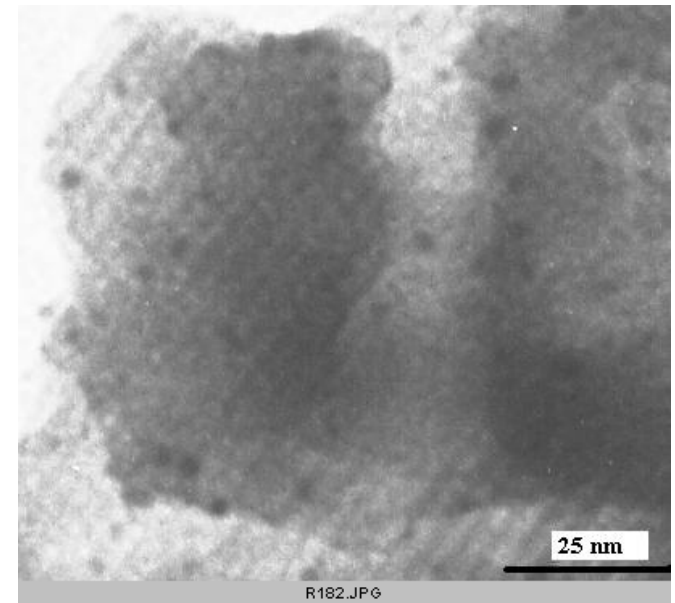
*TEM photos- Au nano particles stabilized in the channels
of nanoporous materials of different pore diameters*

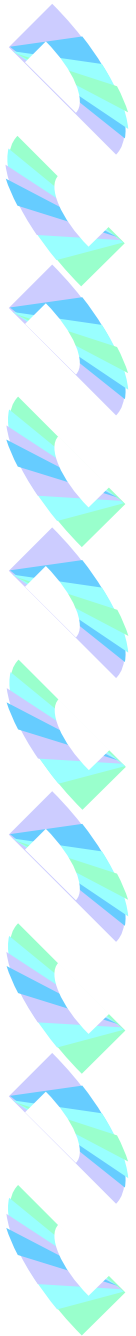


Au-rMCM-41(14)



Au-rMCM-41(18)





Biomedical Applications

Classical

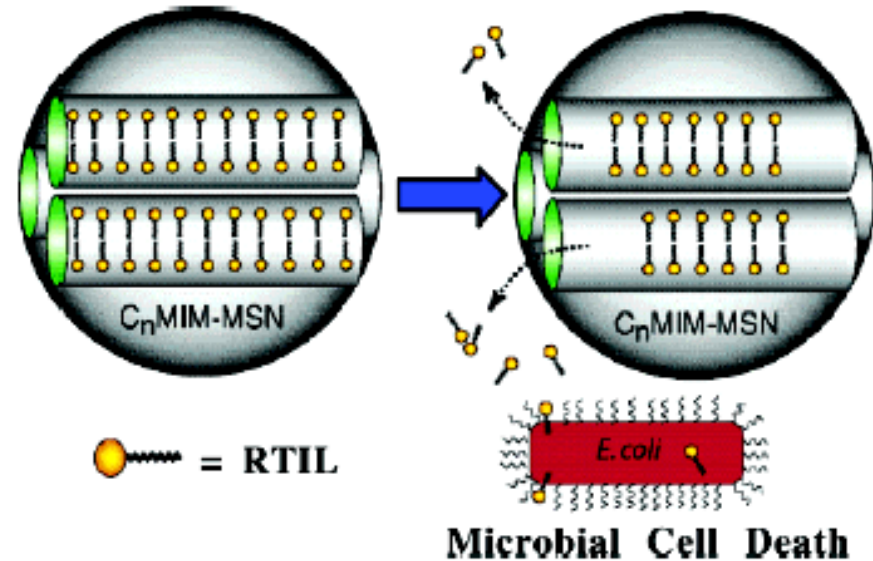
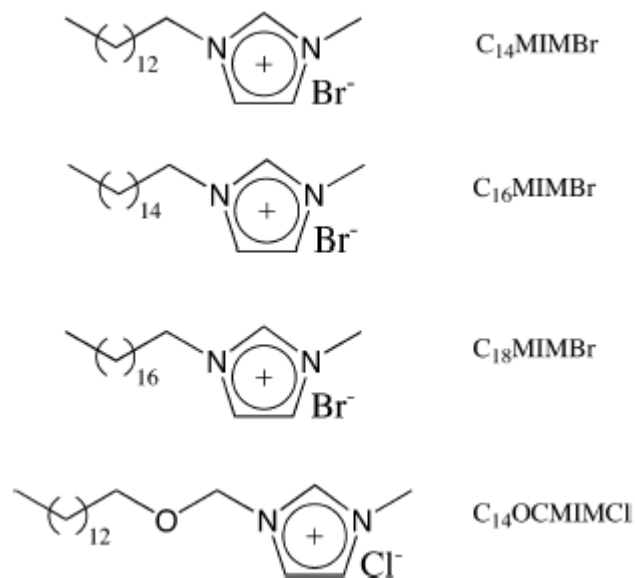
- ◆ **Decontamination and antibacterial agents**
- ◆ **Slow release drugs**
- ◆ **Filter in Hemodialysis**

Potential

- ◆ **Enzyme mimetics and Biosensors**
- ◆ **Adjuvant in anticancer therapy**

Morphological Control of Room-Temperature Ionic Liquid (RTIL) Templated Mesoporous Silica Nanoparticles for Controlled Release of Antibacterial Agents

B.G. Trewyn, C.M. Whitman, V.S.-Y. Lin
NANO LETTERS, 2004, 4, 2139



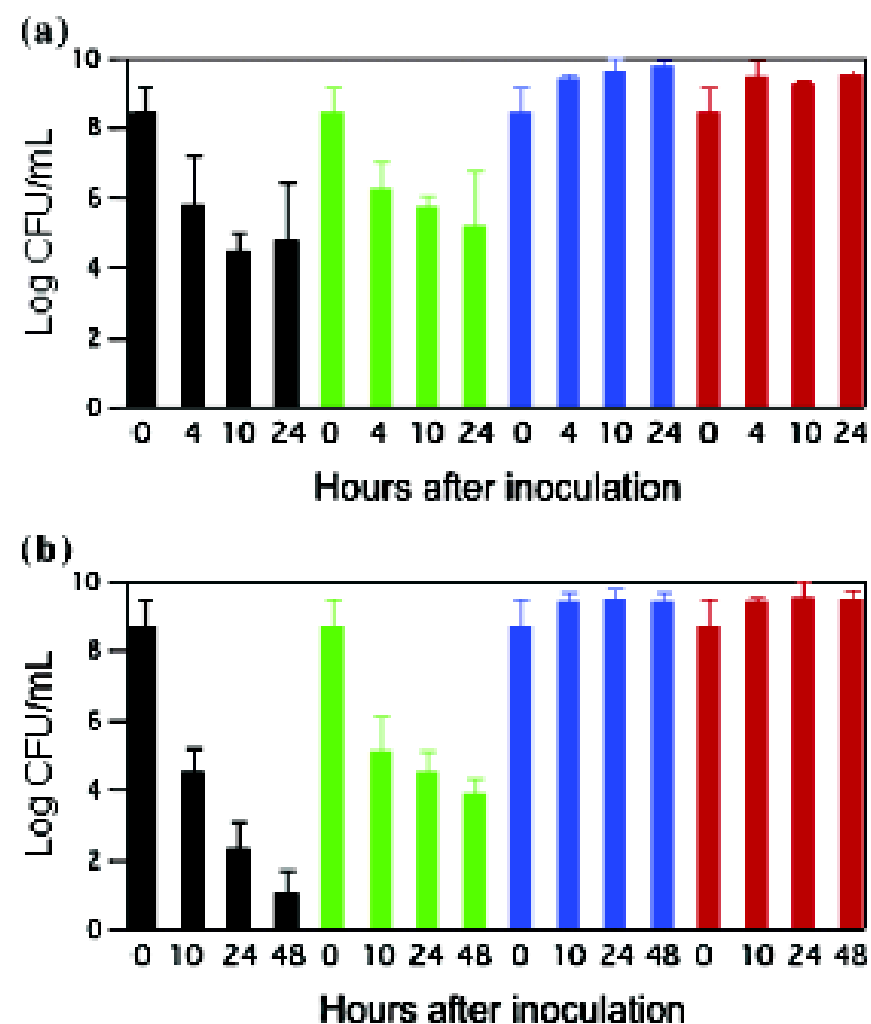
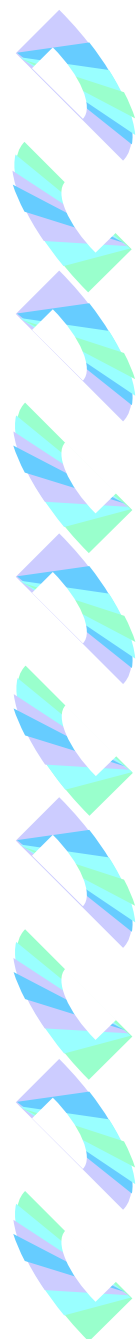


Figure 6. Histogram of the antibacterial activity of C₆MIM-MSNs against *E. coli* K12 at 25 °C (a) and 37 °C (b). Four samples were measured at each temperature: C₁₆MIM-MSN (black bars), C₁₄-OCMIM-MSN (green bars), RTIL-removed C₁₆MIM-MSN (blue bars), and blank control (no silica material) (red bars).

Separation of sterols using zeolites

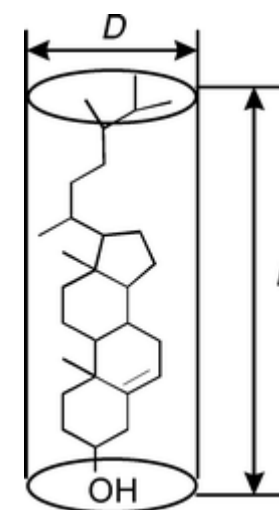
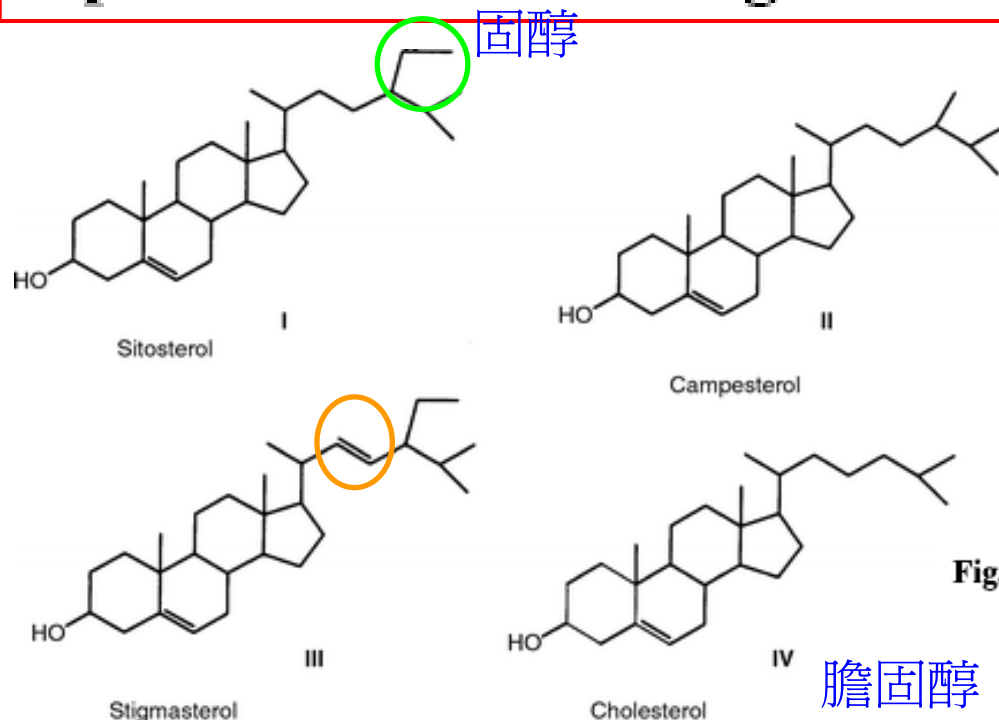
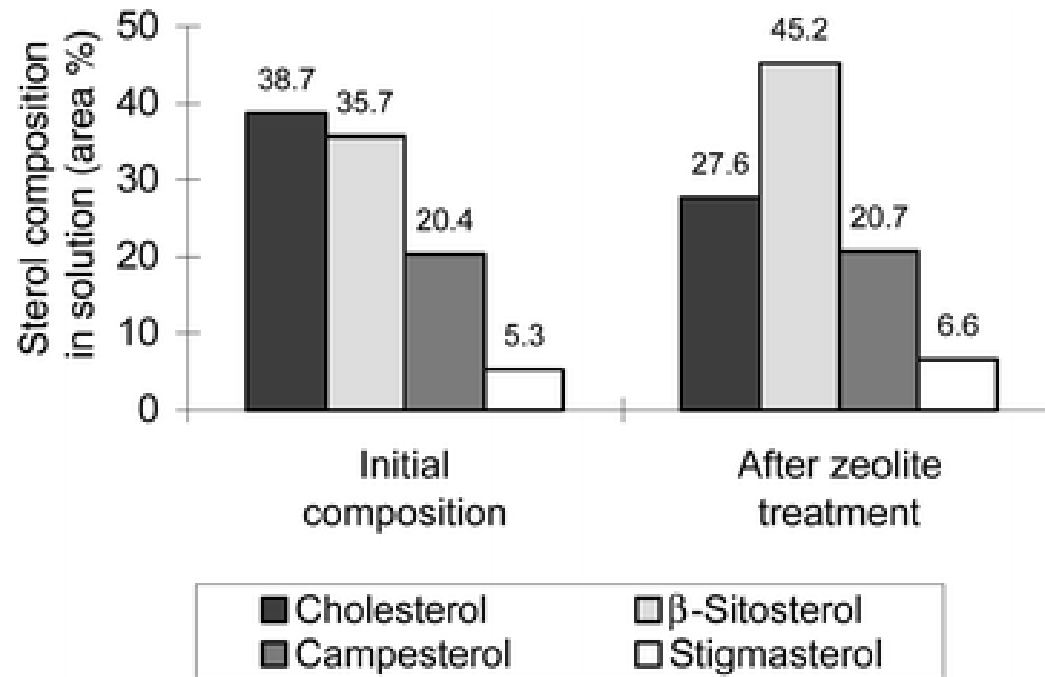
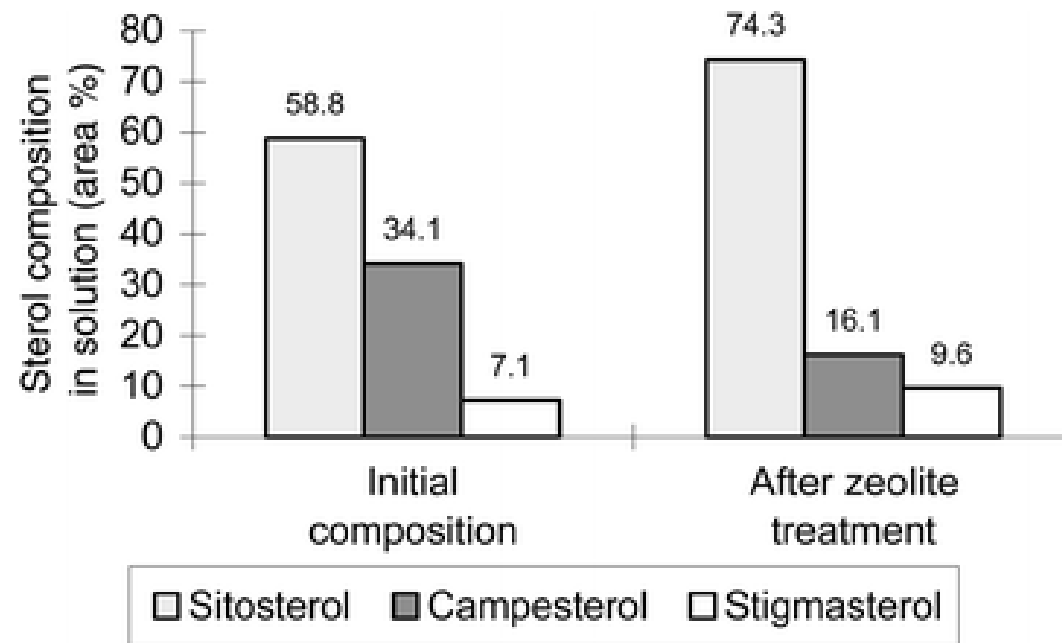
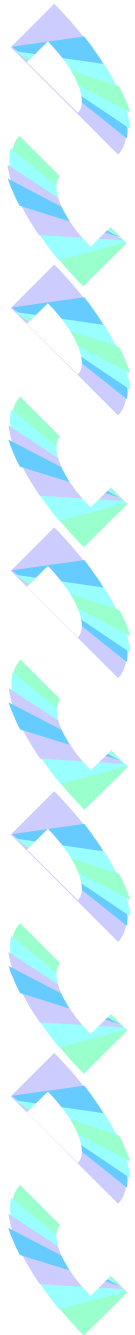


Fig. 12 Cylindrical size model of a sterol molecule.

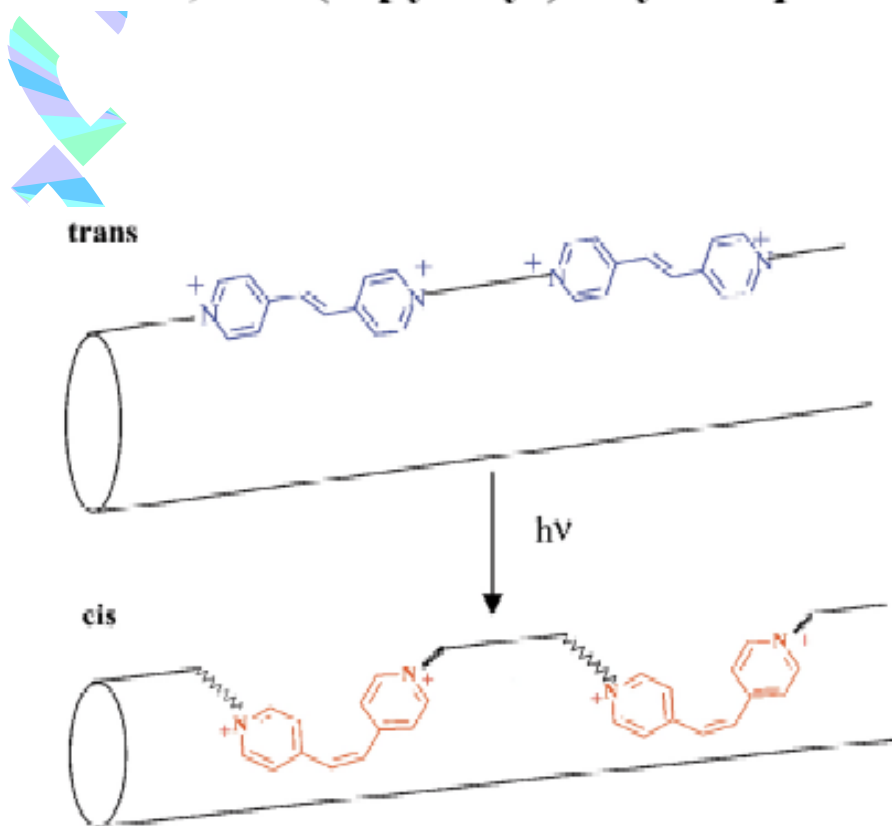
Table 1 Dimensions of sterols based on molecular modeling

	Length, $L/\text{\AA}$	Diameter, $D/\text{\AA}$
Cholesterol	19.0	6.1
Campesterol	18.7	6.3
β -Sitosterol	17.8	7.5
Stigmasterol	17.1	7.7



Photochemical modification of the surface area and tortuosity of a *trans*-1,2-bis(4-pyridyl)ethylene periodic mesoporous MCM organosilica

[Chem. Commun. 2012 (2002)]



Scheme 2

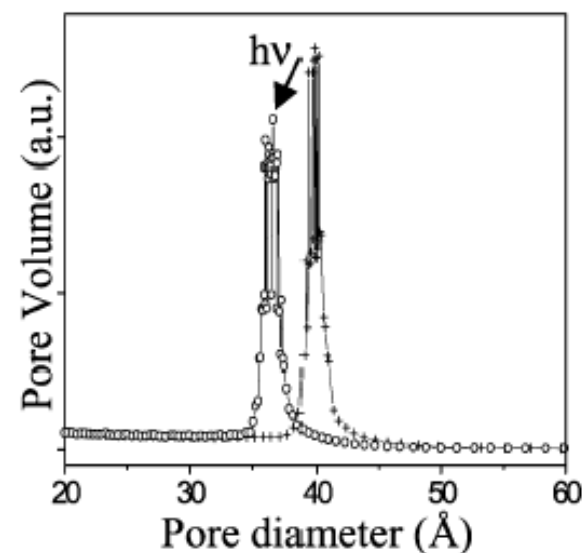


Fig. 3 Pore size distribution for *t*-BES-PMO before (+, 39.8 Å) and after (o, 36.5 Å) UV irradiation deduced by the Horvath–Kawazoe equation from the Ar adsorption isotherm.

Photocontrolled reversible release of guest molecules from coumarin-modified mesoporous silica

[Nature 421, 350 (2003)]

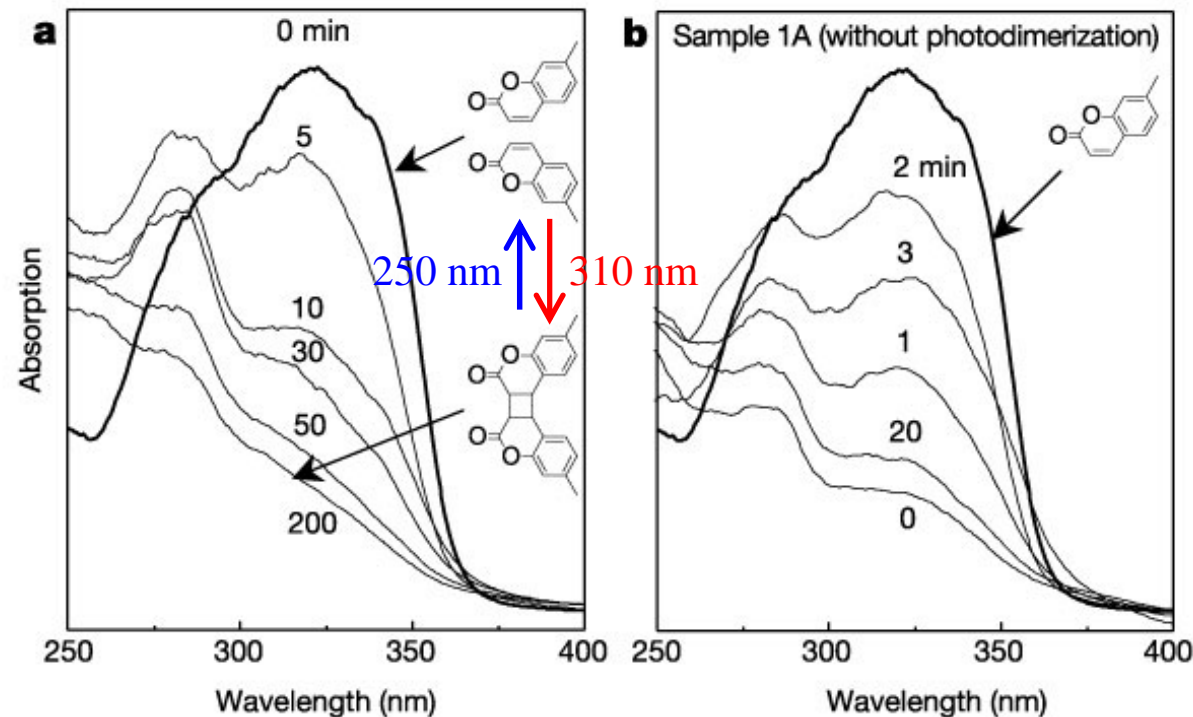


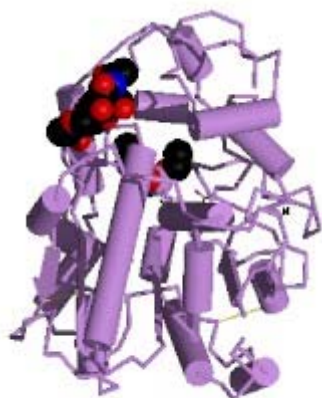
Figure 1 Changes in UV-visible spectra of modified MCM-41 samples during UV irradiation. **a**, Sample **1A** (MCM-41 with 4 wt% coumarin substituent, prepared with a grafting time of 15 min) during photo-irradiation with UV light of wavelength >310 nm. **b**, Sample **2A** (cholestane absorbed to sample **1A**, followed by photodimerization and washing) during photo-irradiation with UV light of wavelength around 250 nm. The structures of coumarin monomer and dimer are also shown,

Immobilization of lipase in a mesoporous reactor based on MCM-41

Hui Ma, Jing He, David G. Evans, Xue Duan.

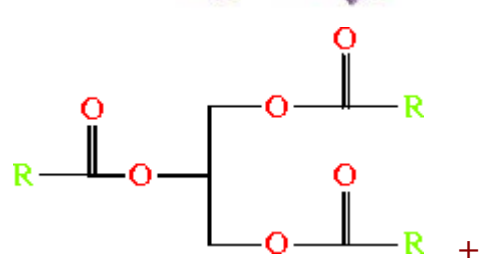
Journal of Molecular Catalysis B: Enzymatic **30** 2004 209–217

Lipases are enzymes which catalyze the hydrolysis of triglycerides to give fatty acids and glycerol, both essential chemicals in the oleochemical industry.

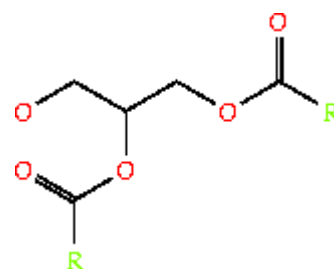


MW: 45000-50000

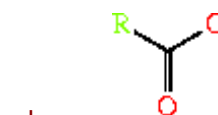
Dimension : 4.6nm*2.6nm*1.1nm



Triacylglycerol



diacylglycerol



$a \times$ fatty acid anion

Schematic representation of the structure of the mesoporous reactor

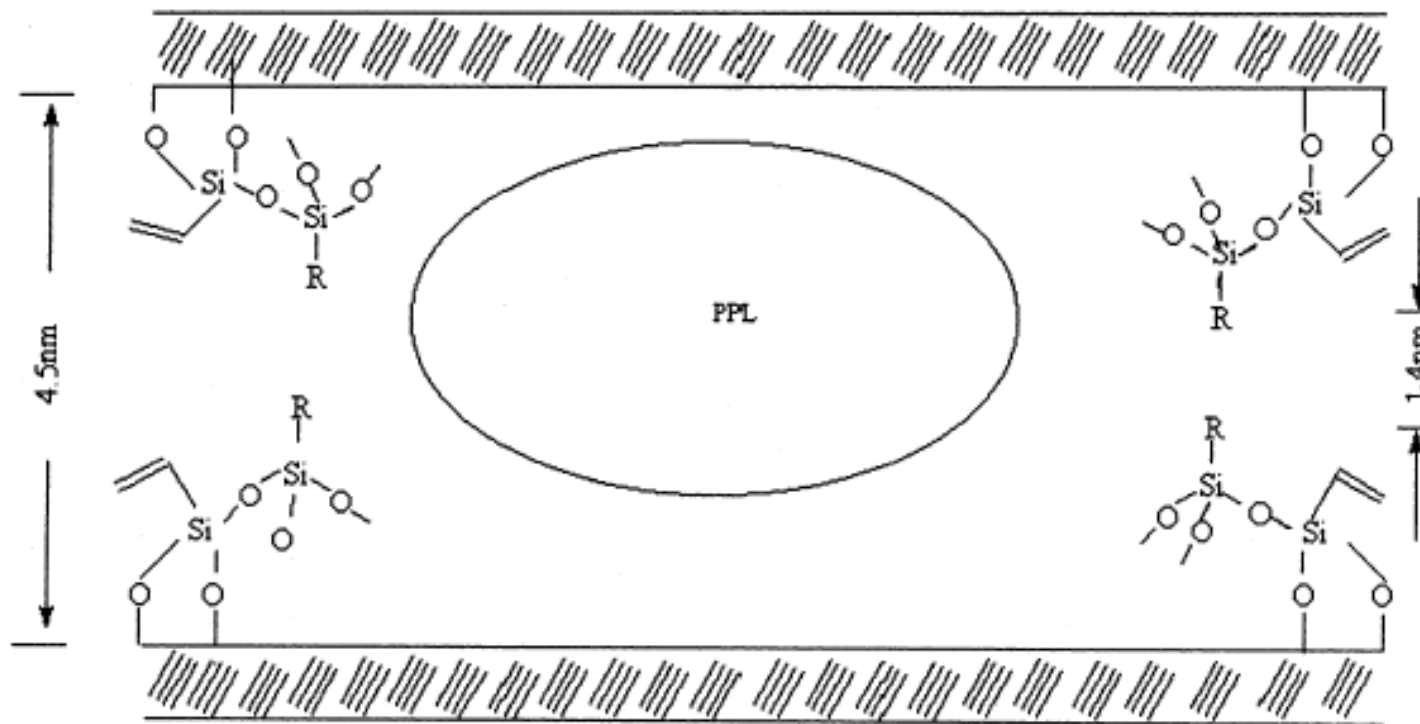


Fig. 9. Schematic representation of the structure of the mesoporous reactor.

Activity of PPL immobilized in the mesoporous reactor

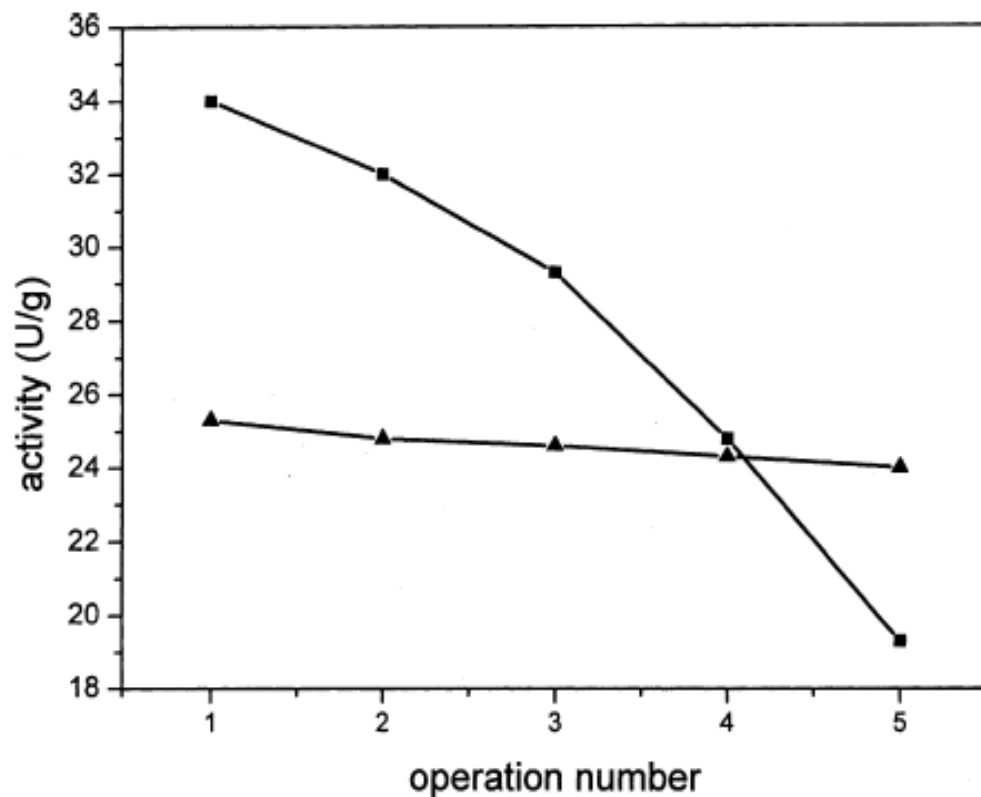
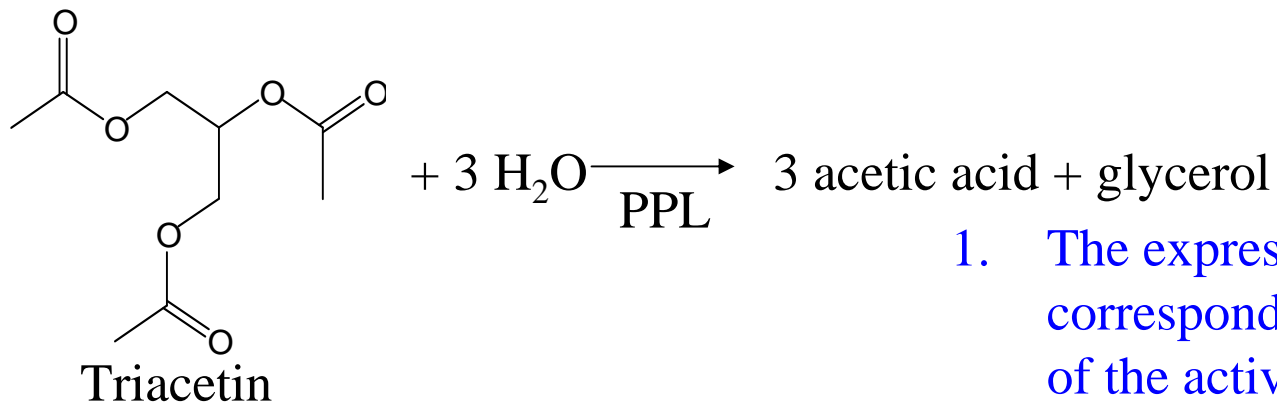


Fig. 10. Activity of IME-MCM (■) and IME-MCM-VS (▲) upon repeated use.

1. The expressed activity (34U/g) corresponds to just over 50% of the activity of the same amount of free PPL.
2. PPL is being leached out of the support during the reaction because it is only attached by relatively weak hydrogen bonding with the silanol groups of the support.
3. Silylation of the material has indeed led to a **reduction in the size of the pore mouth**, thus **preventing leaching** of the immobilized enzyme from material.

A Polyamidoamine Dendrimer-Capped Mesoporous Silica Nanosphere-Based Gene Transfection Reagent

J. AM. CHEM. SOC. 2004, 126, 13216

D.R. Radu, C.-Y. Lai, K. Jeftinija, E.W. Rowe, S. Jeftinija, V.S.-Y. Lin

Diameter
~ 230 nm

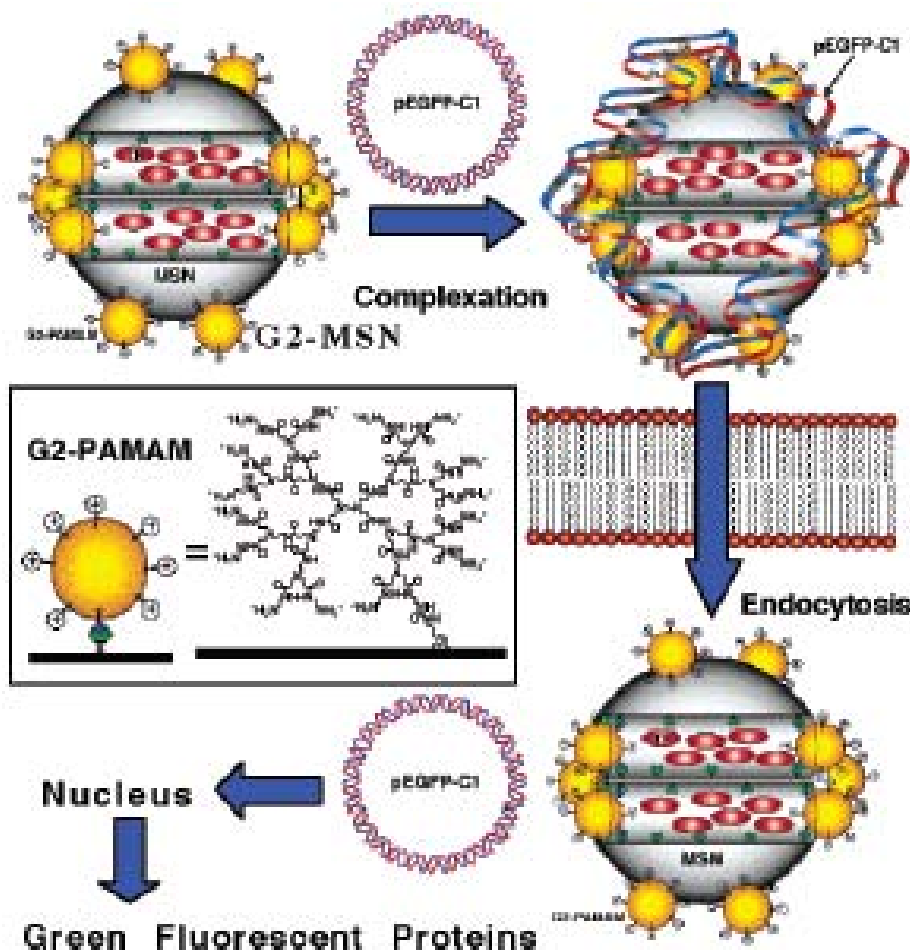


Figure 1. Schematic representation of a nonviral gene transfection system based on a **Texas Red (TR)**-loaded, **G2-PAMAM dendrimer**-capped MSN material complexed with an enhanced **green fluorescence protein** (*Aequorea Victoria*) plasmid DNA (pEGFP-C1).

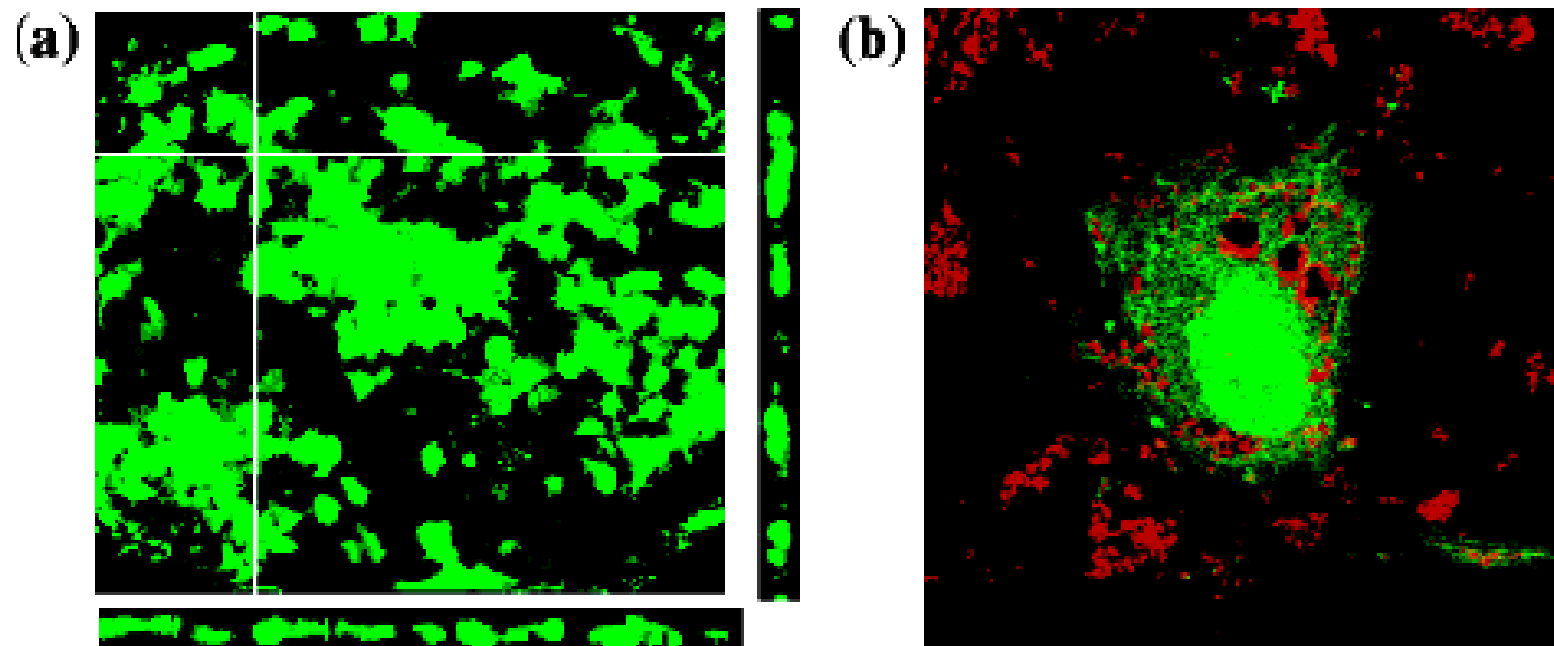
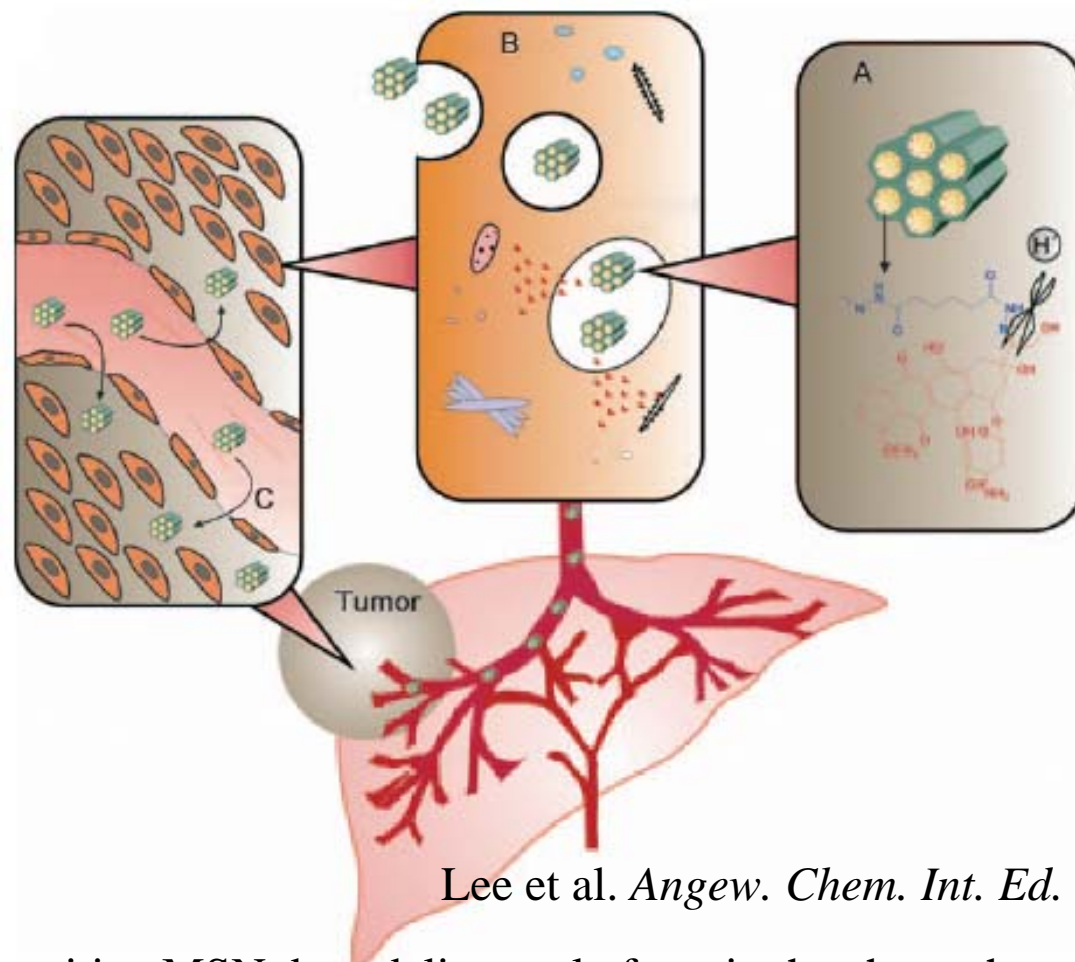
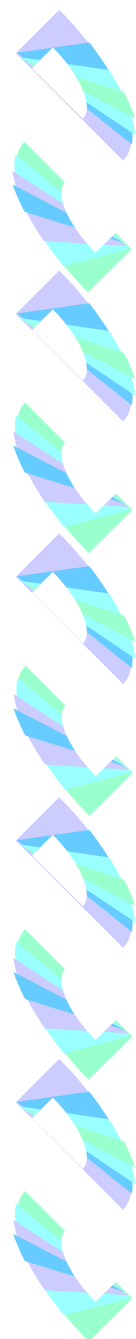


Figure 3. Fluorescence confocal micrographs of cells transfected by the pEGFP-C1-coated G2-MSN system. Panel a presents GFP-transfected HeLa cells showing cross-sections through a cell layer. Orthogonal images indicated the monolayer packing of cells. Panel b presents Texas Red-loaded G2-MSNs inside a GFP-transfected rat neural glia cell (astrocyte).



Lee et al. *Angew. Chem. Int. Ed.* **2010**, 49, 8214–8219

The pH-sensitive MSN drug delivery platform in the chemotherapeutic treatment of liver cancer. Nonspecific uptake of MSN-hydrazone-Dox from the **blood stream (C)** by the liver cancer cells occurs through **endocytosis (B)**. Hydrolysis of hydrazone bond of the **pH-sensitive linkers (A)** in the acidic environment of endosomes/lysosomes (pH 5–6) releases doxorubicin (red) intracellularly from the MSN nanochannels.



% Release profile of MSN hydrazone-Dox for different pH values

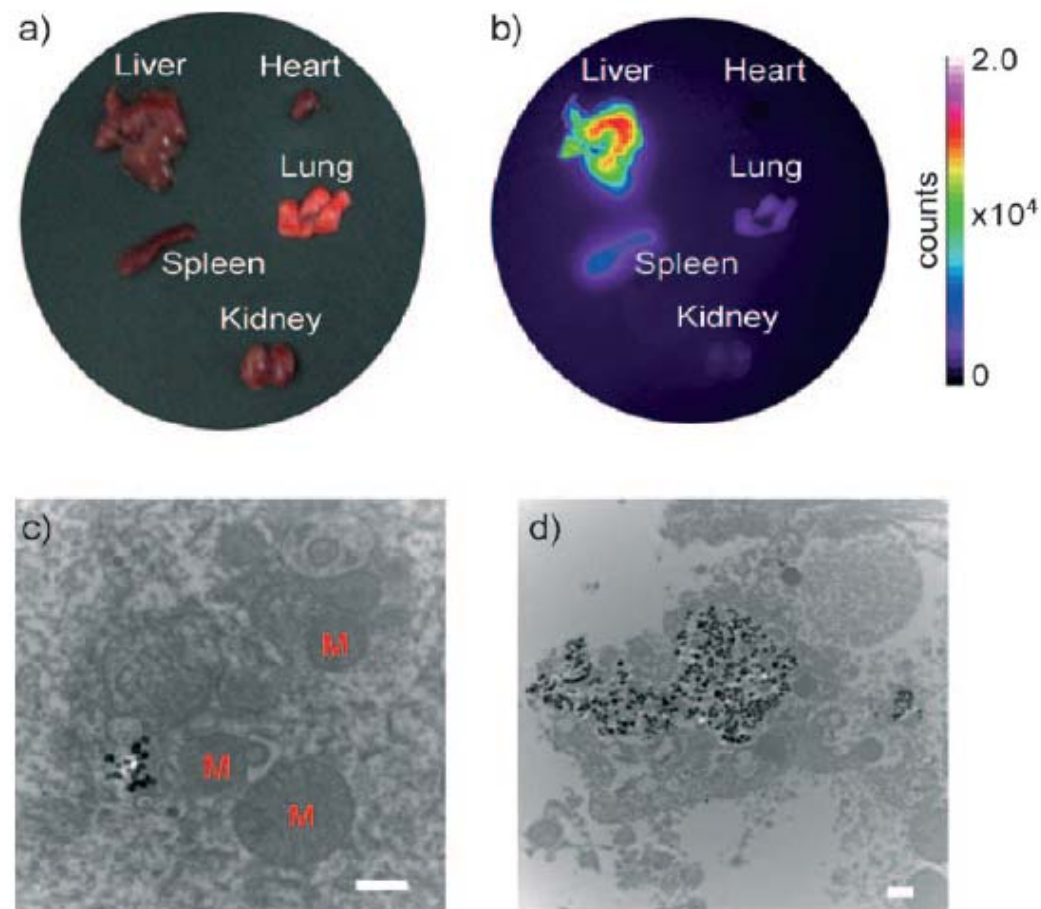
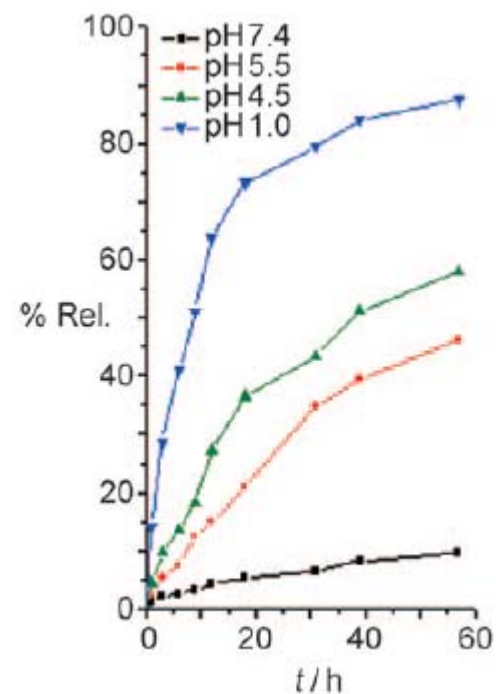
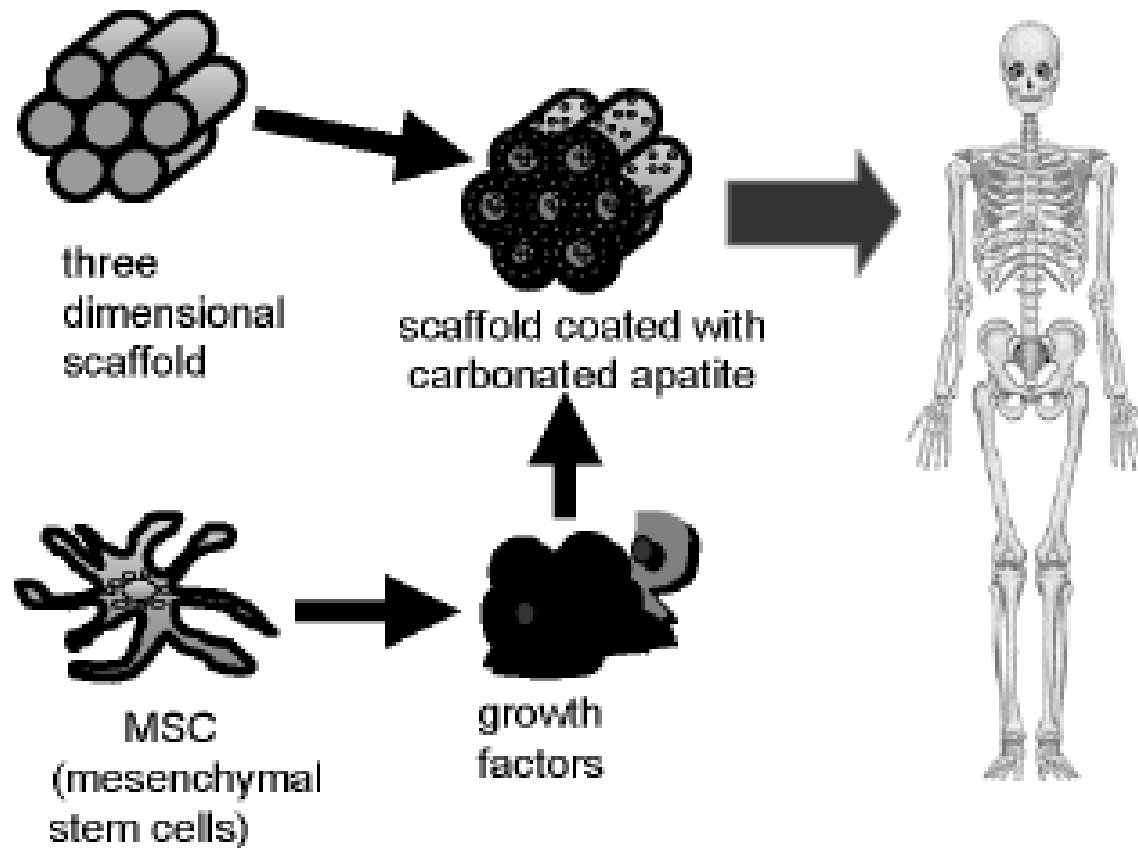


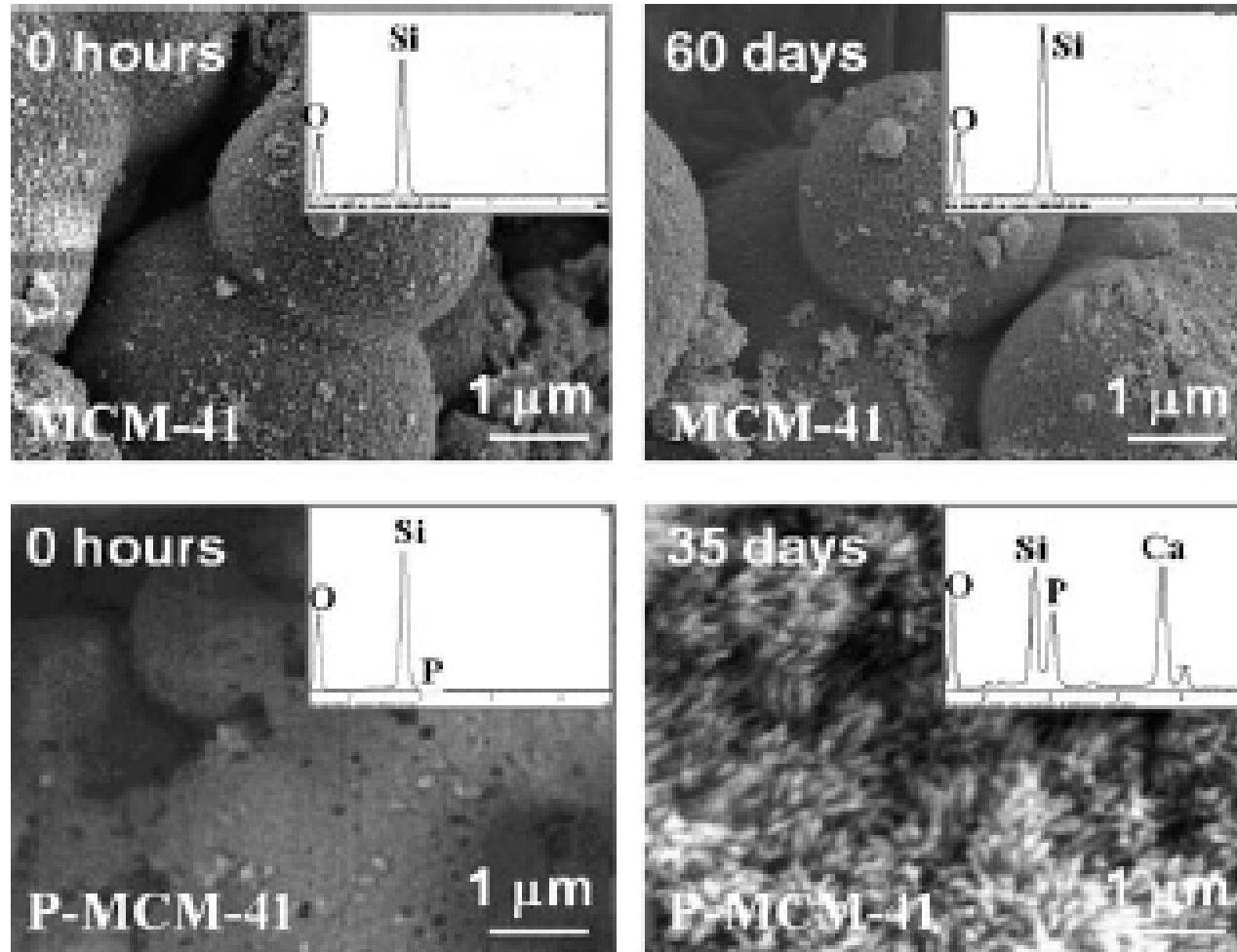
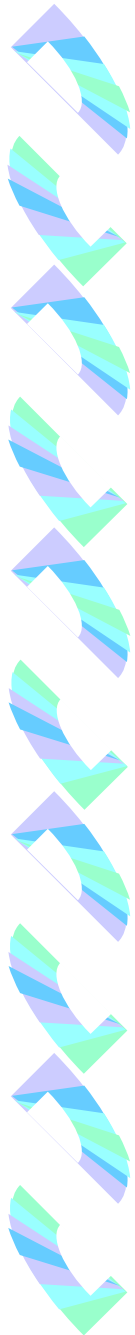
Figure 6. Organs from a mouse dissected 3 h after intravenous injection of Atto-647-MSN-hydrazone-Dox. a) Representative white-light and b) NIR fluorescent images of the organs; c) TEM images of a 70 nm-thick section of liver viscerated from an anesthetized mouse 3 h after intravenous injection of Atto-647-MSN-hydrazone-Dox. (Scale bars 500 nm; M = mitochondria.)

Phosphorous-doped MCM-41 as bioactive material

Solid State Sciences 7 (2005) 233–237



Biomimetic scheme of bioactive MCM-41 matrix as bone tissue engineering; useful in the preparation of bioceramic implants with previously adsorbed antibiotic and/or antiinflammatory drugs, allowing treating locally the infections or inflammatory response of the living tissue surrounding the implantation area.

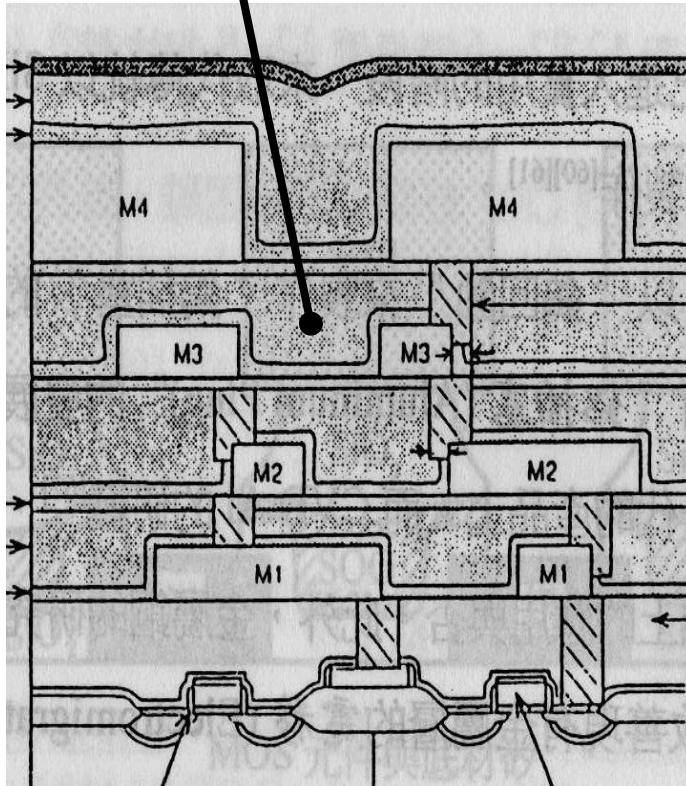


SEM micrographs and EDS analysis of MCM-41 and P-MCM-41 samples before and after soaking in SBF.

An Introduction to the Low-k Film

台大化工製程研究室

Interlayer Dielectric



A typical semiconductor device

○ k : Dielectric Constant

$$k = \frac{C(\text{substance})}{C(\text{vacuum})}$$

C : capacitance

○ Why develop low-k films?

To reduce R-C delay
when device is small

○ Requirements for Low-k Films

1. Electrical Performance
 - a). Low dielectric constant.
 - b). Low leakage current density.
2. Mechanical strength
 - a). Stiffness and film stress.
 - b). Adhesion.

How to reduce the k (dielectric constant) value of a material?

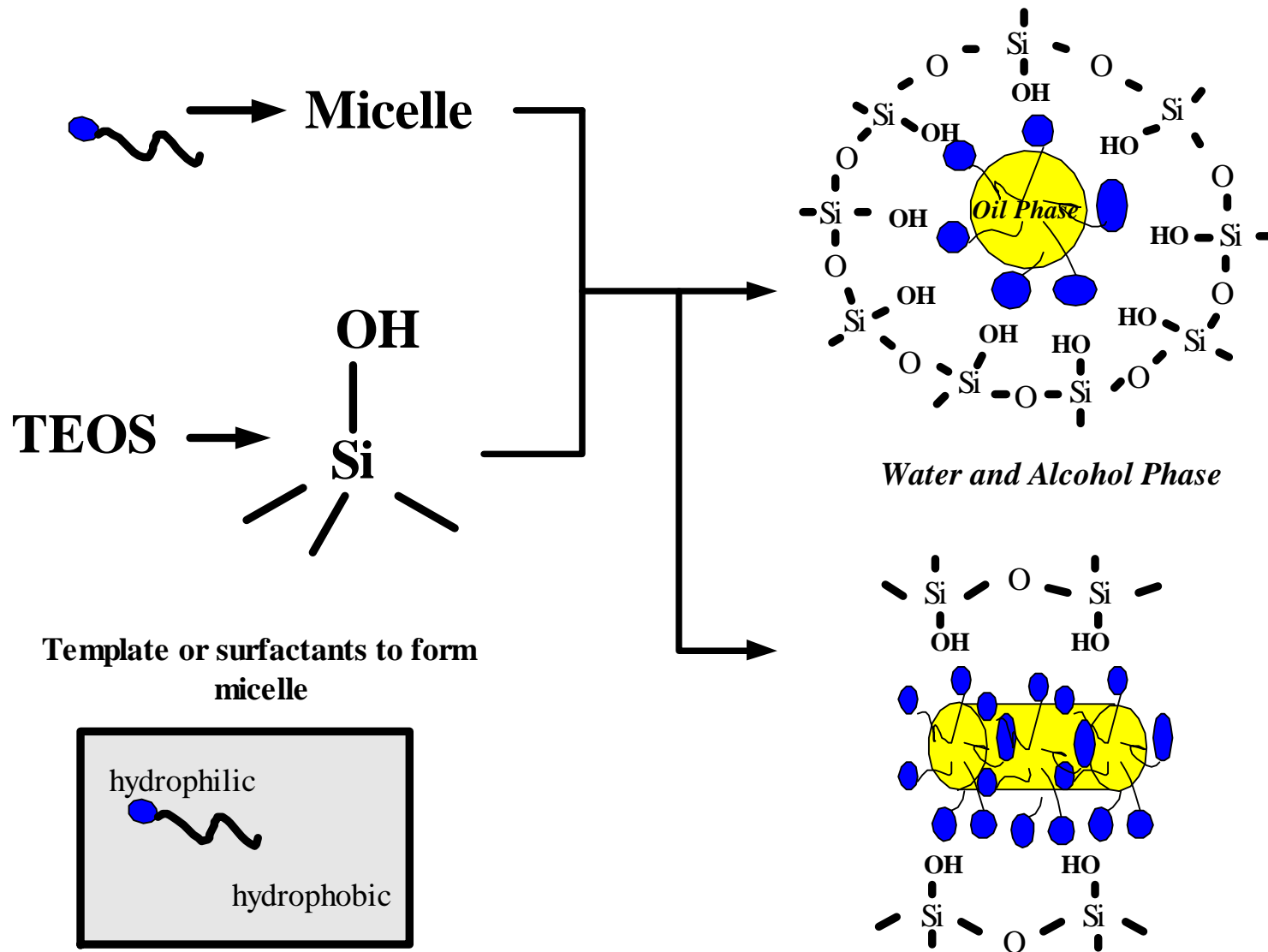
台大化工製程研究室

○ $k = 4.0$ for SiO_2
 $k \sim 1.0$ for air

○ Possible strategies:

1. Introducing nano-pores into the material.
2. Reducing the number of polar sites on the pore surfaces

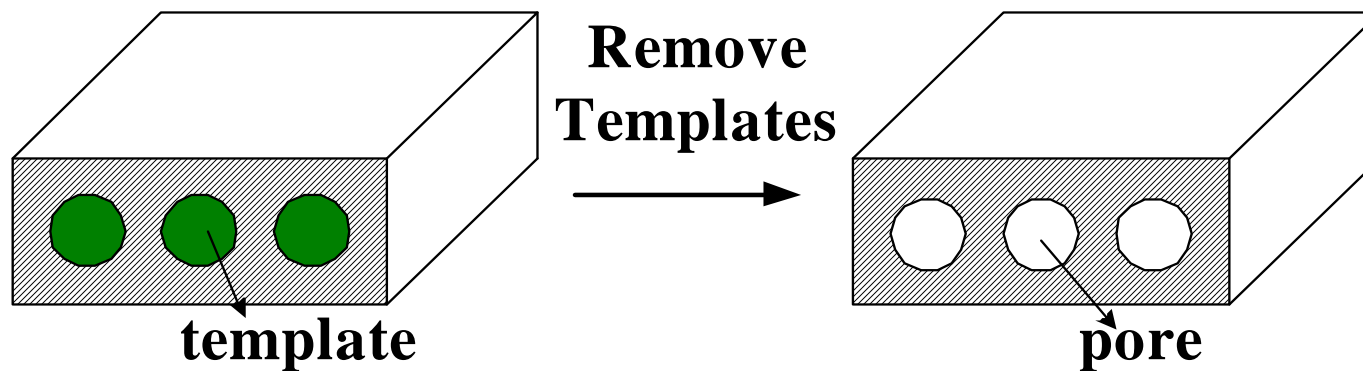
Proposed Mechanism for Surfactant-templating Porous Silica Formation



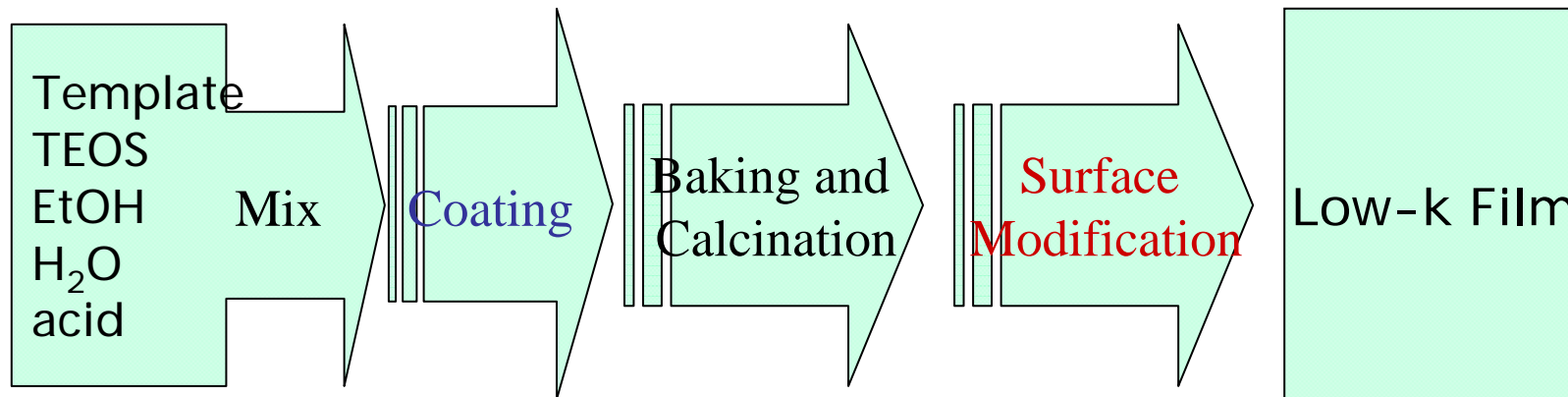
The Nanoporous Low-k Film

台大化工製程研究室

Strategy : Introducing air ($k \sim 1$) in the film by making pores in it.



Preparation :



Electrical Performance of Nano-porous Silica film

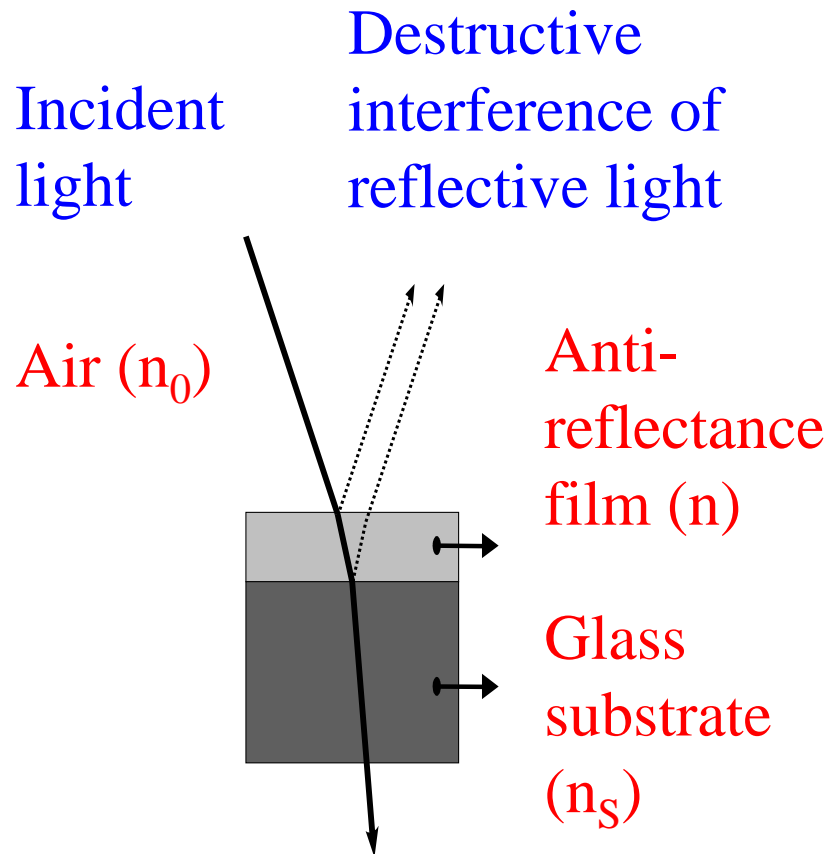
台大化工製程研究室

Performance of films prepared by Tween 80/TEOS = 41wt%

HCl/TEOS (molar ratio)	Thickness (nm)	k	I (A/cm ²)
0.37	397.7	1.80	3.28E-07
0.25	451.2	1.77	6.51E-09

Theory of Anti-reflectance film

台大化工製程研究室



By controlling the reflective index (n) and the thickness of the film, anti-reflectance can be achieved through the destructive interference of light reflective from the film surface and that from the interface of film and glass.

Anti-reflectance film

台大化工製程研究室

$$d = \frac{1}{4} \left(\frac{\lambda}{n} \right)$$

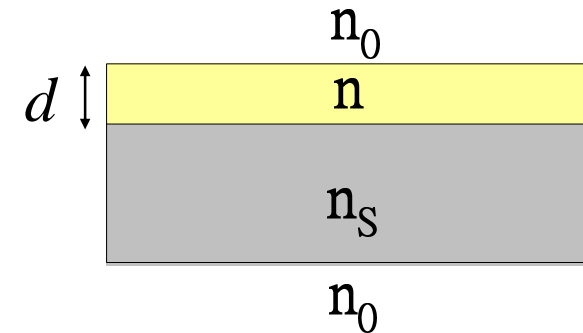
$$n^2 = n_0 n_s$$

n_0 : reflective index of air ($n_0=1$)

n_s : reflective index of glass ($n_s=1.52$)

n : reflective index of thin film

d : thicknes of the film

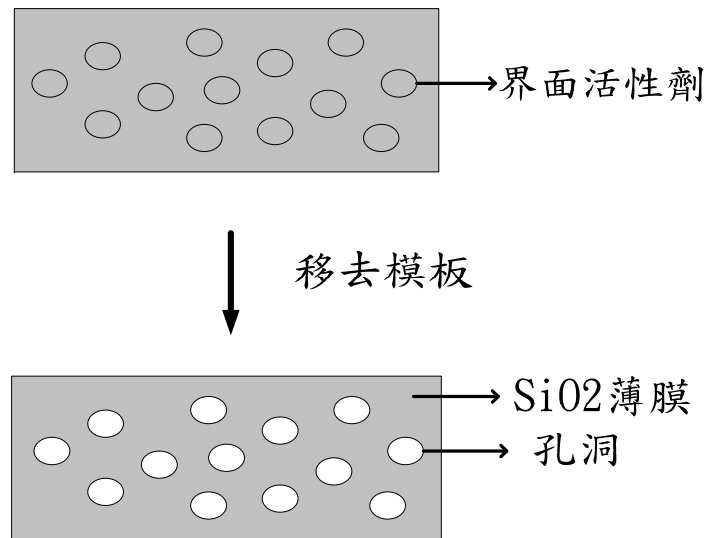


$$n_0=1, n_s=1.52 \Rightarrow n = \sqrt{n_0 n_s} \approx 1.23$$

$$\lambda = 510 \text{ nm} \Rightarrow d = \frac{\lambda}{4n} \approx 100 \text{ nm}$$

Preparation of anti-reflectance silica film with pore-directing agents

台大化工製程研究室



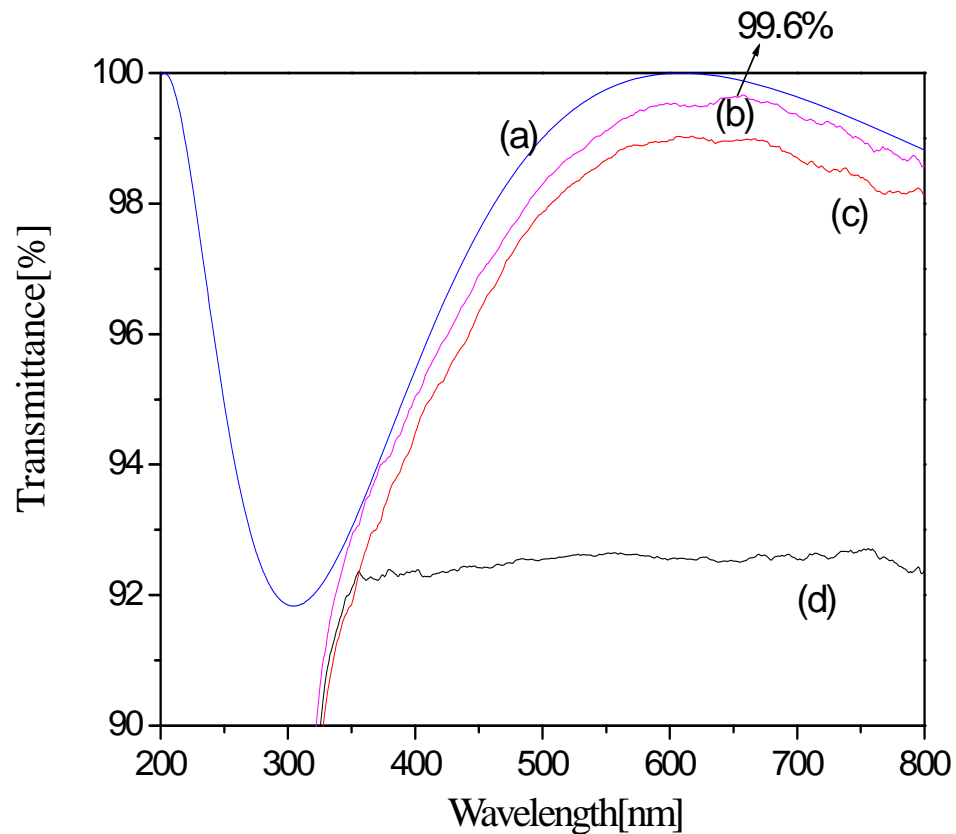
Formation of porous SiO₂ film

The reflective index (n) is adjusted by varying the volume ratio of air (pore) and silica.

The thickness of the film (d) is controlled by varying the composition of the sol-gel.

Effect of pre-treatment

台大化工製程研究室



(a) simulation, (b) KOH pre-treatment (c)
HF+SC1 pre-treatment, (d) glass substrate

Thickness and reflective index

reagent	n	d (nm)
(b) KOH	1.238	123
(c) HF+SC1	1.238	123

KOH pre-treatment seems
to give better result!



*Can Nono-porous Materials be
Made of Compounds Other than
Silica*

